NOTE TO USERS

Page(s) not included in the original manuscript and are unavailable from the author or university. The manuscript was scanned as received.

104

This reproduction is the best copy available.

UMI®

DISSERTATION

DEVELOPMENT OF A MAMMALIAN CELL MUTATION ASSAY BASED ON FLOW CYTOMETRY AND ITS USE IN ANALYZING MUTATIONS INDUCED BY IONIZING RADIATION AND CHEMICALS

Submitted by

Carley Denise Ross

Cell and Molecular Biology

In partial fulfillment of the requirements

For the Degree of Doctor of Philosophy

Colorado State University

Fort Collins, Colorado

Summer 2006

COLORADO STATE UNIVERSITY

June 21, 2006

WE HEREBY RECOMMEND THAT THE DISSERTATION PREPARED UNDER OUR SUPERVISION BY CARLEY ROSS ENTITLED *DEVELOPMENT OF A MAMMALIAN CELL MUTATION ASSAY BASED ON FLOW CYTOMETRY AND ITS USE IN ANALYZING MUTATIONS INDUCED BY IONIZING RADIATION AND CHEMICALS* BE ACCEPTED AS FULFILLING IN PART REQUIREMENTS FOR THE DEGREE OF DOCTOR OF PHILOSOPHY.

Committee on Graduate Work

Dr. William Hanneman William H. Hanneman

Dr. Joel Bedford J Bedford

Dr. Deborah Roess Deborah A Roess

Dr. Michael Fox Michael H. Fox

Adviser

Dr. Norman Curthoys N. C. Curthoys

Department Head/Director

ABSTRACT OF DISSERTATION

DEVELOPMENT OF A MAMMALIAN CELL MUTATION ASSAY BASED ON FLOW CYTOMETRY AND ITS USE IN ANALYZING MUTATIONS INDUCED BY IONIZING RADIATION AND CHEMICALS

The purpose of this study is to develop and utilize a mammalian mutation assay to analyze mutations caused by various toxic agents in a Chinese Hamster Ovary-Human hybrid cell line (CHO A_L).

The CHO A_L cell line contains a single unrearranged copy of human chromosome 11 stably transfected for the last 30 yrs. Measuring a loss of CD59, a gene localized to chromosome 11, is the basis of the mutation assay. By treating CHO A_L cells with various mutagens, the loss of CD59 can be measured as an indicator of genotoxicity. Linear dose responses from ^{137}Cs γ radiation and MNNG (N-methyl-n-nitrosoguanidine) showed that the flow cytometry mutation assay (FCMA) allows a rapid, sensitive, and inexpensive method for detecting the mutations.

The kinetics of CD59 mutant expression was analyzed by flow cytometry. The CD59 protein was removed from the plasma membrane by phosphatidyl inositol phospholipase C (PI-PLC) to measure the rate of exocytosis. At 8 hr, the CD59 expression had returned to control values. CD59 siRNA was also used to knock down CD59 mRNA and determine the duration of the CD59 protein on the cell surface before endocytosis. At 48 hr, CD59 expression had 85% reduction in CD59 expression. Cell cycle analysis was also measured by flow cytometry for lead acetate and MNNG. Lead acetate had a cell cycle delay on day2

whereas MNNG had a prolonged G_2 block until day 4 and fully recovered by day 7. CD59 mutant expression is more likely controlled by cell cycle alterations than protein turnover rate since, through PI-PLC and siRNA treatment, the minimum time before CD59 mutants could be measured was 48 hr.

All mutagens measured by FCMA exhibited a peak in CD59 mutant expression at various time points. To examine the mutant peak region, the CHO A_L cells were irradiated and sorted on the CD59 mutant peak by flow cytometry. The sorted populations were analyzed for survival, growth rate and phenotypic expression of CD44/CD59/CD90. The peak in CD59 mutant expression may be explained by cell lethality of $CD44^-CD59^-CD90^-$ mutants for radiation.

The mutant spectra was determined for irradiated CHO A_L cells using flow cytometry to measure cell surface markers CD59/CD44/CD90/CD98/CD151 and GPI-anchor control. PCR results reflected flow cytometry results. The FCMA gives researchers the tools to measure mutant yield and mutant spectra rapidly and efficiently and provides new insights into the mechanisms of action of mutagenic agents such as ionizing radiation.

Using this system, researchers could quickly ascertain the mutagenic potential of novel chemicals and pharmaceuticals as well as clarify the method of mutagenesis without large expense. Additionally, the FCMA would be able to quickly analyze mutated populations during extended time periods to evaluate the evolution of phenotypic expression.

Carley Denise Ross
Cell and Molecular Biology
Colorado State University
Fort Collins, CO 80523
Summer 2006

Acknowledgements

I first would like to thank Dr. Michael Fox for all of the time, effort, intellectual stimulation he has put into this project and my education. I couldn't have done it without him. My committee members, Dr. Joel Bedford, Dr. Gerald Callahan, Dr. William Hanneman, and Dr. Deborah Roess also made this happen.

All of my laboratory colleagues including Chang Uk-Lim, Dhanashree Joshi, Tenley French, Steve Keysar, and Henri Jean-Francois Dengah have been great fun and wonderful collaboration. I will miss you all!

Leslie Armstrong-Lea, the flow cytometry technician, did a fantastic job training me in flow cytometry and being a wonderful companion and support.

The administrative staff, including Norma Bulera, Julie Asmus and Lori Williams aided in all of the paperwork. Thanks so much!

Lastly, my family has helped me through all of the good and hard times, including my husband, David Ross, my two children, Iain and Dorian and my parents, Rex and Nita Berg. My sister, Kimberly Berg-Collins, kept me company on the phone and my in-laws, Richard and Rosemary Ross have been great support. Thank you to everyone for all of your help, even those that I haven't mentioned!

Table of Contents

CHAPTER 1

INTRODUCTION

Scope of Work

Throughout this work, I have used the CHO A_L Chinese-human hybrid cell line to detect mutations from several mutagens including MNNG and gamma radiation. I developed an assay to measure CD59 mutations by detecting the presence or absence of CD59 with flow cytometry after a 5-12 day growth period following treatment. Since the flow cytometry mutation assay (FCMA) is rapid and measures CD59 presence at any time point, I analyzed the kinetics of CD59 mutagenesis and how the glycosylphosphatidyl inositol (GPI) linkage modulates this process. Also, I examined the types of mutations caused by radiation using a multiple marker analysis and flow cytometry. Finally, using several markers along chromosome 11, I determined the size of the genetic lesion by the presence or absence of markers flanking CD59.

The majority of this work focuses on the effects of radiation on the CHO A_L cell line and how CD59 is modulated by this mutagenesis. Before proceeding, I will include a general literature review encompassing the history of the CHO A_L cell line and mammalian mutation assays, a description of CD59 biochemistry and genetics, detailed information about the GPI anchoring of CD59, an explanation of mutagenesis and repair as well as a focus on radiation as a mutagen in the CHO A_L clonogenic assay.

History of the CHO A_L cell line

Dr. Puck from the University of Colorado Medical Center first isolated the Chinese Hamster Ovary (CHO) cells from hamster tissues. Their cells are of particular interest because of their low chromosome number of 2n = 22. After ten months of continuous incubation, researchers saw no decrease of growth rate or change in cellular colony morphology making CHO cells excellent candidates for genetic studies (103). The colonies develop the typical rough edges which characterize clonal growth of fibroblast-like cells in other media. When CHO cells were treated with mutagenic agents such as radiation, there was a significant portion (in comparison to human cells) that had 21 or 23 chromosomes. With the isolation of CHO cells, researchers were now able to compare patterns and frequencies of radiation-induced cellular abnormalities when treated with radiation (103). A few years later, Puck and Ham determined that the CHO cells grew best in an incubator controlling the temperature, humidity and an addition of 5% CO_2 to a buffered media solution (48). After isolating the CHO cells, toxicity data was accumulated for numerous chemicals including radiation (102,104), puromycin, actinomycin (125), proline (64), colcemid (29) among others.

Through the toxicity studies, researchers found that CHO cell mutants were easily isolated using auxotrophic selection such as glycine, hypoxanthine, inositol, and proline (106). Using the auxotrophic mutants, Puck *et al.* fused parental CHO-K1 cells with human fibroblasts and lymphocytes using an ultraviolet-inactivated Sendai virus (62). Through this fusion, only binucleated cells predominated. Cells were then plated down into selection medium (either lacking glycine or hypoxanthine) and 1-2% of the cells survived. Since the reversion rate of the auxotrophic mutants was $5X10^{-8}$, those surviving clones arose from a

fusion between the human and CHO cells (62). The hybrid clones then became stable as the chromosome number decreased to 36 and concomitantly their plating efficiency and their growth rate increased. Through this study, the first hamster-hybrid cells were developed and utilized for genetic mutation studies.

The clones were tested for their possession of a human lethal antigen (A_L) by treating them with antisera to human cells (AHC) (106) which is lethal to human cells but has little or no effect on CHO-K1 cells. Using this method, Puck *et al.* isolated several hybrid clones that were negative for the A_L marker and contained a range of chromosomes from 26 to 45 (106) (where CHO-K1 contains ~20 and human cells have 46 chromosomes) (103). They developed the idea of using a hybrid cell hemizygous for a human chromosome complementing the auxotrophic CHO mutant for a high throughput mutagenic screening system.

Next, Wuthier, Puck and Jones determined that the hybrid clones deficient in the A_L gene were protected from lysis by rabbit antiserum (147). The usage of the antigenic activity in the CHO hybrid clones allowed researchers to determine other possible human genes and forecast the human chromosomes located within the hybrid clones. Since the A_L marker is lysed by rabbit complement, a cell surface protein expressed by the hybrid clones must be involved in an immunological response to foreign bodies. The marker, A_L was not only found on CHO hybrid clones, but also found on human tissues and human cultured cells (61).

Another key discovery was the linkage of the human lactic dehydrogenase gene(LDH-A) to the A_L marker (61). LDH-A is present on human chromosome 11 and therefore the A_L marker must also be linked to that chromosome. Jones *et al.* also found that the A_L marker was found on human red blood cells (RBC), but the A_L antigen did not completely protect the

RBC from lysis. They proposed that RBCs lack a component of the A_L protein present in the CHO-hybrid clones that modulate the lysis by complement. The RBC, it seems, lack either a_1 or a_2, cell surface antigens found only in surviving CHO-human hybrid clones. They suggest that the surface complex protecting the CHO has at least two if not three (a_3) cell surface components protecting the cell from lysis. Moore *et al.* then found that the CHO-human hybrid cells treated with antiserum prepared against glycophorin are killed only if they express a_1 (84).

At that time, researchers narrowed their CHO-hybrid usage to one clone resulting from a fusion of a glycine-deficient mutant and a human fibroblast from amniotic fluid (61). This particular clone had 20 CHO chromosomes and a human chromosome 11. Spontaneous loss of the A_L marker occurs rarely at a rate of $1X10^4$ and therefore only a qualitative description of mutagenesis could occur (61).

Further characterization of the a_1 antigen demonstrated that human erythrocytes also express a_1 but not a_2 (60). Later that same year, Kao found that the A_L cell-surface antigen complex localized to the indicated regions of chromosome 11, where a_1 and a_3 were localized to 11p13 $\rightarrow$11pter and a_2 was linked to 11q13$\rightarrow$11qter (63). Results of genetic analysis demonstrate that there are at least four complementation groups involved in the expression of the a_1 antigen and three of these involve the Chinese hamster genome (59). Through biochemical analysis, Jones *et al.* found that the cell surface antigen resides in the macroglycolipid which biosynthesis requires participation of several different gene actions (59). The CHO genes required possibly reflect the need for additional information for glycosylation on the protein.

Mammalian Mutation Assays

A_L clonogenic mutagenesis assay

After the development of the CHO human-hamster hybrid cell line and the demonstration that marker a_1 was present and sensitive to mutations, Waldren *et al.* developed a mutation assay dependent on the mutagenesis of the CHO A_L cell line (134). Most of the mutations found in humans are chromosomal defects such as aneuploidy and translocations so there was a need to develop a test for chromosomal loss and errors as well as for single gene mutations. Chromosomal errors are often involved in human disease, especially cancer. The single most immediate cause of newly produced genetic disease is chromosomal damage, of which loss of all or a significant portion of a chromosome may be the most important event (134).

The A_L clonogenic mutagenesis assay utilizes the loss of a_1 as a marker for mutagenesis, with markers a_2, a_3, and LDH-A used as a measure of whether the entire marker was lost. Cells were treated with X-radiation, MNNG and caffeine for their ability to cause an increase in a_1 mutants. After treatment, cells were allowed to reach normal growth rates and then plated down into tissue culture flasks. Once cells attached, they were treated with sheep antiserum for the antibodies to a_1 and then rabbit complement. Those cells that kept the a_1 antigen were not protected from lysis and then cell death occurred. Colonies were allowed to be grown up and then the plates were scored for their mutant fraction: number of cells surviving/number of cells plated after being corrected for plating efficiency (134). After demonstrating the applicability of this assay, Waldren and coworkers then studied a variety of different mutagens and measured their mutant yield including but not limited to: ultraviolet radiation (27), cigarette condensate (79), chrysotile fiber (53), heavy ions (71),

human NAD(P)H: quinone oxidoreductase (DT-diaphorase) (44), alpha particles (54), colcemid (70), arsenic (52), heterocyclic amines MeIQ and PhIP (137), Vanillin (3-methoxy-4-hydroxybenzaldehyde) (45), nitrogen ions and protons (68), and others listed in Table 1-1.

The A_L clonogenic mutagenesis assay developed during the 1980s was one of the few mammalian mutation assays competing with the standard Bacterial Reverse Mutation assay, also known as the Ames Test. The Bacterial Ames test is based on several strains of *Salmonella typhimurium* that require histidine for growth (6,4,5,7,120,9,8). When mutagenized cells are grown in histidine-free medium, the resultant bacteria have a reversion to allow growth without histidine. Strains have been developed that have both frameshift and point mutations in the genes required for bacterial growth, allowing researchers to quickly target the category of mutation occurring. There are also other strains developed that focus on the genes responsible for lipopolysaccharide synthesis and the excision repair system to make the test more sensitive. Addition of liver extract such as S9 may also simulate the effects of metabolism which is especially useful if the metabolites are toxic even if the compound is not mutagenic in itself.

Relying on a reverse mutation for the expression of the histidine gene and resultant colony growth, the Ames test focuses on small or point mutations. Unfortunately, this test excludes all other mutations including chromosomal aberrations and deletions, which are at least as important in carcinogenesis and birth defects as are point mutations (134). With the vital differences between prokaryotes and eukaryotes, mutation yield may not reflect the same results. In processing mutations, the membrane permeability, genome organization and the method of DNA repair all differ in bacterial mutations. In addition, about 5-10% of the chemicals chosen at random are false positives in the test (1).

Table 1-1. Mutant yield measured by the Mouse Lymphoma Assay and the A_L clonogenic assay. Table provided by Dr. Michael Fox.

COMPOUND CLASS	COMPOUND	MLA	A_L	Sources Cited
Clastogens	γ radiation	+	+	(134)
	Bleomycin	+	NT	
Heavy metals	Sodium arsenite	+	+	(52,87)
	Lead acetate (LA)	-	+	(49)
Alkylating agents & other direct acting mutagens	Ethyl methanesulfonate (EMS)	+	NT	(50)
	MNNG	+	+	(66)
	n-Nitroso n-ethylurea (ENU)	+	NT	(25)
	UV radiation	+	+	(133,35)
Oxidizing agents	Hydrogen peroxide (H_2O_2)	+	+	(66)
	Paraquat	NT	+	
	Ascorbate	-	-	(130,138,3)
Cross linker	Mitomycin C (MMC)	+	+	(66)
DNA intercalater	Ethidium bromide (EtBr)	-	NT	(96)
Mutagens requiring S9 activation	3- Methyl cholanthrene	+	+	(66)
	Benzo(a)Pyrene (BaP)	+	+	(66)
	Dimethyl benzanthracene	+	NT	(33)
MLA false negatives	Asbestos (chrysotile)	NT	+	(53)
	1,1,1,2-Tetrachloroethane	+/-	NT	(66)
	1,4 – Dioxane	-	NT	(66)
	Diethylstilbestrol	-	NT	(96)
	Colchicine	+	+	(70,56)
	Benzene	+/-	NT	
	Urethane	-	NT	(96)
MLA false positives	1,2-dichlorobenzene	+	NT	(92)
	Chlorpheniramine maleate (CM)	-	NT	(80)
Negative control	Thalidomide	-	-	(12)

The A_L assay, in contrast, is based on a mammalian system where the cells are much more sensitive to cell killing, allowing low levels of mutagens such as x-rays to be detected (133). Chromosome 11, located within the CHO-hybrid cell line, is a large target for mutagenesis as only a very small portion is required for CHO cell survival. In other mammalian mutation tests, if the genetic marker is deleted it may be that the flanking markers are also deleted. This may cause cell killing and therefore larger deletions and nondisjunction processes would not be detected (133). Nondisjunction and deletions are associated with several important human diseases such as Burkitt's lymphoma (151) and so therefore are essential in determining mutagenic potential of chemicals. Waldren *et al.* propose that the A_L clonogenic assay is able to (1) remove distortion of data via cell killing, (2) directly measure mutations at low doses, (3) analyze different types of genetic mutations in relation to human disease, (4) effectively analyzes a range of mutagens with convenient, and accurate experimental procedures (133). Analyzing mutations from low dose x-ray radiation, the mutagenesis rate was more than 200 times greater than reported by studies using conventional measurements with mammalian cells. After treating the cells with various mutagens including x-ray, UV, MNNG, ethyl methyl sulfonate, Benzo(a)Pyrene (BaP), Waldren *et al.* were able to determine the complexity of the mutants by the presence or absence of a_1, a_2, and a_3 and LDH-A. Researchers challenged the sensitivity of the A_L assay stating that the loss of repair mechanisms may cause the difference, but cells were also analyzed at the HGPRT locus and yield the same low values of mutagenesis. This confirmed that the A_L assay did exhibit standard mutagenesis and repair (133). Bridging the gap between human disease and various doses of mutagenic agents and combinations of agents may explain the epidemiology of certain mutational responses.

At that time, the a_1, a_2, and a_3 were described as antigens S_1, S_2 and S_3 (53) which were encoded by gene *MIC1* at 11p13. With the advent of PCR, markers such as Wilms' tumor (WT) were utilized to determine the size of the genetic lesions found in the A_L clonogenic assay (Table 1-2).

In 1999, a major discovery determined that the antigen S1, or a_1, were encoded by the *MIC1* gene and was characterized as the epitope of human CD59. With the advent of monoclonal antibody techniques, researchers were able to specifically identify the cell surface antigens. Wilson *et al.* (145) developed a monoclonal antibody E7 which was a mouse IgM produced by inoculation with a human squamous cell carcinoma. The gene for the E7 antigen, similar to *MIC1*, was mapped to 11p13→11pter using complement-mediated lysis of A_L series of subclones. Researchers set out to demonstrate that E7 and *MIC1* were an epitope of CD59, a well-characterized complement regulatory protein (145). The E7.1 IgM reacted with the purified cell membrane CD59 on a Western Blot, giving a band at 20 kDa, characteristic of CD59. Flow cytometric analysis using a CD59 monoclonal antibody demonstrated coincidental expression of S1 and CD59 across several cell lines. Further evidence that CD59 was S1 was confirmed by ELISA, in which E7.1 IgM reacted strongly with CD59 protein. Cross-inhibition assays between E7.1 and CD59 indicated that the E7.1 binding site on CD59 protein was localized close to the epitopes for *MIC1*. In addition, the ability of E7.1 to block complement-mediated cell lysis suggests that E7.1/CD59/*MIC1* are the same in the CHO A_L cell line (145).

Table 1-2. PCR markers utilized to determine the size of the genetic lesion in the A_L clonogenic assay (81).

Marker	Locus	Chromosome Location	Distance from CD59 Mbp
CD59	CD59	11p13	0
WT	Wilms' tumor	11p13	1.3
P5	P5	11p13	1.5
CAT	Catalase	11p13	2
D16	D11S16	11p13	3
LDHA	Lactate dehydrogenase-A	11p14-15	11
HBE	Hemoglobin	11p15	46
RAS	H-ras	11p15.5	60
ACP2	Acid phosphatase-2	11p11	60
FTH	Ferritin	11q13	48
APOA1	Apolipoprotein A1	11q23	103

Standard Mammalian Mutation Assays

A mammalian mutation assay was developed in the 1970's by Thacker *et al.* (124,123) to estimate the possible mutation rate in humans. Chinese Hamster Ovary cell line V79 are deficient in the hypoxanthine-guanine phosphoribosyltransferase (HPRT) and when treated with 6-thioguanine, cells mutated in the *hprt* gene survive to give the mutant frequency of a particular chemical. The *hprt* locus is located on the X-chromosome and it cannot detect large scale mutations such as mitotic recombination, very large deletions and aneuploidy (75). It is also sensitive to cell death because flanking regions surrounding the *hprt* gene are required for cell survival. This mutation assay has been historically used, but since the FDA prefers the Mouse Lymphoma Assay (MLA), CHO/HPRT assay popularity has declined.

The MLA L5178Y/TK$^{+/-}$ (2) assay system is the most prevalent *in vitro* mammalian mutation assay system. The use of the toxic nucleoside analog trifluorothymidine (TFT) forms the basis for cell selection following treatment. Cells without a mutation in the *tk* gene are poisoned by TFT, while mutant cells survive and form colonies. Those cells that are able to form colonies are assumed to be mutant cells resulting from either spontaneous DNA damage or from mutagen-related damage. Specifically, this assay determines whether mutations or chromosome deletions have occurred involving the *tk* locus of L5178Y *tk*+/- lymphoma cells. L5178Y cells have one functional copy of the gene that codes for thymidine kinase (TK), which has enzyme activity that is critical for DNA synthesis (26). After treatment, colonies that form in the presence of TFT are sized . Small colonies are thought to reflect clastogenic (chromosomal) damage, while large colonies are considered to be the result of mutational events involving the *tk* locus (34,86). Positive and negative controls are incorporated into each test. Metabolic activation using rat liver S9 is included to mimic the

in vivo activity of the liver enzymes in activating some pro-mutagens to mutagens. The MLA assay is more effective in detecting compounds that are clastogenic (86) and several other chromosomal events that are not determined by Ames or CHO/HGPRT mutation assay. It also has been demonstrated, though, that it only detects chromosomal aberrations that are compatible with cell survival and according to the NIEHS assay of 114 chemicals and 4 *in vitro* assays, the MLA *in vitro* mutation assay demonstrated a relatively high level of false positive results (122).

Figure 1-1 describes the mammalian mutation rate for gamma radiation in the *hprt*, MLA, and A_L clonogenic mutation assay. As is evident in the figure, the A_L mutation assay is much more sensitive than the others (over 200 fold). The *hprt* gave the lowest mutant yield due to the location of the gene on the X chromosome and the flanking genes required for cell survival (40). The MLA assay sensitivity was lower than the A_L clonogenic assay due to the same issue as for *hprt*, that the genes near the *tk* locus may be mutated, causing cell death to occur from mutations. The *CHO AL* assay, on the other hand, is extremely sensitive because the genes on chromosome 11 are not required for cell survival so large deletions therefore will not cause lethality. Using the A_L clonogenic assay allows researchers, pharmaceuticals, and the Food and Drug Administration (FDA) to determine the mutagenic potential of chemicals at a lower dosage than currently measured.

Molecular Biology of CD59 Expression

CD59

The CD59 cell surface antigen is an 18-20 kDa complement regulatory protein that stops the plasma membrane insertion and polymerization of a complement component

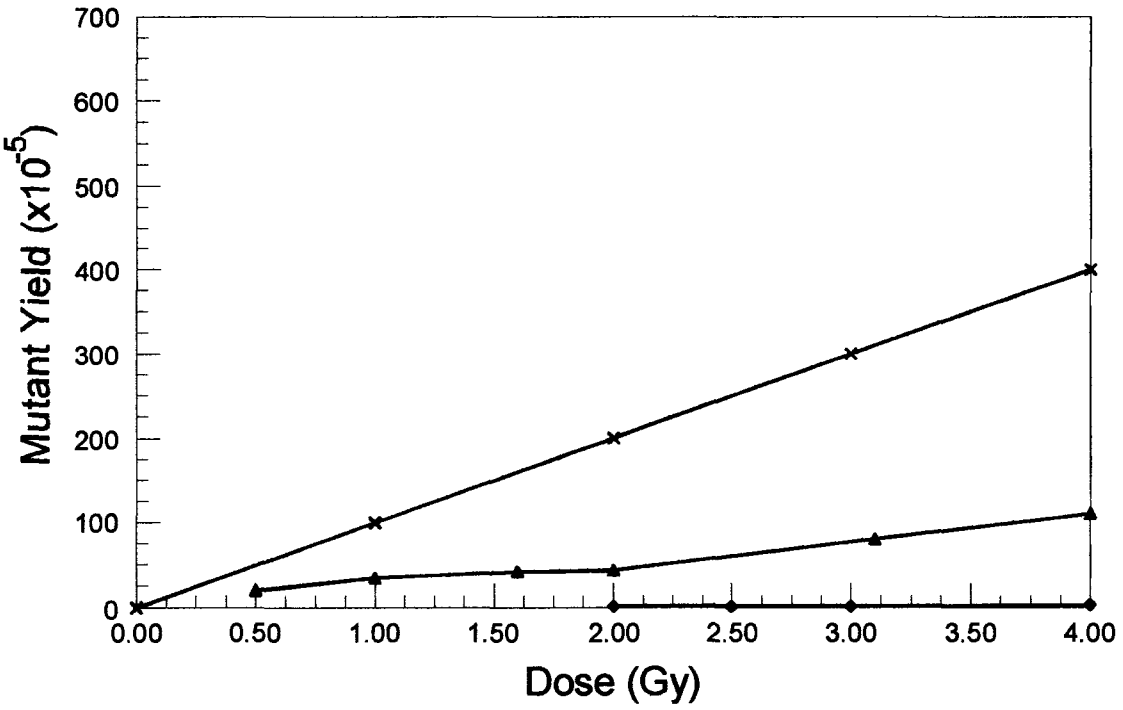

Figure 1-1. Dose response curve for gamma radiation with various mutation assays. Results are normalized to 0 at 0 Gy; (x) Clonogenic A_L assay, data taken from Waldren 1998 (135); (▲) MLA assay, data taken from Moore 1985 (85); (♦) HPRT assay, data taken from Thacker 1977 (124).

C9 (109,108). CD59, since it protects the cell from lysis, is known as "protectin". It is colocalized to chromosome 11 at 11p13.5 (15) determined by chromosomal *in situ* suppression hybridization and pulsed-field gel electrophoresis (50). Similar to the CD55 cell surface antigen, CD59 is cleaved by the bacterial phosphatidyl inositol phospholipase C (PI-PLC) indicating that the CD59 protein is linked via a glycosylphosphatidyl inositol (GPI) anchor in the plasma membrane (74). A rare human disease, paroxysmal nocturnal haemoglobinuria (PNH), may be described as a loss of GPI-anchoring proteins such as CD59. This antigen is found in ductal epithelia of pancreatic, biliary, and salivary systems, bronchi, and kidney collecting ducts (83). The mature protein consists of 103 amino acids arranged in a single cysteine-rich domain composed of two antiparallel β-sheets, 5 protruding surface loops and a short helix (149) (Figure 1-2). The structure is characterized by a hydrophobic signal sequence of 25 amino acid residues, a cysteine-rich sequence with at least two potential N-glycosylation sites, and a hydrophobic carboxyl terminus characteristic of proteins that post-translationally attach the glycosylphosphatidylinositol anchor (100). The structure of the CD59 gene contains 4 exons: exon 2 is the leader sequence, exon 3 is the amino terminus of the mature protein, and exon 4 contains the hydrophobic region near the site of the GPI-anchor addition (100) (see Figure 1-3).

CD59 belongs to the Ly6 superfamily of proteins which includes functional CD59 analogues from other species, snake venom neurotoxins, urokinase-type plasminogen activator receptor and murine Ly6 differentiation antigens (150). As shown in Figure 1-4, the active site of CD59 is located on the front (facing away from membrane) face of the molecule and involves residues located along a hydrophobic groove defined by evolutionarily conserved residues (149).

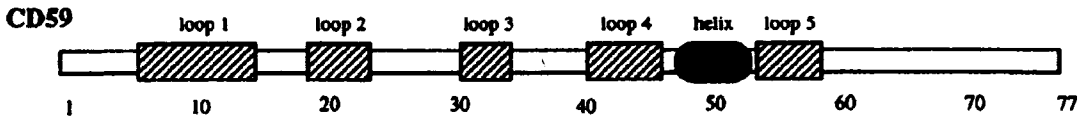

Figure 1-2 The secondary structure of CD59 found in humans (149).

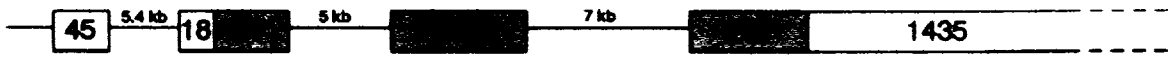

CD59

Figure 1-3 The structure of the gene CD59. The number of nucleotide base pairs in each exon is given; the translated exons and portions of exons are shaded (100).

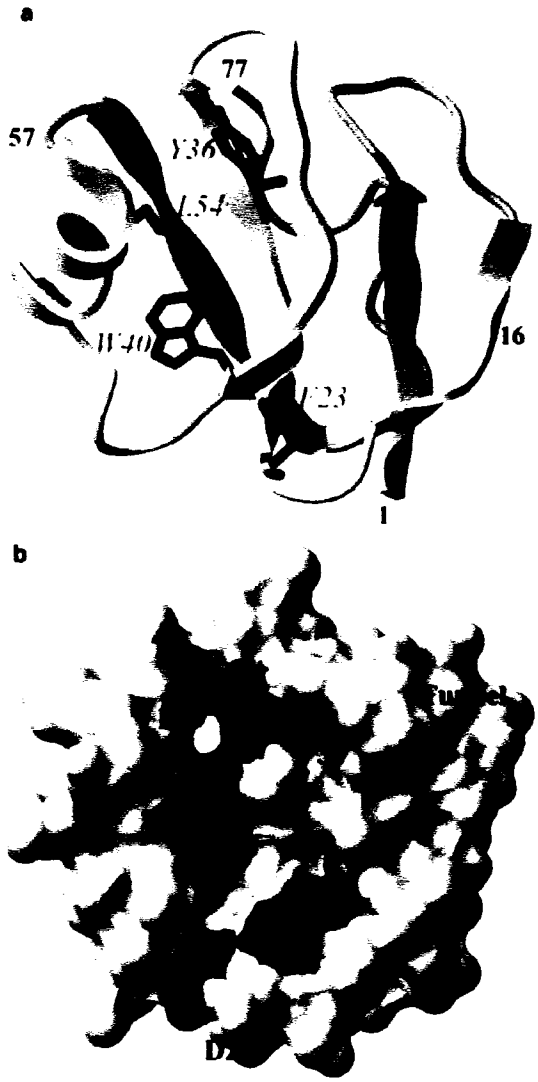

Figure 1-4. Tertiary structure of CD59 in humans with the active site defined by residues in green, blue and yellow (149).

GPI anchor

An essential element of CD59 is the attachment to the plasma membrane via a GPI-anchor. The GPI anchor was first discovered in 1963 as a protein-lipid anchor that was lysed by a crude extract of PI-PLC (116). Later, researchers analyzed the variant surface glycoprotein (sVSG) of trypanosomes and determined that the lipid-anchor was synthesized in the endoplasmic reticulum (ER) (13). In 1985, the structural analysis of the sVSG determined that a glycolipid attached the VSG to the plasma membrane and described this anchor as the glycosylphosphatidylinositol (37). There are several classes of GPI-proteins including cell surface hydrolases, adhesion molecules, protozoal and mammalian antigens as well as other such as the scrapie prion protein, folate receptor and decay accelerating factor (39). Figure 1-4 shows the essential components of the GPI anchor including the core structure of ethanolamine phosphate, trimannoside, glucosamine and inositol phospholipid , including cleavage sites for PI-PLC. Without exception, GPI anchors are covalently linked to carboxyl-terminals of proteins (58). The glycosylation, however, on each GPI anchor is not homogenous, but a mixture of microheterogeneity in the number of galactose molecules (112,111). CD59 is not the only heterogeneous GPI-anchor as it is also found in organisms such as *T. brucei*(37)and 5'-nucleotidase of bovine liver (121).

The biosynthesis of the GPI anchors has been well-studied, not only in *T. brucei*, but also in mammalian cells and the core structure is evolutionarily conserved over many different species. The first step in GPI synthesis (the transfer of GlcNAc to PI) requires at least four physically associated protein components (141) including PIG-A, PIG-C, PIG-H and hGPI-1 (see Figure 1-5). Similarly, the last step (the transfer of the intact GPI precursor to protein) requires at least two protein components The full extent to which the components of the GPI pathway exist in multi-protein complexes remains to be determined; however, not all the

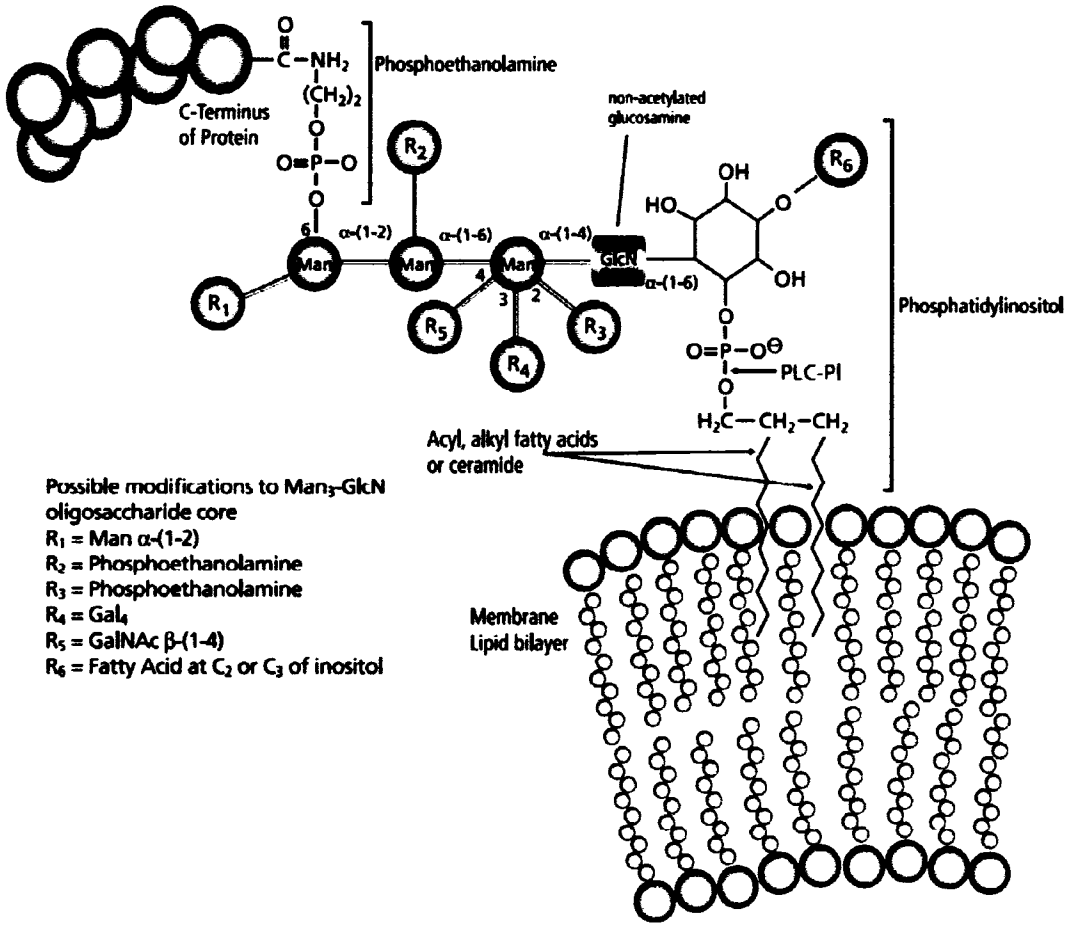

Figure 1-4. Schematic drawing of a glycosylphosphatidyl inositol anchor provided by Sigma Aldrich.

components are associated (93). Through the stepwise procedure in the ER lumen, the GPI anchor is synthesized and at the last step is added to the C-terminus of the protein.

After the GPI anchor moiety is added, the protein, CD59 in our case, is then trafficked to the cell membrane and is then localized to the lipid raft region of the cell membrane. The determining factor that the GPI anchor was lipid raft associated was the resistance of the protein to cold detergent treatment (95). The lipid raft (or lipid-dependent membrane microdomains) localization also indicates that the GPI anchor travels into the *trans*-Golgi network and there forms into glycosphingolipid- and GPI protein-containing rafts (18,19,20). The lipid raft complexes are then trafficked to the plasma membrane according to Nichols *et al.*(95), but even this conclusion has met with some uncertainty. It is known however, that there is a lipid raft clustering in the plasma membrane as seen in the diagram in Figure 1-6. Packaging and presentation of the GPI-linked protein is essential in understanding the overall control of the CD59 protein kinetics. There is no general consensus explaining how the CD59 and GPI-associated proteins (GPI-APs) are endocytosed (113). Given their uniform, diffuse distribution at the cell surface, CD59 may be internalized by multiple routes of endocytosis. CD59 may be endocytosed using dynamin and clathrin-independent means (73). Another possibility is that proteins are associated with detergent resistant membranes (DRMs) may be endocytosed via a clathrin-independent RhoA-regulated pathway followed by DRM- associated interleukin receptors, IL2-R (72). Finally, Nichols *et al.* (95) suggest that CD59 is endocytosed directly to the Golgi bodies and is then recycled between the plasma membrane and the Golgi bodies at a rate of 8 min per cycle with a return rate to the plasma membrane of under 1 min (95). They also demonstrated that the CD59 protein is not

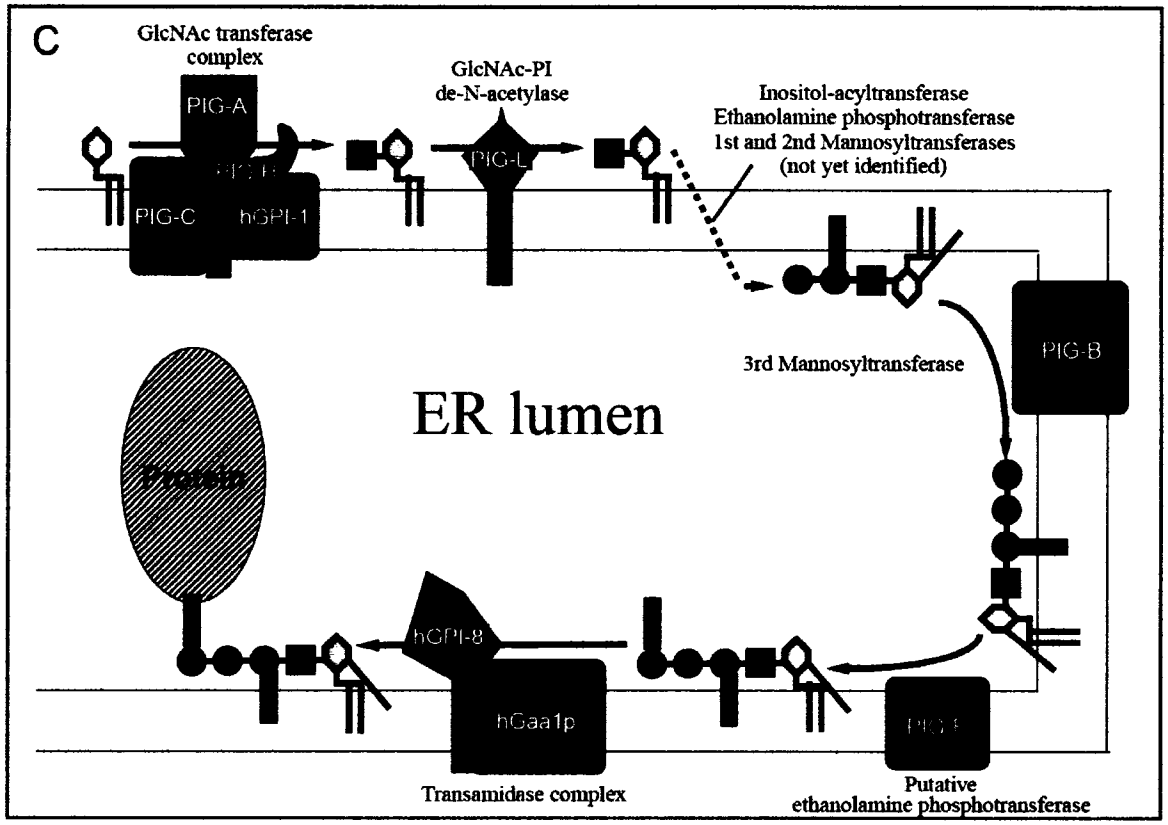

Figure 1-5. GPI mammalian biosynthesis diagram developed by M.A. Ferguson 1999 (36).

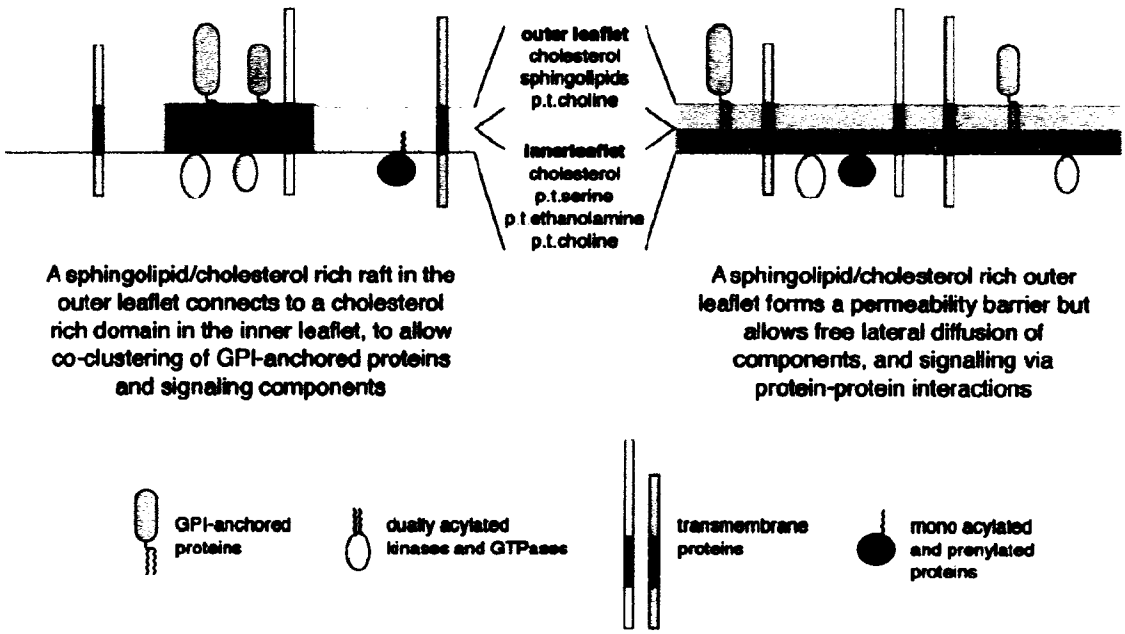

Figure 1-6. Lipid raft localization of GPI anchors in the plasma membrane (91).

newly synthesized, but instead is taken from an already transcribed pool of CD59 proteins within the Golgi Bodies.

Mutagenesis

The detailed characteristics of CD59 and the GPI anchor attachment help clarify the numerous components that may be challenged with mutagenesis. How the cells react to gamma radiation and other genotoxic agents is a key component to this project. In the proceeding sections, I discuss mutations, the methods of mutagenesis by radiation and route for DNA repair.

Mutation

Mutation is defined as a heritable change in genetic material and in multicellular organisms may be divided into two categories: germline mutations (mutations can be passed on to descendents) and somatic mutations. Mutations, when accidental, often lead to the malfunction or death of the cell. Mutations in the DNA sequence are classified into several different categories depending upon the effect of the mutation on the structure, function, expression or outward phenotype of the gene.

Structural mutations are generally on a small scale such as point mutations, insertions and deletions. Point mutations are often caused by a chemical mutagen or malfunction of the DNA and include an exchange of a single nucleotide for another. The most common exchange is a purine for a purine (i.e. A to G) or a pyrimidine for a pyrimidine (C to T) caused by nitrous acid, base mispairing or a mutagenic base analog such as 5-bromo-2-deoxyuridine (BrdU) (2). Transversion (purine for a pyrimidine) is much less common and may be reversed by another point mutation to either its original state (true reversion) or by a second-site reversion where the gene gains functionality from a mutation elsewhere.

Point mutations may be divided into three distinct classes: silent mutations (code for the same amino acid), missense mutations (code for a different amino acid) and nonsense mutations (which code for a stop codon and may truncate the protein) (30). Insertions add one or more extra nucleotides and are usually caused by transposable elements or errors during the replication of repeating elements (i.e. AT repeats) (4). Insertion in the coding region of the DNA could alter the splicing of the mRNA coding region or shift the reading frame (frameshift) which could dramatically change the final gene product (118). The mutation may be resolved by an excision from a transposable element such as a "jumping gene" (38). Deletions remove a section of the DNA causing a shift in the reading frame of the gene and are irreversible.

The DNA structure may also be altered by large-scale mutations in the chromosomal structure such as amplifications, deletions, loss of heterozygosity or gene fusion (105). Amplification of chromosomal regions leads to multiple copies of the genes causing a change in the dosage of the gene product available in the cell. Deletions of large chromosomal regions may cause a loss of the gene within those regions. The loss of heterozygosity occurs when there is a loss of one allele either by a deletion or recombination event when the organism originally had two copies. Finally, the genes may be mutated by juxtaposing two separate pieces of DNA to possibly form distinct fusion genes as in the Philadelphia chromosome (where chromosomes 9 and 22 are fused to make the *bcr-abl* gene) (132). Genes may be fused by chromosomal translocations where there is an interchange of genetic parts from nonhomologous chromosomes. There may also be interstitial deletions which remove regions of DNA from a single chromosome apposing previously distant genes (128).

Finally, DNA may also be mutated by chromosomal inversions which reverse the orientation of the chromosomal segment.

Mutations may also be classified by the effect on the gene function. Cells may have a loss-of-function mutation evident by the loss or reduction of the gene product. When the allele has a complete loss of function (null allele) it is often called an amorphic mutation and this type of mutation is most commonly recessive. There may also be a gain-of-function mutation, generally found as a dominant phenotype, which changes the gene product so that there is a new or abnormal function (47). Dominant negative mutations (also termed antimorphic mutations) have an altered gene product that acts antagonistically to the wild-type allele causing an altered molecular function. Lethal mutations, in contrast, are mutations that completely shut down the gene product ceasing effective reproduction (107).

Gene expression classifies another type of mutation. If the cells have a reduced function of the gene product, it is termed hypomorphic mutation. An increase of function describes a hypermorphic mutation. Neomorphic mutations are delineated by a novel molecular function or expression of gene product (107).

Finally, mutations may also be classified by the phenotype that is affected. Morphological mutations usually effect the outward appearance of an individual, for example, corn plants may be taller or mouse coats may be a different color. Biochemical mutations, on the other hand, result in a change in an enzymatic pathway generally causing changes in the morphological phenotypes (107).

There also is a possibility of spontaneous mutations arising within the cell. In the natural processes of cells, chromosome replication is 99.999% accurate (114). Errors in the actual duplication process happen only about once in 100,000 bases. Since the human genome has

about 6 billion bases, this means that each replication cycle will have about 60,000 errors associated with it (114). The difficulty is determining if the mutation is newly arisen from a mutagen or spontaneous.

DNA repair

Cells utilize several different methods of repairing DNA within the cell, depending on the four types of damage inflicted. First, the bases in DNA (A,T,C, and G) can be covalently modified at various positions, for example, a cytosine being converted to a uracil. There may also be a mismatch of the normal bases because of a proofreading failure during DNA replication. Cross linkage between bases on the same DNA strand ("intrastrand") or on the opposite strand ("interstrand") may also cause mutations. In radiation, the primary type of DNA mutation is a physical break in the DNA helix causing both single strand breaks (SSB) and double strand breaks (DSB).

Sources of DNA damage

DNA damage may be divided into two main types: exogenous and endogenous. Exogenous damage may occur from external agents such as ultraviolet or other radiation, hydrolysis or thermal disruption, plant toxins, human-made mutagenic chemicals and cancer chemotherapy and radiotherapy among others (77). The endogenous damage is created from reactive oxygen radicals produced from normal metabolic byproducts (spontaneous mutation). There are four main classes: oxidation, alkylation, hydrolysis and mismatch of bases attacking the primary structure of the DNA (127).

DNA repair systems

DNA repair systems are divided into three distinct classes of function: damage reversal, removal and tolerance (77). Damage reversal includes an enzymatic action to restore normal structure without breaking the helix and includes such actions as photoreactivation and

ligation of SSB. The cells may also remove the mutation by base excision repair (BER), nucleotide excision repair (NER) and mismatch repair (MMR). If neither of these mechanisms work, then the cells may repair the DNA damage by homologous recombination or non-homologous end-joining (NHEJ) for DSBs (142,139).

Repairing Damaged Bases

Damaged or inappropriate bases can be repaired by direct chemical reversal or by excision repair. Direct chemical reversal repair mechanisms focus on the point mutations arising in human cells triggered by methylation of a cytosine causing deamination to a thymidine. Most of these changes are repaired by enzymes called glycosylases that remove the mismatched T to restore the correct C. This process does not require DNA helix breakage, but is not highly efficient (142).

Cells utilize either BER or NER to remove the damaged base. In BER, the incorrect base is released from the DNA helix and then repaired by DNA glycosylases and AP endonucleases (77). The DNA glycosylase is used to break the glycosidic bond to create an AP site (apurinic or apyrimidinic site). The AP endonuclease recognizes this site and nicks the damaged DNA on the 5' side of the AP site creating a free 3'-OH. DNA polymerase, Pol I, extends the DNA from the free 3'-OH using its exonuclease activity to replate the nucleotide of the damaged base as well as a few bases downstream, followed by sealing of the new DNA strand by DNA ligase (142).

NER enzymes, in contrast, recognize bulky distortions in the shape of the DNA double helix. Recognition of these distortions leads to the removal of a short single-stranded DNA segment that includes the lesion, creating a single-strand gap in the DNA, which is subsequently filled in by a DNA polymerase that uses the undamaged strand as a template.

NER can be divided into two subpathways (global genomic NER and transcription coupled NER) that differ only in their recognition of helix-distorting DNA damage (42).

MMR

DNA damaging agents such as MNNG cause a mismatch in the DNA during replication and are generally corrected by the mismatch repair system (MMR) (42). The cells replace the mismatched bases in newly synthesized daughter strands by first cleaving off the damage and then inserting the correct nucleotides. The MMR system recruits Mut proteins to detect and fix the mismatch. MutS recognizes the mismatched base on the daughter strand and binds the mutated DNA. It is then joined by MutL, which binds the MutS-DNA complex. MutL activates the endonuclease MutH, which incises the daughter strand near the mismatch with the help of the helicase UvrD. An exonuclease then digests the nicked strand, moving in the direction of the mismatch, and ending past the mismatch site. Which exonuclease is used is dependent on which side of the mismatch MutH incises the strand - 5' or 3'. If the nick is on the 5' end of the mismatch, either RecI or exonuclease VIII, both 5' to 3' exonucleases, are used; if however, MutH nicks on the 3' end of the mismatch, the 3' to 5' exonuclease I is used. These exonucleases create a single-stranded gap that can be repaired by DNA Polymerase III, which uses the other strand as a template, and sealed by DNA ligase (43).

Double-Strand Breaks

Breaking the DNA helix across both DNA strands may be potentially fatal if not repaired. The cells resolve DSB by two methods: homologous recombination (HR) and NHEJ (139). Homologous recombination requires the presence of an identical or nearly identical sequence to be used as a template for repair of the break. The enzymatic machinery responsible for this repair process is nearly identical to the machinery responsible for chromosomal

crossover in germ cells during meiosis. The recombinational repair mechanism is predominantly used during the phases of the cell cycle when the DNA is replicating or has completed replicating its DNA. This allows a damaged chromosome to be repaired using the newly created sister chromatid as a template, i.e. an identical copy that is paired to the damaged region. Many genes in the human genome are present in multiple copies providing many possible sources of identical sequences. But recombinational repair that relies on these copies as templates for each other is problematic because it leads to chromosomal translocations and other types of chromosomal rearrangements (127).

Three steps have been suggested for the repair of DSBs *via* NHEJ: (i) end-binding and bridging, (ii) terminal processing, and (iii) ligation. In the initial step Ku binds the DNA ends (the end-binding activity of Ku suggests that it may be the primary damage detector in NHEJ), aligns them and thus prepares for ligation and protects from degradation (98,99).

Origins of radiation

The discovery of gamma radiation was attributed to French physicist Henri Becquerel in 1896 (46). He discovered that uranium minerals could expose a photographic plate through a heavy opaque paper. Roentgen had recently discovered x-rays, and Becquerel reasoned that uranium emitted some invisible light similar to x-rays. He called it "metallic phosphorescence." In reality, Becquerel had found gamma radiation being emitted by ^{226}Ra .

Throughout this project, gamma radiation from ^{137}Cs has been the primary mode of mutagenesis. The irradiator generates gamma photons, which are the most energetic photons in the electromagnetic spectrum and are emitted from the nuclei of some unstable radioactive atoms. Specifically, ^{137}Cs emits gamma rays by radioactive decay caused by a neutron transforming into a proton and a beta particle. ^{137}Cs decays to ^{137}Ba and the nucleus ejects

the beta particle (1.176 MeV).. However, the nucleus still has too much energy and ejects a gamma photon (0.662 MeV) to become more stable. Gamma rays are able to penetrate various materials including human tissues and can readily damage DNA (46).

Radiation damage to cells

The DNA strand is composed of nucleotides being held together by a phosphodiester (P-E) bond. When DNA is exposed to gamma radiation, the ionization may destroy the P-E bond causing single-strand breaks (SSB). Significant damage to a DNA molecule occurs when the SSBs in opposite strands occur near to each other causing a double strand break (DSB) or DSBs may results from a single cluster of damage. This takes place very quickly, in much less than a second. It takes much longer for the biological effects to become apparent. If the damage is sufficient to kill the cell, the effect may become noticeable in hours or days. Cell "death" can be of two types. First, the cell may no longer perform its function due to internal ionization; this requires a dose to the cell of about 100 Gy (10,000 rad). Second, "reproductive death" (mitotic inhibition) may occur when a cell can no longer reproduce, but still performs its other functions. This requires a dose of 2 Gy (200 rad), which will cause reproductive death in half the cells irradiated (hence such a quantity is called a "mean lethal dose.") (47). Treatment of gamma radiation to cells induces different types of DNA damage including double strand breaks, single strand breaks, and base modifications. These forms of damage, in turn, cause a variety of mutational events including base-pair substitutions, frame shifts, and deletions to the cell (140).

Radiation Induced Damage Measured by the A_L Clonogenic Assay

Extensive research has been done using the A_L clonogenic assay and Cesium^{137} gamma radiation. Parker *et al.* first demonstrated the inducible mutant fraction (97) for radiation for

doses of 0-6 Gy. Comparing the data between studies, the mutant yield induced by 3 Gy varied between 180-289 per 10^5 cells. The mutant fraction induced by gamma radiation seem to increase in a curvilinear response with dose and the CHO A_L assay has a much higher sensitivity than the *hprt* assay (Figure 1-7).

In several experiments, researchers also analyzed the *hprt* locus to allow for mutant yield comparison between the CHO-HPRT and A_L clonogenic assay. The *hprt* results were 100-fold less than the A_L clonogenic assay (Table 1-3).

The type of mutations caused by gamma radiation in the A_L clonogenic assay were also quantified. The mutant spectra for cloned populations were determined by using several PCR markers discussed previously. Simple mutations were defined as missing only CD59 and complex contiguous mutations indicated large multilocus deletions (81) (Table 1-4) . Later, Waldren (135) and Kraemer (70) decided that both the CD59 and multilocus deletions should be designated "simple". The overriding conclusion from this data is that gamma radiation causes mostly simple large deletions with very few complex mutations. It is well-known that radiation is a clastogen (14) and that is reflected in the mutant spectra.

In 2001, Kraemer *et al.* (70) analyzed the karyotypes of several $CD59^-$ mutant clones for their simple and complex mutations. As seen in Figure 1-8, karyotypes were separated by the chromosomal aberrations found. Spontaneous mutants found at 0 Gy had a myriad of chromosomal mutations including translocation of a CHO chromosome onto human chromosome 11. Induced mutant clones were increasingly complex as 43% could be described as "complicated". Those cells that contained just human chromosome 11 were a more stable population resisting mutant spectra change over time. On the other hand,

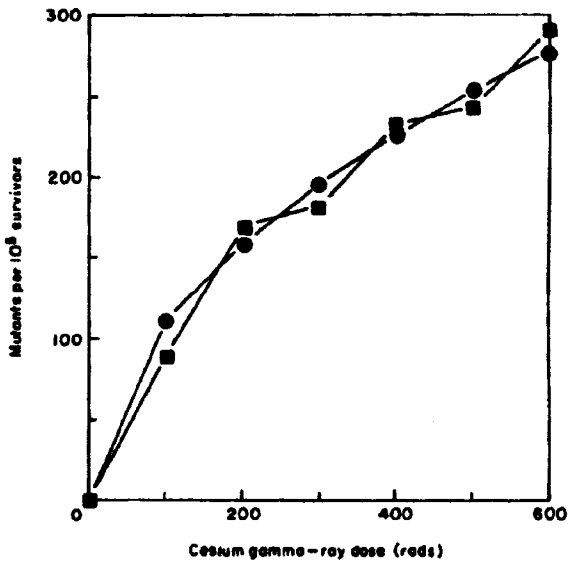

Figure 1-7. Gamma radiation results for A_L clonogenic assay by Parker 1988 et al , ■ = CD59 measured mutants, ● = curve fitted (97).

Study	Dose (Gy)	AL clonogenic Assay	*hprt* assay
Parker 1988	0	0	
	1	90	
	2	150	
	3	180	
	4	225	
	5	245	
	6	280	
McGuinness 1995	0	158±42	
	0.5	181±65	
	1.5	229±73	
	3	289±95	
Ueno 1996	0	136±35	1.3±0.8
	0.04	146±37	1.6±0.1
	3	350±30	3.5±1.0
	3.04	256±57	2.4±0.7
Kraemer 2001	0	9	
50±4 per Gy	1	50	
	2	100	
	3	150	
	4	200	
Waldren 1998	0	90±25	5±4
	1	100	2
	2	200	4
	3	300	6
	4	400	8
Zhou 2006	0	56±18	
	1	125±33	
	3	211±47	
	5	334±76	

Table 1-3 Mutant yield for AL clonogenic and *hprt* assay induced by gamma radiation (97,81,131,45,69,154).

Table 1-4. Mutation spectra defined for A_L clonogenic assay using gamma radiation.

Study	Dose (Gy)	Mutants analyzed	CD59- only		Contiguous and Complex		Complex	
			Number	Percentage	Number	Percentage	Number	Percentage
McGuinness 1995	0	60	16	27%	44	73%	16	27%
	3	63	11	17%	52	83%	1	2%
Ueno 1996	3	75	12	16%	61	81%	2	4%

	Dose (Gy)	Mutants analyzed	Simple		Complex	
			Number	Percentage	Number	Percentage
Waldren1998	0	94	68	72%	26	28%
	3	94	91	97%	3	3%
Kramer 2001	0	153	106	69%	47	31%
	3	73	71	97%	2	3%

complex and complicated mutations seemed to evolve into subpopulations with varying genotypes over time.

In all cases, the A_L clonogenic assay effectively measured the mutation yield and helped elucidate the mechanisms of chromosomal aberrations caused by gamma radiation. It has become evident, though, that direct mutagenesis is not the only mechanism causing cell damage.

Role of reactive oxygen species and the bystander effect

Not only is there direct damage from radiation, but recent research also demonstrates that secondary toxic effects from reactive oxygen species causes a bystander effect. The bystander effect can be defined as the detection of responses in unirradiated cells that can reasonably be assumed to have occurred as a result of exposure of other cells to radiation (90,89). One demonstration of a bystander effect occurs when cells are irradiated and the medium from the irradiated cells is transferred into a unirradiated tissue culture flasks and those cells demonstrate toxic effects from the medium alone. Mothersill *et al.* (90) determine there are several mechanisms and controls to the secondary toxic effect dependent on the cell system. At times proteins or reactive oxygen species are transferred via gap junctions and in other systems the trigger is varied. The ending result, in addition, may include apoptosis (88), induction of genomic instability or delayed death (78), induction of enhanced cell growth (146), or induction of mutations (117).

Zhou *et al.* (153) showed that when only 20% of the cells were irradiated with a lethal dose of alpha particles, the resultant mutant fraction using the A_L clonogenic assay was 3-fold higher than expected, assuming no interaction between the irradiated and non-irradiated

Mutant Type	0 Gy	4 Gy
	3/9 (33%)	7/14 (50%)
	2/9 (22%)	0/14
	1/9 (11%)	0/14
	0/9	1/14 (7%)
Complicated	3/9 (33%)	6/14 (43%)

Figure 1-8. Cartoon of FISH analysis of CD59- mutant clones designated as containing simple or complicated mutations. Human chromosome 11 is shown in yellow; CHO chromosomes in red. Mutants with the "simple mutations" tend to remain clonal over time in culture in relation to the state of human chromosome 11, whereas "complicated" mutants evolve into several subpopulations. In simple mutants, on the other hand, the state of human chromosome 11 found at day 15 was essentially unchanged after an additional 42 days in culture (69).

cells. This demonstrated that irradiated A_L cells clearly induced a bystander mutagenic response in neighboring cells not directly traversed by alpha particles(153). Zhou *et al.*(152) showed that when a single alpha particle traversed a small fraction of A_L cells (10–20%), it induced a mutagenic response similar to that occurring when 100% of the cells in the population were hit.

Conclusion

In this introduction, I have explained how the *CHO AL* clonogenic assay was developed and how CD59 was discovered and utilized as the primary marker. Describing the effects of radiation on mutations gives background information necessary when studying mutagenesis. The challenge in using the CHO A_L clonogenic assay is that it requires a clonal growth period of 7-10 days after treatment, it requires the use of rabbit complement, and the mutant yield is a dichotomous measurement of either present or absent. There is a need for a mammalian mutation assay that can analyze the kinetics of CD59 mutant expression rapidly. We have discovered that utilizing flow cytometry, we are able to accurately, rapidly and efficiently measure mutations at CD59 in the A_L assay. In the following chapters, I describe in detail the flow cytometry mutation assay and how it can be applied to analyzing the kinetics of CD59 mutant expression.

Reference List

1. Aaron CS, Harbach PR, Mattano SS, Mayo JK, Wang Y, Yu RL, Zimmer DM: Risk and benefit evaluation in development of pharmaceutical products. Environ Health Perspect 101 Suppl 3:291-295, 1993.

2. Amacher DE, Paillet S, Ray VA: Point mutations at the thymidine kinase locus in L5178Y mouse lymphoma cells. I. Application to genetic toxicological testing. Mutat Res 64:391-406, 1979.

3. Amacher DE, Paillet SC: Ascorbate is detectably mutagenic in the L5178Y TK+/- cell mutation assay. Cancer Lett 14:151-158, 1981.

4. Ames BN: Carcinogens are mutagens: their detection and classification. Environ Health Perspect 6:115-118, 1973.

5. Ames BN, Ames GF, Young JD, Tsuchiya D, Lecocq J: Illicit transport: the oligopeptide permease. Proc Natl Acad Sci U S A 70:456-458, 1973.

6. Ames BN, Durston WE, Yamasaki E, Lee FD: Carcinogens are mutagens: a simple test system combining liver homogenates for activation and bacteria for detection. Proc Natl Acad Sci U S A 70:2281-2285, 1973.

7. Ames BN, Lee FD, Durston WE: An improved bacterial test system for the detection and classification of mutagens and carcinogens. Proc Natl Acad Sci U S A 70:782-786, 1973.

8. Ames BN, McCann J, Yamasaki E: Methods for detecting carcinogens and mutagens with the Salmonella/mammalian-microsome mutagenicity test. Mutat Res 31:347-364, 1975.

9. Ames BN, McCann J, Yamasaki E: Proceedings: carcinogens are mutagens: a simple test system. Mutat Res 33:27-28, 1975.

10. Amundson SA, Liber HL: A comparison of induced mutation at homologous alleles of the tk locus in human cells. Mutat Res 247:19-27, 1991.

11. Araten DJ, Luzzatto L: The mutation rate in PIG-A is normal in patients with Paroxysmal Nocturnal Hemoglobinuria (PNH). Blood 2006.

12. Ashby J, Tinwell H, Callander RD, Kimber I, Clay P, Galloway SM, Hill RB, Greenwood SK, Gaulden ME, Ferguson MJ, Vogel E, Nivard M, Parry JM, Williamson J: Thalidomide: lack of mutagenic activity across phyla and genetic endpoints. Mutat Res 396:45-64, 1997.

13. Bangs JD, Hereld D, Krakow JL, Hart GW, Englund PT: Rapid processing of the carboxyl terminus of a trypanosome variant surface glycoprotein. Proc Natl Acad Sci U S A 82:3207-3211, 1985.

14. Barbour L, Hanna M, Xiao W: Mutagenesis. Methods Mol Biol 313:121-127, 2006.

15. Bickmore WA, Longbottom D, Oghene K, Fletcher JM, Van H, V: Colocalization of the human CD59 gene to 11p13 with the MIC11 cell surface antigen. Genomics 17:129-135, 1993.

16. Bodian DL, Davis SJ, Morgan BP, Rushmere NK: Mutational analysis of the active site and antibody epitopes of the complement-inhibitory glycoprotein, CD59. J Exp Med 185:507-516, 1997.

17. Brodsky RA, Mukhina GL, Li S, Nelson KL, Chiurazzi PL, Buckley JT, Borowitz MJ: Improved detection and characterization of paroxysmal nocturnal hemoglobinuria using fluorescent aerolysin. Am J Clin Pathol 114:459-466, 2000.

18. Brown D, Waneck GL: Glycosyl-phosphatidylinositol-anchored membrane proteins. J Am Soc Nephrol 3:895-906, 1992.

19. Brown DA: Interactions between GPI-anchored proteins and membrane lipids. Trends Cell Biol 2:338-343, 1992.

20. Brown DA, Rose JK: Sorting of GPI-anchored proteins to glycolipid-enriched membrane subdomains during transport to the apical cell surface. Cell 68:533-544, 1992.

21. Buckley JT: Purification of cloned proaerolysin released by a low protease mutant of Aeromonas salmonicida. Biochem Cell Biol 68:221-224, 1990.

22. Buckley JT: Secretion and mechanism of action of the hole-forming toxin aerolysin. Experientia 47:418-419, 1991.

23. Buckley JT, Howard SP: Aerolysin from Aeromonas hydrophila. Methods Enzymol 165:193-199, 1988.

24. Cai S, Bulus N, Fonseca-Siesser PM, Chen D, Hanks SK, Pozzi A, Zent R: CD98 modulates integrin beta1 function in polarized epithelial cells. J Cell Sci 118:889-899, 2005.

25. Chen T, Harrington-Brock K, Moore MM: Mutant frequency and mutational spectra in the Tk and Hprt genes of N-ethyl-N-nitrosourea-treated mouse lymphoma cellsdagger. Environ Mol Mutagen 39:296-305, 2002.

26. Clive D, Johnson KO, Spector JF, Batson AG, Brown MM: Validation and characterization of the L5178Y/TK+/- mouse lymphoma mutagen assay system. Mutat Res 59:61-108, 1979.

27. Collins A, Waldren C: Cell-cycle kinetics and ultraviolet light survival in UV-1, a Chinese hamster ovary cell mutant defective in post-replication recovery. J Cell Sci 57:261-275, 1982.

28. Costes S, Sachs R, Hlatky L, Vannais D, Waldren C, Fouladi B: Large-mutation spectra induced at hemizygous loci by low-LET radiation: evidence for intrachromosomal proximity effects. Radiat Res 156:545-557, 2001.

29. Cox DM, Puck TT: Chromosomal nondisjunction: the action of colcemid on Chinese hamster cells in vitro. Cytogenetics 8:158-169, 1969.

30. Davies MJ, Phillips BJ, Rumsby PC: Molecular analysis of mutations at the tk locus of L5178Y mouse-lymphoma cells induced by ethyl methanesulphonate and mitomycin C. Mutat Res 290:145-153, 1993.

31. Diaz LA, Jr., Fox DA: A role for CD98 in cellular activation. J Biol Regul Homeost Agents 12:25-32, 1998.

32. Diep DB, Nelson KL, Raja SM, Pleshak EN, Buckley JT: Glycosylphosphatidylinositol anchors of membrane glycoproteins are binding determinants for the channel-forming toxin aerolysin. J Biol Chem 273:2355-2360, 1998.

33. Dobrovolsky VN, Shaddock JG, Heflich RH: 7,12-dimethylbenz[a]anthracene-induced mutation in the Tk gene of Tk(+/-) mice: automated scoring of lymphocyte clones using a fluorescent viability indicator. Environ Mol Mutagen 36:283-291, 2000.

34. el Tarras A, Dubins JS, Warner J, Hoffman C, Cobb RR: Molecular analysis of the TK locus in L5178Y large and small colony mouse lymphoma cell mutants induced by hycanthone methanesulfonate. Mutat Res 332:89-95, 1995.

35. Evans HH, Mencl J, Horng MF, Ricanati M, Sanchez C, Hozier J: Locus specificity in the mutability of L5178Y mouse lymphoma cells: the role of multilocus lesions. Proc Natl Acad Sci U S A 83:4379-4383, 1986.

36. Ferguson MA: The structure, biosynthesis and functions of glycosylphosphatidylinositol anchors, and the contributions of trypanosome research. J Cell Sci 112 (Pt 17):2799-2809, 1999.

37. Ferguson MA, Low MG, Cross GA: Glycosyl-sn-1,2-dimyristylphosphatidylinositol is covalently linked to Trypanosoma brucei variant surface glycoprotein. J Biol Chem 260:14547-14555, 1985.

38. ffrench-Constant R, Daborn P, Feyereisen R: Resistance and the jumping gene. Bioessays 28:6-8, 2006.

39. Fivaz M, Vilbois F, Thurnheer S, Pasquali C, Abrami L, Bickel PE, Parton RG, van der Goot FG: Differential sorting and fate of endocytosed GPI-anchored proteins. EMBO J 21:3989-4000, 2002.

40. Fuscoe JC, Ockey CH, Fox M: Molecular analysis of X-ray-induced mutants at the HPRT locus in V79 Chinese hamster cells. Int J Radiat Biol Relat Stud Phys Chem Med 49:1011-1020, 1986.

41. Geary SM, Cambareri AC, Sincock PM, Fitter S, Ashman LK: Differential tissue expression of epitopes of the tetraspanin CD151 recognised by monoclonal antibodies. Tissue Antigens 58:141-153, 2001.

42. Griffith WLGSM: Introduction to Genetic Analysis. 8th Edition Edition. W.H. Freeman and Company, 2006.

43. Griffiths AJea: Introduction to Genetic Analysis (8th Ed.). 2005.

44. Gustafson DL, Beall HD, Bolton EM, Ross D, Waldren CA: Expression of human NAD(P)H: quinone oxidoreductase (DT-diaphorase) in Chinese hamster ovary cells: effect on the toxicity of antitumor quinones. Mol Pharmacol 50:728-735, 1996.

45. Gustafson DL, Franz HR, Ueno AM, Smith CJ, Doolittle DJ, Waldren CA: Vanillin (3-methoxy-4-hydroxybenzaldehyde) inhibits mutation induced by hydrogen peroxide, N-methyl-N-nitrosoguanidine and mitomycin C but not (137)Cs gamma-radiation at the CD59 locus in human-hamster hybrid A(L) cells. Mutagenesis 15:207-213, 2000.

46. Hall EJ: Radiobiology for the Radiobiologist. 6th ed. Edition. Lippincott Williams & Wilkins, c2006, Philadelphia, 2006.

47. Hall EJ: Radiation for the Radiobiologist. 6th Ed. Edition. 2006.

48. HAM RG, Puck TT: A regulated incubator controlling CO2 concentration, humidity and temperature for use in animal cell culture. Proc Soc Exp Biol Med 111:67-71, 1962.

49. Hartwig A, Schlepegrell R, Beyersmann D: Indirect mechanism of lead-induced genotoxicity in cultured mammalian cells. Mutat Res 241:75-82, 1990.

50. Heckl-Ostreicher B, Ragg S, Drechsler M, Scherthan H, Royer-Pokora B: Localization of the human CD59 gene by fluorescence in situ hybridization and pulsed-field gel electrophoresis. Cytogenet Cell Genet 63:144-146, 1993.

51. Hei TK, Hall EJ, Waldren CA: Mutation induction and relative biological effectiveness of neutrons in mammalian cells. Experimental observations. Radiat Res 115:281-291, 1988.

52. Hei TK, Liu SX, Waldren C: Mutagenicity of arsenic in mammalian cells: role of reactive oxygen species. Proc Natl Acad Sci U S A 95:8103-8107, 1998.

53. Hei TK, Piao CQ, He ZY, Vannais D, Waldren CA: Chrysotile fiber is a strong mutagen in mammalian cells. Cancer Res 52:6305-6309, 1992.

54. Hei TK, Wu LJ, Liu SX, Vannais D, Waldren CA, Randers-Pehrson G: Mutagenic effects of a single and an exact number of alpha particles in mammalian cells. Proc Natl Acad Sci U S A 94:3765-3770, 1997.

55. Hernandez-Campo PM, Almeida J, Sanchez ML, Malvezzi M, Orfao A: Normal patterns of expression of glycosylphosphatidylinositol-anchored proteins on different subsets of peripheral blood cells: a frame of reference for the diagnosis of paroxysmal nocturnal hemoglobinuria. Cytometry B Clin Cytom 70:71-81, 2006.

56. Honma M, Momose M, Sakamoto H, Sofuni T, Hayashi M: Spindle poisons induce allelic loss in mouse lymphoma cells through mitotic non-disjunction. Mutat Res 493:101-114, 2001.

57. Horikawa M, Suzuki F, Ban S: Mammalian cell mutagenesis: comparison of the sensitivity in assay systems of mutations induced by radiations and chemicals [proceedings]. Mutat Res 38:3371976.

58. Ikezawa H: Glycosylphosphatidylinositol (GPI)-anchored proteins. Biol Pharm Bull 25:409-417, 2002.

59. Jones C, Moore EE, Lehman DW: Genetic and biochemical analysis of the a1 cell-surface antigen associated with human chromosome 11. Proc Natl Acad Sci U S A 76:6491-6495, 1979.

60. Jones C, Puck TT: Further studies on hybrid cell-surface antigens associated with human chromosome 11. Somatic Cell Genet 3:407-420, 1977.

61. Jones C, Wuthier P, Puck TT: Genetics of somatic cell surface antigens. III. Further analysis of the AL marker. Somatic Cell Genet 1:235-246, 1975.

62. Kao FT, Johnson RT, Puck TT: Complementation analysis on virus-fused Chinese hamster cells with nutritional markers. Science 164:312-314, 1969.

63. Kao FT, Jones C, Puck TT: Genetics of cell-surface antigens: regional mapping of three components of the human cell-surface antigen complex, AL, on chromosome 11. Somatic Cell Genet 3:421-429, 1977.

64. Kao FT, Puck TT: Genetics of somatic mammalian cells. IV. Properties of Chinese hamster cell mutants with respect to the requirement for proline. Genetics 55:513-524, 1967.

65. Karamatic C, V, Burton N, Kagan A, Green CA, Levene C, Flinter F, Brady RL, Daniels G, Anstee DJ: CD151, the first member of the tetraspanin (TM4) superfamily detected on erythrocytes, is essential for the correct assembly of human basement membranes in kidney and skin. Blood 104:2217-2223, 2004.

66. Kirkland D, Aardema M, Henderson L, Muller L: Evaluation of the ability of a battery of three in vitro genotoxicity tests to discriminate rodent carcinogens and non-carcinogens I. Sensitivity, specificity and relative predictivity. Mutat Res 584:1-256, 2005.

67. Korte W, Heijnen IA: [Paroxysmal nocturnal hemoglobinuria--consequences of a missing anchor]. Ther Umsch 63:71-77, 2006.

68. Kraemer SM, Kronenberg A, Ueno A, Waldren CA: Measuring the spectrum of mutation induced by nitrogen ions and protons in the human-hamster hybrid cell line A(L)C. Radiat Res 153:743-751, 2000.

69. Kraemer SM, Vannais DB, Kronenberg A, Ueno A, Waldren CA: Gamma-ray mutagenesis studies in a new human-hamster hybrid, A(L)CD59(+/-), which has two human chromosomes 11 but is hemizygous for the CD59 gene. Radiat Res 156:10-19, 2001.

70. Kraemer SM, Waldren CA: Chromosomal mutations and chromosome loss measured in a new human-hamster hybrid cell line, ALC: studies with colcemid, ultraviolet irradiation, and 137Cs gamma-rays. Mutat Res 379:151-166, 1997.

71. Kronenberg A, Gauny S, Criddle K, Vannais D, Ueno A, Kraemer S, Waldren CA: Heavy ion mutagenesis: linear energy transfer effects and genetic linkage. Radiat Environ Biophys 34:73-78, 1995.

72. Lamaze C, Dujeancourt A, Baba T, Lo CG, Benmerah A, Dautry-Varsat A: Interleukin 2 receptors and detergent-resistant membrane domains define a clathrin-independent endocytic pathway. Mol Cell 7:661-671, 2001.

73. Lamaze C, Schmid SL: The emergence of clathrin-independent pinocytic pathways. Curr Opin Cell Biol 7:573-580, 1995.

74. Lehto MT, Sharom FJ: PI-specific phospholipase C cleavage of a reconstituted GPI-anchored protein: modulation by the lipid bilayer. Biochemistry 41:1398-1408, 2002.

75. Li AP, Aaron CS, Auletta AE, Dearfield KL, Riddle JC, Slesinski RS, Stankowski LF, Jr.: An evaluation of the roles of mammalian cell mutation assays in the testing of chemical genotoxicity. Regul Toxicol Pharmacol 14:24-40, 1991.

76. Liu SX, Athar M, Lippai I, Waldren C, Hei TK: Induction of oxyradicals by arsenic: implication for mechanism of genotoxicity. Proc Natl Acad Sci U S A 98:1643-1648, 2001.

77. Lodish H BAMPKCKMSMZSDJ: Molecular Biology of the Cell. 5th ed Edition. WH Freeman, New York, NY, 2004.

78. Lorimore SA, Kadhim MA, Pocock DA, Papworth D, Stevens DL, Goodhead DT, Wright EG: Chromosomal instability in the descendants of unirradiated surviving cells after alpha-particle irradiation. Proc Natl Acad Sci U S A 95:5730-5733, 1998.

79. Matsukura N, Willey J, Miyashita M, Taffe B, Hoffmann D, Waldren C, Puck TT, Harris CC: Detection of direct mutagenicity of cigarette smoke condensate in mammalian cells. Carcinogenesis 12:685-689, 1991.

80. McGregor DB, Brown AG, Howgate S, McBride D, Riach C, Caspary WJ: Responses of the L5178Y mouse Lymphoma cell forward mutation assay. V: 27 coded chemicals. Environ Mol Mutagen 17:196-219, 1991.

81. McGuinness SM, Shibuya ML, Ueno AM, Vannais DB, Waldren CA: Mutant quantity and quality in mammalian cells (AL) exposed to cesium-137 gamma radiation: effect of caffeine. Radiat Res 142:247-255, 1995.

82. McGuinness SM, Shibuya ML, Ueno AM, Vannais DB, Waldren CA: Mutant quantity and quality in mammalian cells (AL) exposed to cesium-137 gamma radiation: effect of caffeine. Radiat Res 142:247-255, 1995.

83. Meri S, Waldmann H, Lachmann PJ: Distribution of protectin (CD59), a complement membrane attack inhibitor, in normal human tissues. Lab Invest 65:532-537, 1991.

84. Moore EE, Jones C, Puck TT: Cell surface antigens. IV. Immunological coorespondence between glycophorin and the a1 human cell surface antigen. Cytogenet Cell Genet 17:89-97, 1976.

85. Moore MM, Clive D, Howard BE, Batson AG, Turner NT: In situ analysis of trifluorothymidine-resistant (TFTr) mutants of L5178Y/TK+/- mouse lymphoma cells. Mutat Res 151:147-159, 1985.

86. Moore MM, Doerr CL: Comparison of chromosome aberration frequency and small-colony TK-deficient mutant frequency in L5178Y/TK(+/-)-3.7.2C mouse lymphoma cells. Mutagenesis 5:609-614, 1990.

87. Moore MM, Harrington-Brock K, Doerr CL: Relative genotoxic potency of arsenic and its methylated metabolites. Mutat Res 386:279-290, 1997.

88. Mothersill C, O'Malley K, Murphy D, Seymour CB: Apoptosis and other effects of radiation in normal human urothelial cells. Radiat Oncol Investig 5:150-153, 1997.

89. Mothersill C, Rea D, Wright EG, Lorimore SA, Murphy D, Seymour CB, O'Malley K: Individual variation in the production of a 'bystander signal' following irradiation of primary cultures of normal human urothelium. Carcinogenesis 22:1465-1471, 2001.

90. Mothersill C, Seymour C: Radiation-induced bystander effects: past history and future directions. Radiat Res 155:759-767, 2001.

91. Munro S: Lipid rafts: elusive or illusive? Cell 115:377-388, 2003.

92. Myhr BC, Caspary WJ: Chemical mutagenesis at the thymidine kinase locus in L5178Y mouse lymphoma cells: results for 31 coded compounds in the National Toxicology Program. Environ Mol Mutagen 18:51-83, 1991.

93. Nakamura N, Inoue N, Watanabe R, Takahashi M, Takeda J, Stevens VL, Kinoshita T: Expression cloning of PIG-L, a candidate N-acetylglucosaminyl-phosphatidylinositol deacetylase. J Biol Chem 272:15834-15840, 1997.

94. Nelson KL, Raja SM, Buckley JT: The glycosylphosphatidylinositol-anchored surface glycoprotein Thy-1 is a receptor for the channel-forming toxin aerolysin. J Biol Chem 272:12170-12174, 1997.

95. Nichols BJ, Kenworthy AK, Polishchuk RS, Lodge R, Roberts TH, Hirschberg K, Phair RD, Lippincott-Schwartz J: Rapid cycling of lipid raft markers between the cell surface and Golgi complex. J Cell Biol 153:529-541, 2001.

96. Oberly TJ, Michaelis KC, Rexroat MA, Bewsey BJ, Garriott ML: A comparison of the CHO/HGPRT+ and the L5178Y/TK+/- mutation assays using suspension treatment and soft agar cloning: results for 10 chemicals. Cell Biol Toxicol 9:243-257, 1993.

97. Parker R, Waldren C, Hei TK, Wong DF, Puck TT: Analysis of mutant frequency curves and survival curves applied to the AL hybrid cell system. J Theor Biol 132:113-117, 1988.

98. Pastwa E, Lubner EM, Mezhevaya K, Neumann RD, Winters TA: DNA uptake and repair enzyme access to transfected DNA is under reported by gene expression. Biochem Biophys Res Commun 306:421-429, 2003.

99. Pastwa E, Neumann RD, Mezhevaya K, Winters TA: Repair of radiation-induced DNA double-strand breaks is dependent upon radiation quality and the

structural complexity of double-strand breaks. Radiat Res 159:251-261, 2003.

100. Petranka JG, Fleenor DE, Sykes K, Kaufman RE, Rosse WF: Structure of the CD59-encoding gene: further evidence of a relationship to murine lymphocyte antigen Ly-6 protein. Proc Natl Acad Sci U S A 89:7876-7879, 1992.

101. Pfeifer GP: Involvement of DNA damage and repair in mutational spectra. Mutat Res 450:1-3, 2000.

102. Puck TT: In vitro studies on the radiation biology of mammalian cells. Prog Biophys Mol Biol 10:237-258, 1960.

103. Puck TT, CIECIURA SJ, ROBINSON A: Genetics of somatic mammalian cells. III. Long-term cultivation of euploid cells from human and animal subjects. J Exp Med 108:945-956, 1958.

104. Puck TT, Steffen J: Life Cycle Analysis of Mammalian Cells. I. A Methods for Localizing Metabolic Events Within the Life cycle, and Its Application to the Action of Colcemide and Sublethal Doses of X-irradation. Biophys J 3:379-397, 1963.

105. Puck TT, Waldren CA: Mutation in mammalian cells: theory and implications. Somat Cell Mol Genet 13:405-409, 1987.

106. Puck TT, Wuthier P, Jones C, Kao FT: Genetics of somatic mammalian cells: lethal antigens as genetic markers for study of human linkage groups. Proc Natl Acad Sci U S A 68:3102-3106, 1971.

107. R.Scott Hawley and Michelle Y.Walker.: Advanced genetic analysis : finding meaning in a genome. Blackwell Pub, Malden, MA, 2003.

108. Ratnoff WD, Brockman WW, Hasty LA: Immunohistochemical localization of C9 neoantigen and the terminal complement inhibitory protein CD59 in human endometrium. Am J Reprod Immunol 34:72-79, 1995.

109. Ratnoff WD, Knez JJ, Prince GM, Okada H, Lachmann PJ, Medof ME: Structural properties of the glycoplasmanylinositol anchor phospholipid of the complement membrane attack complex inhibitor CD59. Clin Exp Immunol 87:415-421, 1992.

110. Ross CD, Lim CU, Fox MH: Assay to measure CD59 mutations in CHO A(L) cells using flow cytometry. Cytometry A 66:85-90, 2005.

111. Rudd PM, Dwek RA: Glycosylation: heterogeneity and the 3D structure of proteins. Crit Rev Biochem Mol Biol 32:1-100, 1997.

112. Rudd PM, Morgan BP, Wormald MR, Harvey DJ, van den Berg CW, Davis SJ, Ferguson MA, Dwek RA: The glycosylation of the complement regulatory protein, human erythrocyte CD59. J Biol Chem 272:7229-7244, 1997.

113. Sabharanjak S, Sharma P, Parton RG, Mayor S: GPI-anchored proteins are delivered to recycling endosomes via a distinct cdc42-regulated, clathrin-independent pinocytic pathway. Dev Cell 2:411-423, 2002.

114. Sambamurty AVSS: **Genetics** . 2nd ed. Edition. Alpha Science International, Harrow, U.K., 2005.

115. Schafer H, Bartels T, Hahn G, Otto A, Burger R: T-cell-activating monoclonal antibodies, reacting with both leukocytes and erythrocytes, recognize the guinea pig Thy-1 differentiation antigen: characterization and cloning of guinea pig CD90. Cell Immunol 197:116-128, 1999.

116. SCHWARTZ JH: The phosphorylation of alkaline phosphatase. Proc Natl Acad Sci U S A 49:871-878, 1963.

117. Seymour CB, Mothersill C: Delayed expression of lethal mutations and genomic instability in the progeny of human epithelial cells that survived in a bystander-killing environment. Radiat Oncol Investig 5:106-110, 1997.

118. Smith LE, Grosovsky AJ: Evidence for high-frequency allele loss at the aprt locus in TK6 human lymphoblasts. Mutat Res 289:245-254, 1993.

119. Sowdhamini R, Mitchell TJ, Andrew PW, Morgan PJ: Structural and functional analogy between pneumolysin and proaerolysin. Protein Eng 10:207-215, 1997.

120. Straus DS, Ames BN: Histidyl-transfer ribonucleic acid synthetase mutants requiring a high internal pool of histidine for growth. J Bacteriol 115:188-197, 1973.

121. Taguchi R, Hamakawa N, Harada-Nishida M, Fukui T, Nojima K, Ikezawa H: Microheterogeneity in glycosylphosphatidylinositol anchor structures of bovine liver 5'-nucleotidase. Biochemistry 33:1017-1022, 1994.

122. Tennant RW: Evaluation and validation issues in the development of transgenic mouse carcinogenicity bioassays. Environ Health Perspect 106 Suppl 2:473-476, 1998.

123. Thacker J: The nature of mutants induced by ionising radiation in cultured hamster cells. III. Molecular characterization of HPRT-deficient mutants induced by gamma-rays or alpha-particles showing that the majority have deletions of all or part of the hprt gene. Mutat Res 160:267-275, 1986.

124. Thacker J, Stretch A, Stephens MA: Th induction of thioguanine-resistant mutants of Chinese hamster cells by gamma-rays. Mutat Res 42:313-326, 1977.

125. Tobey RA, Petersen DF, Anderson EC, Puck TT: Life cycle analysis of mammalian cells. 3. The inhibition of division in Chinese hamster cells by puromycin and actinomycin. Biophys J 6:567-581, 1966.

126. Tomita-Mitchell A, Kat AG, Marcelino LA, Li-Sucholeiki XC, Goodluck-Griffith J, Thilly WG: Mismatch repair deficient human cells: spontaneous and MNNG-induced mutational spectra in the HPRT gene. Mutat Res 450:125-138, 2000.

127. Tornaletti S, Pfeifer GP: UV damage and repair mechanisms in mammalian cells. Bioessays 18:221-228, 1996.

128. Turker MS, Pieretti M, Kumar S: Molecular evidence for the induction of large interstitial deletions on mouse chromosome 8 by ionizing radiation. Mutat Res 374:201-208, 1997.

129. Tzircotis G, Thorne RF, Isacke CM: Chemotaxis towards hyaluronan is dependent on CD44 expression and modulated by cell type variation in CD44-hyaluronan binding. J Cell Sci 118:5119-5128, 2005.

130. Ueno A, Vannais D, Lenarczyk M, Waldren CA: Ascorbate, added after irradiation, reduces the mutant yield and alters the spectrum of. J Radiat Res (Tokyo) 43 Suppl:S245-S2492002.

131. Ueno AM, Vannais DB, Gustafson DL, Wong JC, Waldren CA: A low, adaptive dose of gamma-rays reduced the number and altered the spectrum of S1-mutants in human-hamster hybrid AL cells. Mutat Res 358:161-169, 1996.

132. Valle L, Fernandez V, Perez-Pons C, Sanchez FG, Benitez J, Urioste M: Generation of the BCR/ABL fusion gene in a Philadelphia chromosome-negative chronic myeloid leukaemia: insertion of 5.6 Mb of 9q34 into the BCR region of chromosome 22. Hematol Oncol 24:86-88, 2006.

133. Waldren C, Correll L, Sognier MA, Puck TT: Measurement of low levels of x-ray mutagenesis in relation to human disease. Proc Natl Acad Sci U S A 83:4839-4843, 1986.

134. Waldren C, Jones C, Puck TT: Measurement of mutagenesis in mammalian cells. Proc Natl Acad Sci U S A 76:1358-1362, 1979.

135. Waldren C, Vannais D, Drabek R, Gustafson D, Kraemer S, Lenarczyk M, Kronenberg A, Hei T, Ueno A: Analysis of mutant quantity and quality in human-hamster hybrid AL and AL-179 cells exposed to 137Cs-gamma or HZE-Fe ions. Adv Space Res 22:579-585, 1998.

136. Waldren CA, Ueno AM, Schaeffer BK, Wood SG, Sinclair PR, Doolittle DJ, Smith CJ, Harvey WF, Shibuya ML, Gustafson DL, Vannais DB, Puck TT, Sinclair JF: Mutant yields and mutational spectra of the heterocyclic amines MeIQ

and PhIP at the S1 locus of human-hamster AL cells with activation by chick embryo liver (CELC) co-cultures. Mutat Res 425:29-46, 1999.

137. Waldren CA, Ueno AM, Schaeffer BK, Wood SG, Sinclair PR, Doolittle DJ, Smith CJ, Harvey WF, Shibuya ML, Gustafson DL, Vannais DB, Puck TT, Sinclair JF: Mutant yields and mutational spectra of the heterocyclic amines MeIQ and PhIP at the S1 locus of human-hamster AL cells with activation by chick embryo liver (CELC) co-cultures. Mutat Res 425:29-46, 1999.

138. Waldren CA, Vannais DB, Ueno AM: A role for long-lived radicals (LLR) in radiation-induced mutation and persistent chromosomal instability: counteraction by ascorbate and RibCys but not DMSO. Mutat Res 551:255-265, 2004.

139. Wang H, Perrault AR, Takeda Y, Qin W, Wang H, Iliakis G: Biochemical evidence for Ku-independent backup pathways of NHEJ. Nucleic Acids Res 31:5377-5388, 2003.

140. Wang Q, Ponomareva ON, Lasarev M, Turker MS: High frequency induction of mitotic recombination by ionizing radiation in Mlh1 null mouse cells. Mutat Res 594:189-198, 2006.

141. Watanabe R, Inoue N, Westfall B, Taron CH, Orlean P, Takeda J, Kinoshita T: The first step of glycosylphosphatidylinositol biosynthesis is mediated by a complex of PIG-A, PIG-H, PIG-C and GPI1. EMBO J 17:877-885, 1998.

142. Watson JD: Molecular Biology of the Gene. 5th ed. Edition. Peason Benjamin Cummings, 2004.

143. Wedemeyer N, Greve B, Uthe D, Potter T, Denklau D, Severin E, Hacker-Klom U, Kohnlein W, Gohde W: Frequency of CD59 mutations induced in human-hamster hybrid A(L) cells by low-dose X-irradiation. Mutat Res 473:73-84, 2001.

144. Wetzel A, Wetzig T, Haustein UF, Sticherling M, Anderegg U, Simon JC, Saalbach A: Increased neutrophil adherence in psoriasis: role of the human endothelial cell receptor Thy-1 (CD90). J Invest Dermatol 126:441-452, 2006.

145. Wilson AB, Seilly D, Willers C, Vannais DB, McGraw M, Waldren CA, Hei TK, Davies A: Antigen S1, encoded by the MIC1 gene, is characterized as an epitope of human CD59, enabling measurement of mutagen-induced intragenic deletions in the AL cell system. Somat Cell Mol Genet 25:147-157, 1999.

146. Wu LJ, Randers-Pehrson G, Xu A, Waldren CA, Geard CR, Yu Z, Hei TK: Targeted cytoplasmic irradiation with alpha particles induces mutations in mammalian cells. Proc Natl Acad Sci U S A 96:4959-4964, 1999.

147. Wuthier P, Jones C, Puck TT: Surface antigens of mammalian cells as genetic markers. II. J Exp Med 138:229-244, 1973.

148. Yandell DW, Dryja TP, Little JB: Molecular genetic analysis of recessive mutations at a heterozygous autosomal locus in human cells. Mutat Res 229:89-102, 1990.

149. Yu J, Abagyan R, Dong S, Gilbert A, Nussenzweig V, Tomlinson S: Mapping the active site of CD59. J Exp Med 185:745-753, 1997.

150. Yu J, Dong S, Rushmere NK, Morgan BP, Abagyan R, Tomlinson S: Mapping the regions of the complement inhibitor CD59 responsible for its species selective activity. Biochemistry 36:9423-9428, 1997.

151. Yunis JJ: The chromosomal basis of human neoplasia. Science 221:227-236, 1983.

152. Zhou H, Randers-Pehrson G, Waldren CA, Hei TK: Radiation-induced bystander effect and adaptive response in mammalian cells. Adv Space Res 34:1368-1372, 2004.

153. Zhou H, Randers-Pehrson G, Waldren CA, Vannais D, Hall EJ, Hei TK: Induction of a bystander mutagenic effect of alpha particles in mammalian cells. Proc Natl Acad Sci U S A 97:2099-2104, 2000.

154. Zhou H, Xu A, Gillispie JA, Waldren CA, Hei TK: Quantification of. Mutat Res 594:113-119, 2006.

CHAPTER 2

GENERAL MATERIALS AND METHODS

Cell Culture

The CHO A_L cells were originally obtained from C.A. Waldren (Colorado State University). They have a standard set of Chinese hamster ovary K1 chromosomes along with a single copy of human chromosome 11. Cells designated CHO A_L(N), which we used in these experiments, contain a neomycin resistance gene on chromosome 11 which confers resistance to the antibiotic G418. Spontaneous background mutants were reduced via periodic treatment (alternate passages) of the cells with 800 μM G418 (Sigma-Aldrich, St. Louis, MO. Cells were cultured in Ham's F-12 medium supplemented with 10% fetal bovine serum (Gemini Bio-Products, Woodland, CA), penicillin/streptomycin (0.14 and 0.2 g/L, respectively) and 7.5% w/v sodium bicarbonate, pH 7.3. Cells were maintained in T75 tissue culture flasks at 37° C in a humidified 5% CO_2 incubator. The cells were passed every 3 to 4 days to avoid confluence. After 3 to 4 months of continual use, the flasks of stock cells were discarded and new cells were thawed and maintained as above.

Monoclonal antibody labeling

Cells were trypsinized, washed once in PBS and then again in staining buffer (PBS with 1% BSA, 0.1% sodium azide). Cells were resuspended at $1x10^6$ cells/ml and 1 ml was aliquoted into three separate 1.2 ml microcentrifuge tubes. Control samples were required with individual staining of each marker and combinations of untreated control A_L cells.

After centrifugation at 1500 rpm (450g) in an IEC table-top centrifuge, buffer was aspirated and the cells were resuspended in the residual buffer.

To stain cells simultaneously with CD59, CD44 and CD90 antibodies, CD59-PE (Caltag, Burlingame, CA 1:40 dilution), CD44 biotin (Serotec, Raleigh, NC, 1:5 dilution), and CD90-Alexa 647 (Serotec, Raleigh, NC, 1:5 dilution) directly-conjugated monoclonal antibodies were added to a total volume of 50 µl in staining buffer. The cells were incubated for 30 min on ice and then 1 ml staining buffer was added. After centrifugation and aspiration, cells were resuspended in 99 µl staining buffer and 1 µl Alexa 488 Streptavidin (Molecular Probes, Invitrogen, Carlsbad, CA, 1:100) and stained for 30 min on ice. All buffers and staining solutions were kept on ice throughout the experiment.

After incubation, all samples were washed in cold staining buffer and resuspended in 0.5 ml cold buffer, filtered through a 40 µm nylon mesh and kept on ice prior to analysis by flow cytometry.

Flow Cytometry

A CyAn™ flow cytometer (Dako, Ft. Collins, CO) was used with 488 and 635 nm lasers for excitation. FITC was detected using a 530/40 nm bandpass filter with a 545 nm dichroic long pass, PE was detected using a 575/25 nm bandpass filter with a 595 nm dichroic long pass, and Alexa 647 was excited using the 635 nm laser and detected using a 665/20 nm bandpass filter with a 730 nm dichroic long pass. A total of $1x10^5$ cells were analyzed for each sample. Gating on forward scatter vs. side scatter eliminated cellular debris, thus reducing false negatives. The photomultiplier voltages were set so that the unstained populations with each marker had the same mean value on the histogram with the mutant region gated on 99% of the negative parental cells, which lacked chromosome 11.

Compensation was required between the PE and FITC/Alexa 488 stains and was done with the Summit Software v4.2 (Dako, Ft. Collins, CO). Within the PE histogram, the mutant region was defined as those cells with fluorescence intensity less than 1% of the mean fluorescence intensity of the $CD59^+$ population of control cells. This enabled quantification of $CD59^-$ (mutant) cells for subsequent calculation of the mutant fraction.

Mutation Assay

Cells were treated with G418 (800 μM) for 5 days prior to treatment. The day before treatment, $4x10^5$ cells were plated in a T75 flask, giving $8x10^5$ at time of treatment. The medium was aspirated, then medium containing MNNG (Sigma-Aldrich, St. Louis, MO) in various concentrations (0.0625, 0.125, 0.25, 0.5 μg/ml) was added to the flasks and the cells were incubated at 37 °C in 5% CO_2 for 3 hrs. The clonogenic survival after the highest dose was 20%. The flasks were then washed twice with PBS and fresh medium was returned to the flasks. The cells were returned to the incubator for growth and mutant expression. Cells were grown for 2 days and then at least $1.5x10^5$ cells were passed, the actual number depending on the relative growth compared to the control flasks. The same passing procedure occurred on days 6, 9, and 12. Cells were assayed with flow cytometry every 2 days to determine the day of maximum mutant expression after treatment with 0.5 μg/ml MNNG. Untreated control cells were passed in parallel and were processed along with the treated samples. After determining the mutant expression period, a dose response curve was generated by treating cells with various doses of MNNG that caused 20-80% survival and measuring the mutant yield on the day of maximum expression.

Radiation Treatment

Cells were treated with G418 (800 μM) for 5 days prior to treatment. The day before treatment, $4x10^5$ cells were plated in a T75 flask, giving $8x10^5$ cells at time of treatment. The cells were then irradiated with doses of 0-4 Gy ^{137}Cs γ radiation, a well-known clastogen (57,133) (J.L. Shepherd and Associates, Glendale, CA), at a dose rate of 0.93 Gy/min at 22° C, to test the response of multiple markers on chromosome 11. Treatment and control flasks were passed with a minimum of $1.5x10^5$ cells per T75 flask and assayed using the FCMA protocol with multiple markers on day 6, the maximum day for CD59 mutation expression. The spontaneous background was subtracted to determine the corrected mutant fraction for each marker.

Statistical Analysis

When comparing control and treated samples for statistical analysis, Pro-Stat and PSI-Plot were utilized to determine linear regression, Student's T test and standard error. Microsoft Excel was also used to calculate average values.

CHAPTER 3

AN ASSAY TO MEASURE CD59 MUTATIONS IN CHO A_L CELLS USING FLOW CYTOMETRY

Cytometry 66A:85-90 (2005)

Abstract

Background: A sensitive mammalian cell mutation assay was developed previously using a Chinese hamster ovary cell line (CHO A_L) that stably incorporates human chromosome 11. The assay measures mutations in the *CD59* gene on chromosome 11 but it requires the use of rabbit complement and colony growth for mutant selection. We have developed a more rapid flow cytometry based mutation assay with CHO A_L cells that uses monoclonal antibodies against CD59 to detect mutants and does not require colony formation.

Methods: CHO A_L cells were treated with gamma radiation or N-methyl-N'-nitro-N-nitrosoguanidine (MNNG), then allowed to grow for various times for mutant expression. Cells were labeled with monoclonal antibodies against CD59 and analyzed by flow cytometry.

Results: Negative and positive populations were separated by over 100-fold. Mixing various proportions of CD59 positive and negative cells demonstrated that the assay is highly linear (r^2=0.9999) and sensitive (<0.05% background mutants). The yield of *CD59* inducible mutants was linearly related to dose for both a clastogen (gamma radiation) and point mutagen (MNNG). The mutant yield was both time and treatment specific.

Conclusions: Mutations induced by genotoxic agents can be rapidly and sensitively measured in CHO A_L cells using flow cytometry.

Keywords

Mammalian mutation assay, flow cytometry, CD59, human-hamster hybrid cells, CHO A_L cells, gamma radiation, MNNG, mutagenesis

Introduction

Studies of mutagenesis in cultured mammalian cells can help predict carcinogenesis based upon evidence that mutation plays a vital role in carcinogenesis and the correlation between the ability of an agent to induce mutations *in vitro* and its carcinogenic potency (5). Mutagenesis data are used for heritable risk assessment, as part of the body of information used to make a decision to trigger oncogenicity testing, and as part of the weight-of-evidence for determining a carcinogenicity classification for a chemical when a long-term bioassay has not been performed (12).

Current mammalian cell mutation assay systems, namely the Mouse Lymphoma Assay (MLA) based on the thymidine kinase gene (16,15,2) and the Chinese hamster ovary hypoxanthine guanine phosphoribosyl transferase (HGPRT) assay (22,21), effectively measure specific types of mutations, but are limited in sensitivity by the requirement that flanking genes on the chromosome remain functional for cell survival (14). If the mutation extends beyond the reporter gene location, it may then cause cell death and the mutation is not scored (18). This is especially true in the HGPRT assay, since the gene is located on the X-chromosome and flanking genes may not be rescued by a homologous chromosome. Large deletions, for example, are likely to kill the cell and alter the accurate mutant yield induced by a genotoxic agent, reducing the assay sensitivity (12).

In light of these difficulties, Puck and co-workers (26,18) designed a mammalian cell mutation assay around a Chinese hamster ovary cell line (CHO A_L) that stably incorporated a single copy of human chromosome 11. The CHO A_L hybrid cells were formed by fusion of a human amniotic fluid fibroblast and a gly^- mutant of the Chinese hamster ovary CHO-K1 cell (19). They retain the normal set of CHO-K1 chromosomes and a single human chromosome 11 (13). The hybrid cells express the *CD59* gene on chromosome 11 which encodes a GPI-linked surface protein, CD59, which is not expressed in normal CHO cells. Thus, mutations in *CD59* lead to loss of expression of CD59 protein on the surface of the cells. This cell line has been stable for over 30 years with very little rearrangement (20,4). Waldren and co-workers subsequently used this system to assay mutagenesis from a variety of genotoxic compounds (5,10,14,18,26,13,25,28,28,17,7,14,24,8,6,27,30,5,3). They have found that the mutation assay is a hundred-fold more sensitive than HGPRT and a thousand-fold more sensitive than the bacterial Ames test (5). Those results reflect a major advantage of the A_L system: the cell line does not require chromosome 11 to survive except for an essential gene at the tip of the p arm (9). This makes it possible to quantify the activity of small, non-lethal doses of a mutagen like those to which human populations are likely to be exposed (5).

The original CHO A_L mutation assay system depends on rabbit complement-induced cytotoxicity against cells labeled with monoclonal antibodies against CD59 to detect mutants after clonal growth. Cells which are mutated in the *CD59* gene will not bind the antibody and continue to grow in the presence of rabbit complement. The resulting colonies are counted and mutant yield is calculated. When determining exact mutant yield, researchers have to take into account the toxicity of rabbit complement. Furthermore, results vary with different lots of complement.

Flow Cytometry Mutation Assay

We propose to take this CHO A_L mammalian mutation assay and streamline it using flow cytometry, which we call the flow cytometry mutation assay (FCMA). The cells are stained with a directly-conjugated monoclonal antibody to CD59 and analyzed by a flow cytometer to measure the number of $CD59^-$ mutant cells, avoiding the need for rabbit complement and colony growth. Not only does this eliminate the intrinsic toxicity of the rabbit complement, but it shortens the time required for the assay. Both the clonogenic and flow cytometric methods require a treatment phase (20 min - 24 hrs depending on chemical toxicity), an expression period (5-12 days) and an assay phase. The entire analysis takes 12-22 days for the clonogenic assay but only 7-14 days for the FCMA. The time and labor reduction speeds results from experiments and makes possible the analysis of more variables while allowing for lower laboratory costs.

To validate the flow cytometric mutation assay, we chose both a known clastogen (25,29) (^{137}Cs (radiation) and a point mutagen (1) (N-methyl-N'-nitro-N-nitrosoguanidine, MNNG). Calibration experiments demonstrate that the FCMA is sensitive and linear. Treatment with either radiation or MNNG results in linear mutation dose response curves, which is due in part to the ability of the assay to detect both small (single locus) and large (multilocus) mutations, allowing one to measure the effect of mutagenic agents at low and high doses (5). We assume that detection of a mutation is contingent on the cell surviving and the *CD59* gene not being rescued or repaired. Rescue could occur by a translocation in which the gene is moved from its position on the human chromosome and reintegrated elsewhere in the genome (17).

Methods

Reducing background mutants

The A_L cell line has a naturally-occurring spontaneous background of around 10-50x10^{-5} or less when cells are properly plated and remain at the correct pH (26). Over time, or if cells become confluent or acidic, the background mutation level may increase to 100x10^{-5} or above, making the mutation assay system less sensitive. To combat this problem, we employ three techniques for reducing the background: antibiotic treatment, panning, and sorting. Cells are periodically treated with neomycin (800 μM, Sigma-Aldrich, St. Louis, MO) since it effectively reduces the background if it is less than about 100x10^{-5}. If the background rises higher than this, the cells are panned, which is very effective in reducing background but is time consuming. To pan the cells, sterilized petri plates are labeled with a general goat anti-mouse antibody (Sigma-Aldrich, St. Louis, MO) at 20 μg/ml in Phosphate Buffered Saline (PBS). The cells are labeled with a CD59 monoclonal antibody (E7.1) provided by Dr. Waldren (2 μl anti-CD59 in PBS containing 2% FBS) and then placed in the goat anti-mouse petri plates where they incubate at 4° C for 2 hr. After treatment, the plates are gently washed with cold 2% FBS/PBS and those cells that lack the CD59 antigen are washed away. In one particular experiment, this panning procedure reduced the background from 200x10^{-5} to 20x10^{-5} in two successive treatments (data not shown). Another method to reduce background is to sort $CD59^+$ cells with a cell sorter, with similar results as panning but at a much higher cost. Generally, cells were panned about every 3 months or when cells exhibited a high background.

Calibration

The linearity of the FCMA was determined by mixing parental CHO cells (negative for CD59) with the $CD59^+$ CHO A_L cells in two-fold serial dilutions from 4% to 0.125%. The

cell mixtures were then stained with anti-CD59 antibodies and analyzed with the flow cytometer.

Results

Separation of CD59 Positive and Negative Cells

In order to determine whether flow cytometry could adequately distinguish $CD59^+$ CHO A_L cells from $CD59^-$ mutants, we compared histograms of antibody-labeled CHO A_L cells with unstained CHO A_L cells as a negative control (Figure 3-1). We also used antibody-labeled parental CHO cells which do not contain chromosome 11 (and thus do not express CD59) as negative controls, but they had slightly less fluorescence than unstained CHO A_L cells (data not shown). This is probably because the CHO A_L cells are somewhat larger and thus the unstained cells are a better control. There was more than a 100-fold separation in fluorescence intensity. A region was set that included 97% of the negative cells. This was done to minimize the inclusion of false-negatives but to maximize the number of true mutants. The background proportion of negative cells (presumably mutants) was typically 0.05% or less ($50x10^{-5}$). These results demonstrate that the assay has sufficient sensitivity to be able to measure low levels of mutants in a $CD59^+$ background.

Calibration: System Sensitivity

We then investigated whether we could use flow cytometry to accurately measure known proportions of negative cells in a positive population. Parental CHO cells lacking CD59 were mixed with CHO A_L cells in two-fold serial dilutions from 4.0% to 0.125% and stained with a monoclonal antibody to CD59, then measured with flow cytometry (Figure 3-2). The results demonstrate that flow cytometry can accurately count the proportion of CD59 negative cells in a highly linear fashion (r^2=0.9999).

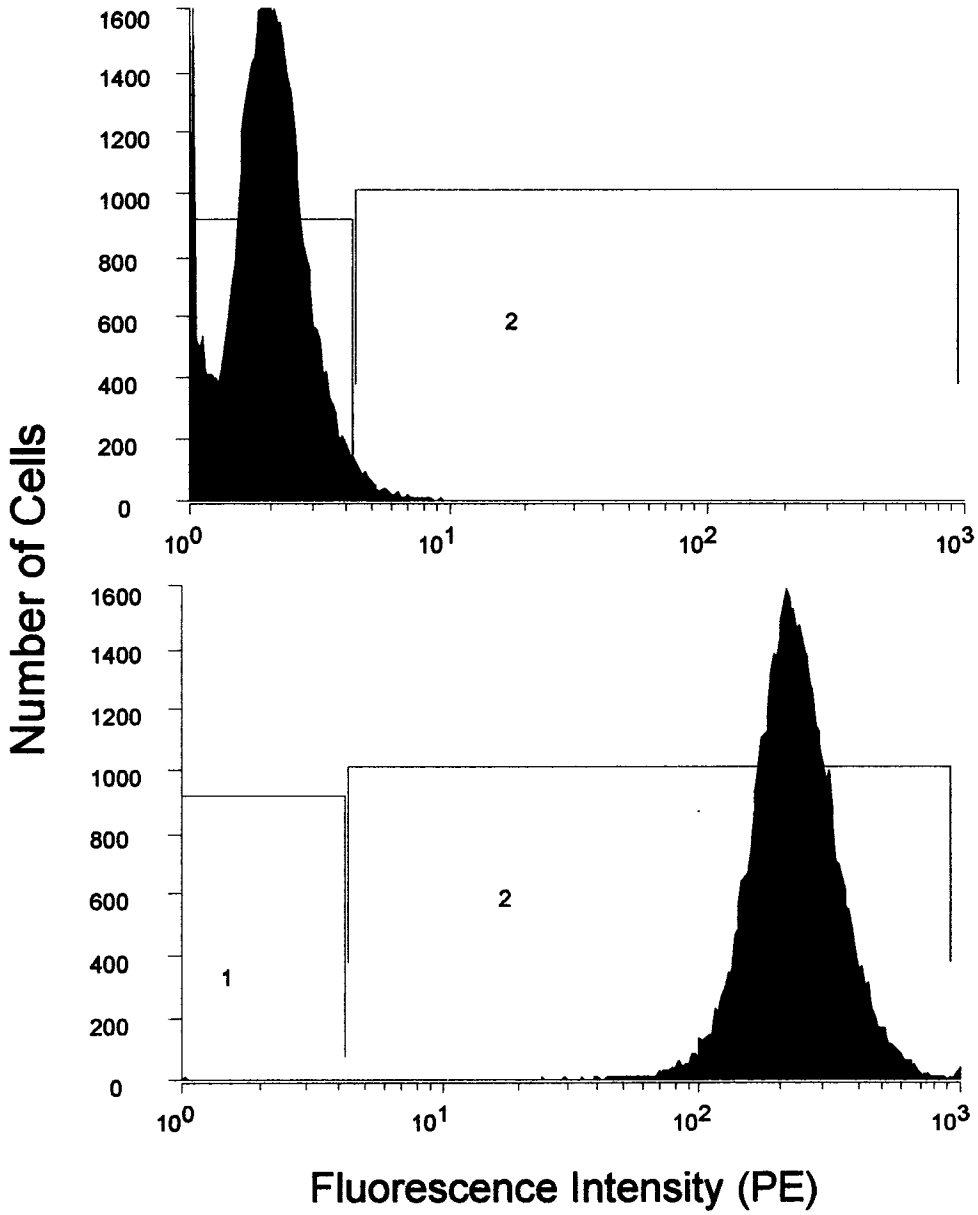

Figure 3-1. Flow cytometry histograms of CHO A_L cells either unstained (top) or stained with antibodies against CD59 (bottom). Region 1 is set to include 97% of the negative cells and is used for counting mutants. This gives a spontaneous background of 0.03% or about 30x10-5 analyzed cells.

MNNG mutagenesis

After the FCMA linearity was determined with mixed populations, we used a well-known mutagen, MNNG, to determine whether mutants could reliably be measured. It was first necessary to determine the kinetics of mutant expression. Cells were treated with 0.5 μg/ml MNNG for 3 hr, a dose giving 20% survival, and assayed for mutants at various times later (Figure 3-3). No excess mutants were detected by day 7, but a high level was detected on day 10 with peak expression on day 12. The mutant yield subsequently decreased by day 15. Cells were then treated with various doses of MNNG that gave surviving fractions of 20%, 40%, 60%, and 80% and assayed on day 12 (Figure 3-4). The MNNG dose response curve increased linearly from 0.0625 μg/ml to 0.5 μg/ml (r^2=0.9980) and was statistically significant from control at 0.125 μg/ml ($p<0.0025$).

Radiation mutagenesis

We also analyzed the ability of the FCMA to measure mutations induced by a well-known clastogen, ^{137}Cs gamma radiation. The maximum day of mutant expression was evaluated by irradiating cells with 4 Gy, a dose giving 50% survival, and assaying the mutant fraction with flow cytometry at various times (Figure 3-5). The mutant yield remained at background levels for 4 days, but was high at 7 days, peaked at 9 days and gradually declined over the next 6 days.

Cells were irradiated at doses that gave surviving fractions of 50%, 65%, 75% and 90% and assayed on day 9 (Figure 3-5). The γ radiation dose response curve increased in a linear manner from 1 to 4 Gy (r^2 = 0.9958) and was statistically significant from control at 1 Gy ($p<0.05$) (Figure 3-6).

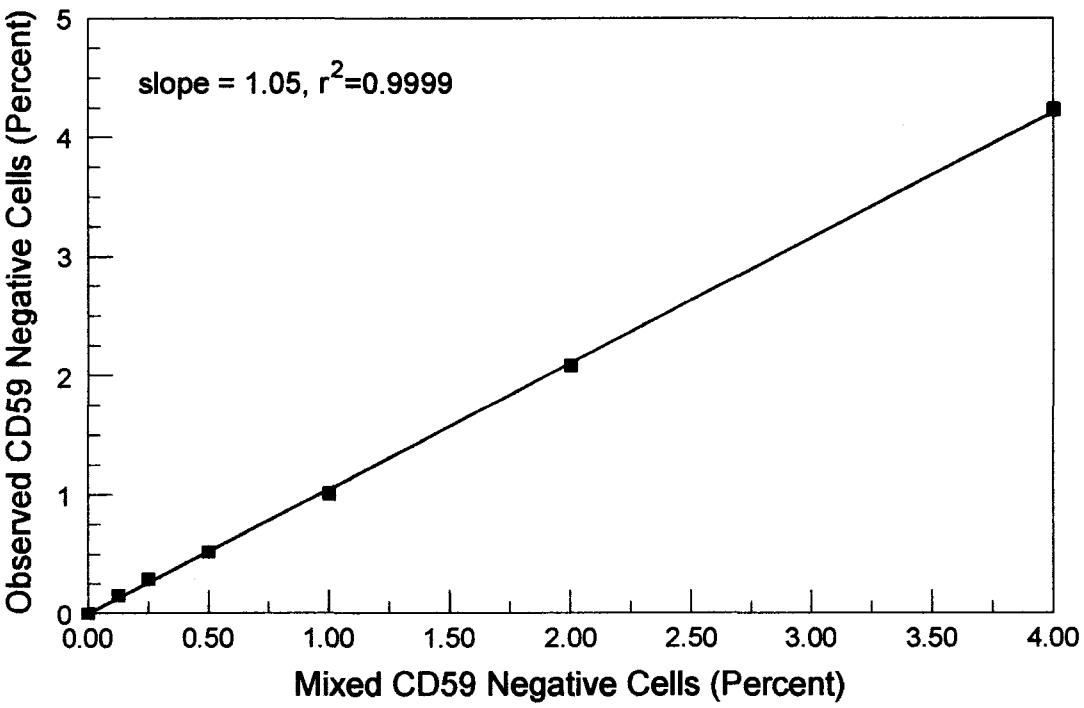

Figure 3-2. Negative CD59 parental cells were mixed with CHO A_L cells in varying proportions and then labeled with anti-CD59 monoclonal antibodies and measured with the EPICS V. The X-axis represents the percentage of negative cells in the mixture and the Y-axis represents the measured percentage. The results are from 3 independent experiments. Error bars representing the standard error of the mean (SEM) are smaller than the data points.

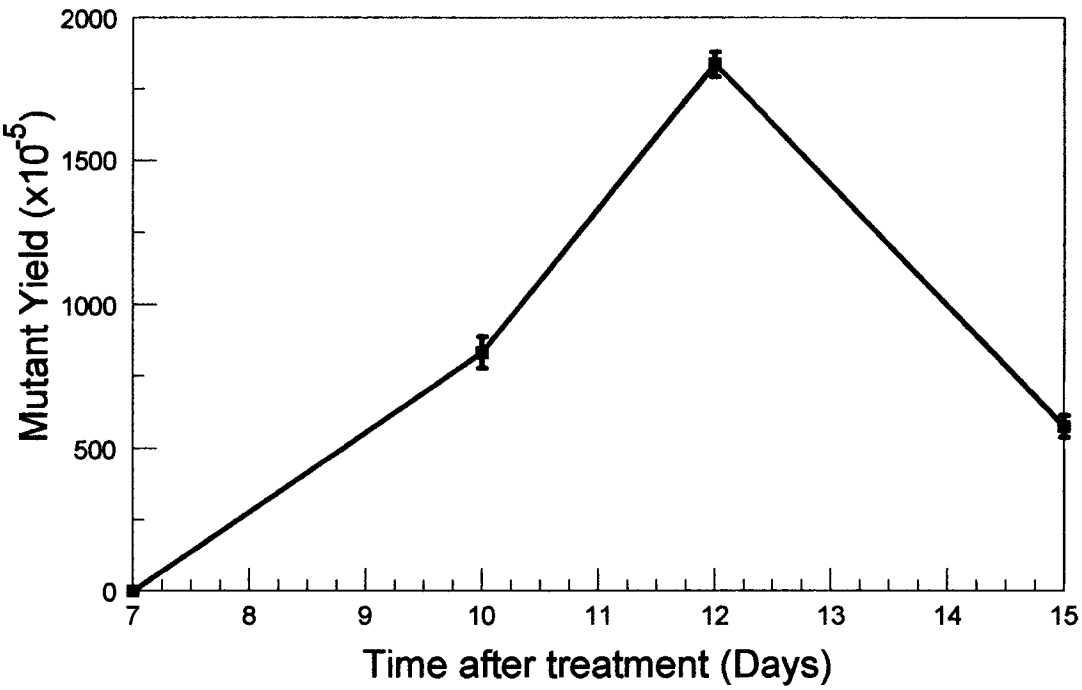

Figure 3-3. Temporal expression of mutants after treatment with 0.5 μg/ml MNNG for 3 hr. The data points are corrected for the background level of mutants from parallel untreated samples. The mutant yield is the number of mutants per 105 cells measured in R1 (see Figure 1). Symbols are the mean values from 3 independent experiments and error bars represent the SEM. Results were obtained with the EPICS V flow cytometer.

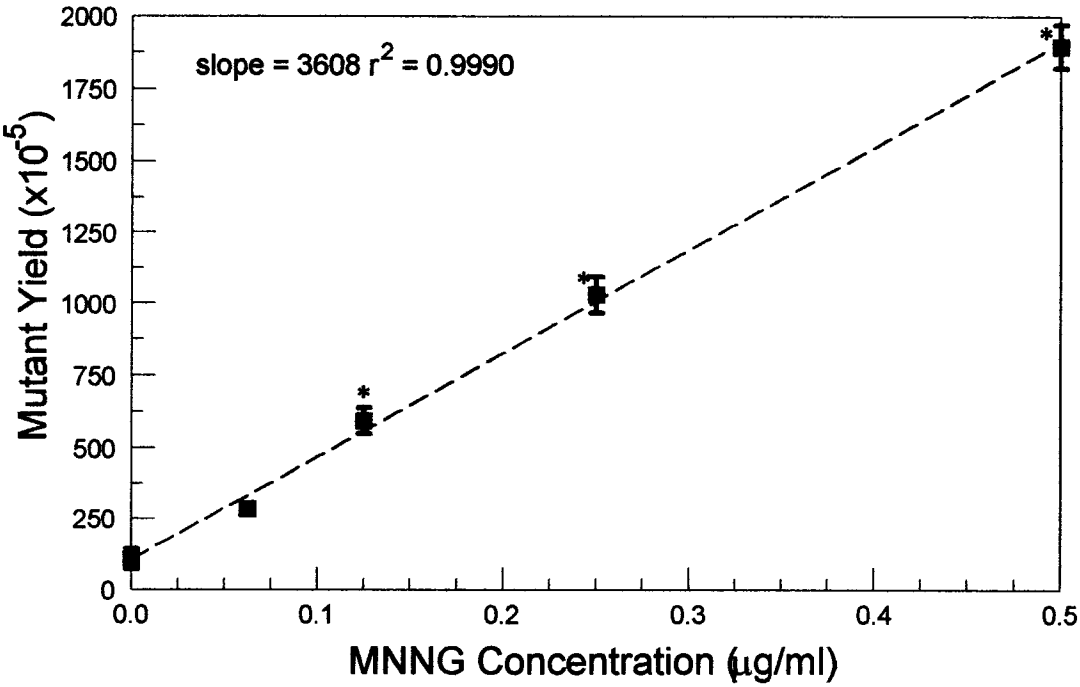

Figure 3-4. Dose response curve for MNNG treatment. Cells were treated with various doses of MNNG for 3hr, and then assayed on day 12. The minimum dose resulted in 80% survival while the maximum dose gave 20% survival. Symbols represent the mean values of 3 independent experiments and error bars represent SEM. *Significantly different from control at p<0.0025.

Discussion

The FCMA method was developed to enable a rapid and quantitative analysis of mutations induced by genotoxic agents that would not require the time and labor of a clonogenic assay. It was first necessary to demonstrate that flow cytometry could measure a very small proportion of negative cells in a positive background, which is opposite the usual case with flow cytometry where positive cells are measured in a background of negative cells. The separation between the CD59 positive and CD59 negative cells in Fig.1 clearly demonstrates that there is sufficient resolution to measure mutants in a background of CD59 positive cells. Background levels of mutants could be measured down to <0.05% ($50x10^{-5}$), which is as low as the background is measured using the standard complement-based cytotoxicity assay for CD59 mutants (Charles Waldren, personal communication). The mixing experiments demonstrate that the FCMA effectively measures CD59 mutants in a linear and sensitive manner.

One important issue is the criteria for setting the mutant region on the histograms. We chose to include 97% of the negative control population in the region. This is a trade-off that was chosen so that only 3% of mutants would be missed but the false-positive rate of non-mutants that have a very low fluorescence would be minimized. It is possible to use other values, 98% or 99%, for example, but the effect is to give a larger background. Using 97% was a reasonable compromise. The main issue is to use a consistent value so that all samples will be analyzed in the same way.

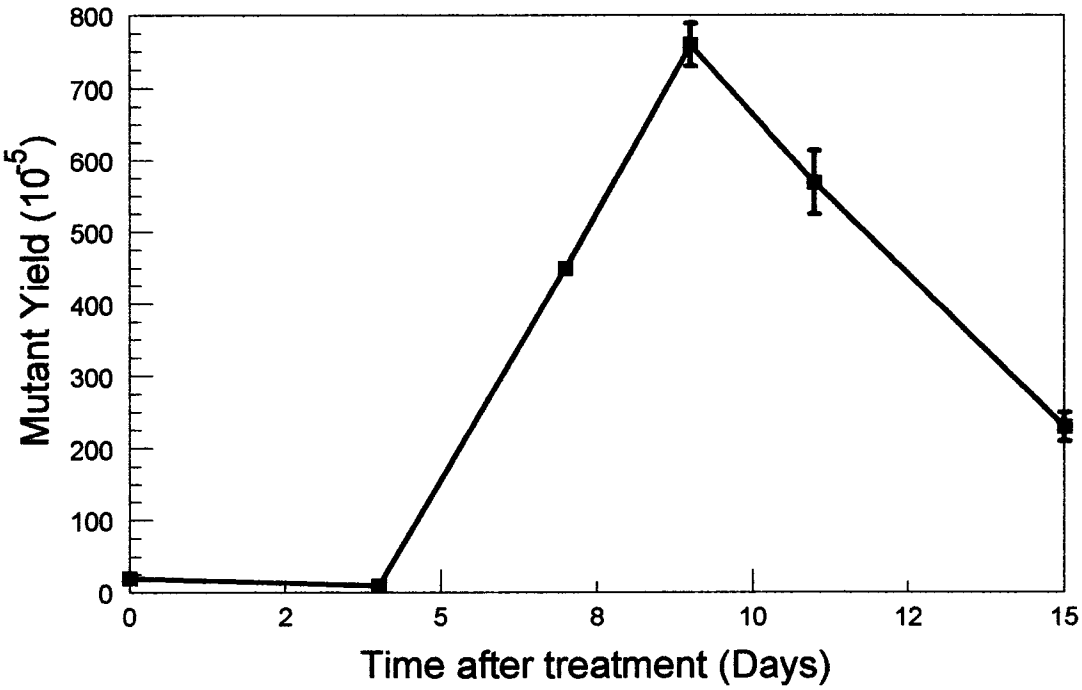

Figure 3-5. Temporal expression of mutants after treatment with 4 Gy gamma radiation. The data points are corrected for the background level of mutants from parallel untreated samples. Symbols are the mean values from 3 independent experiments and error bars represent the SEM.

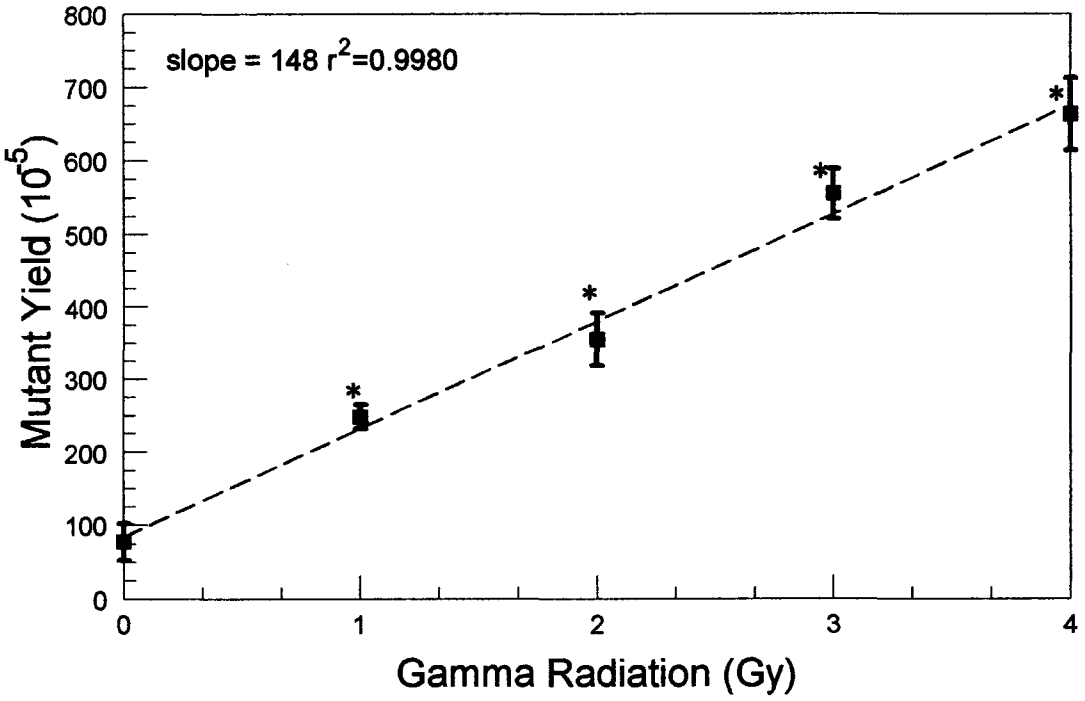

Figure 3-6. Dose response curve for gamma radiation. Cells were treated with various doses of gamma radiation and then assayed on day 9. The minimum dose resulted in 90% survival while the maximum dose gave 50% survival. Symbols represent the mean values of 3 independent experiments and error bars represent SEM. *Significantly different from control at $p<0.0005$.

A previous report using flow cytometry to measure mutations in the CD59 gene had a much higher background level of mutations of 0.2% (29). The separation between the positive and negative cells was much less than the results reported here. Furthermore, they used a cutoff to detect mutants at 10% of the mean value of the positive cell population. This resulted in artificially high mutant induction rates for ionizing radiation.

Mutations were induced both with ionizing radiation, a clastogen, and MNNG, a point mutagen, to determine whether the FCMA could measure a dose response for mutagenesis. Both agents resulted in linear dose response mutation curves over the range of doses studied. This shows that the FCMA assay is able to detect both large and small mutations, similar to what has been shown with the complement-based cytotoxicity assay (17,11,27). In order to demonstrate the widespread applicability of this assay for measuring genotoxicity, we are currently studying a panel of genotoxic agents and appropriate control agents.

As with all mutation assays, an expression period is necessary for mutants to be measured. We have shown that the mutant expression is time-dependent for both radiation and MNNG, but that the kinetics are quite different. The time for maximum expression was 12 days for MNNG but 9 days for radiation. One difference in this assay compared to a clonogenic assay is that dead cells will be present in the cell population for a period of time after mutagenesis and then will eventually be overgrown by the viable cells, including mutants. This will potentially affect the temporal expression of mutants. The expression time is also affected by cell cycle alterations, which can be quite different for different agents. Preliminary cell cycle analysis demonstrates that for MNNG, expression does not occur until the mutated cells begin a normal cell cycle (data not shown). An additional factor that may be reflected in the time of mutant expression with different genotoxic agents is that

other physiological processes may be affected by toxic drugs that could affect the recycling of existing CD59 from the cell surface. Another important observation is that the mutant yield is reduced after the peak expression time. We do not know why it is reduced, but it may be due to a somewhat reduced viability or slower growth rate of the mutant cells. A detailed understanding of the kinetics of mutant expression requires further study, which is currently underway.

The FCMA, using the monosomic *CD59* gene in CHO A_L cells, gives a higher mutant yield for 4 Gy of radiation than other mutation assays, including the A_L clonogenic assay (27), MLA (16), and HPRT (23). Both the MLA and HPRT are limited in sensitivity by having flanking genes near the analysis gene that may be deleted or mutated, causing cell death and artificially low mutant measurements. With the large chromosome 11 as a target, the A_L cell line is immune from that problem. The CHO A_L clonogenic assay is somewhat less sensitive than the FCMA, which also utilizes the CHO A_L hybrid cell line. The reasons for this are unknown but it may be due to the very different methods for detecting mutants. The rabbit complement system is much more complex and may kill some of the mutants if they have a low expression of CD59. Wedemeyer *et al.* (29) reported much higher mutation frequencies using CHO A_L cells (about 2.8% after 4 Gy), but their results are much higher than any previous reports. Furthermore, they reported an induction of mutants within 2 days after 3 Gy of X-rays. We do not see any mutants before 4 days after gamma-irradiation. Both of their results may be due to the fact that they had less separation between mutant and non-mutant cells and set the gating to identify mutants as cells that had 10% or less fluorescence intensity than the peak of the CD59-positive cells. This is a much less stringent condition than we use and would give a much higher mutant fraction.

We have also compared our results for the mutant yield induced by MNNG with the MLA (31), the HPRT assay (3), the CHO A_L clonogenic assay (10). The FCMA measures a substantially higher mutant yield after treatment with MNNG than the other assays. In fact, we could only measure results up to a concentration of 0.5 μg/ml (80% killing) while others used doses up to 4 μg/ml. In our hands, that concentration of MNNG would lead to unacceptable cell killing.

In summary, we have demonstrated that the FCMA is robust, linear, and more sensitive than other currently used mutation assay systems. Results can be obtained more rapidly and easier than with conventional clonogenic assays. It is necessary to determine the optimal mutant expression period, which varies depending on the mutagenic agent, to get the most accurate results.

Acknowledgements

We are very grateful to Charles Waldren and Diane Vannais for giving us the cells and for many helpful discussions on the use of the assay.

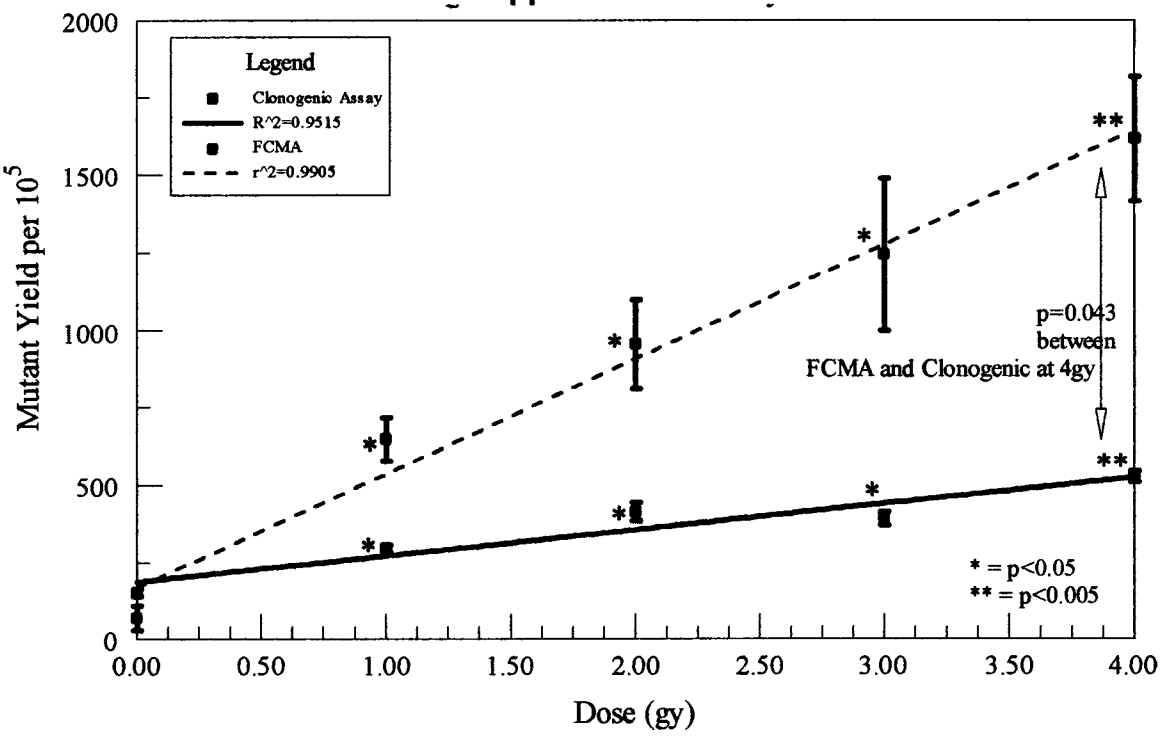

Figure 3-7. Comparison of CD59 mutant yield measured by the FCMA and CHO A_L clonogenic assay for irradiated cells (dose of 0-4 Gy) measured on the Dako CyAn flow cytometer. Regions were set at 1% of the mean positive peak, giving a much higher mutant yield for radiation than cited in chapter 3. Epics and CyAn comparison is discussed in Appendix, Chapter 5. Rabbit complement was graciously provided by Dr. Tom Hei at Columbia University.

Clonogenic methods were executed as described by Waldren and coworkers (28, 29, 30).

Reference List

1. Bempong MA: Mutagenicity and carcinogenicity of N-methyl-N'-nitro-N-nitrosoguanidine I. Induction of chromosome aberrations and mitotic anomalies in Chinese hamster ovary cells. J Environ Pathol Toxicol 2:633-656, 1979.

2. Clive D, Caspary W, Kirby PE, Krehl R, Moore M, Mayo J, Oberly TJ: Guide for performing the mouse lymphoma assay for mammalian cell mutagenicity. Mutat Res 189:143-156, 1987.

3. Costes S, Sachs R, Hlatky L, Vannais D, Waldren C, Fouladi B: Large-mutation spectra induced at hemizygous loci by low-LET radiation: evidence for intrachromosomal proximity effects. Radiat Res 156:545-557, 2001.

4. Glaser T, Housman D, Lewis WH, Gerhard D, Jones C: A fine-structure deletion map of human chromosome 11p: analysis of J1 series hybrids. Somat Cell Mol Genet 15:477-501, 1989.

5. Gustafson DL, Franz HR, Ueno AM, Smith CJ, Doolittle DJ, Waldren CA: Vanillin (3-methoxy-4-hydroxybenzaldehyde) inhibits mutation induced by hydrogen peroxide, N-methyl-N-nitrosoguanidine and mitomycin C but not (137)Cs gamma-radiation at the CD59 locus in human-hamster hybrid A(L) cells. Mutagenesis 15:207-213, 2000.

6. Hei TK, Liu SX, Waldren C: Mutagenicity of arsenic in mammalian cells: role of reactive oxygen species. Proc Natl Acad Sci U S A 95:8103-8107, 1998.

7. Hei TK, Piao CQ, He ZY, Vannais D, Waldren CA: Chrysotile fiber is a strong mutagen in mammalian cells. Cancer Res 52:6305-6309, 1992.

8. Hei TK, Wu LJ, Liu SX, Vannais D, Waldren CA, Randers-Pehrson G: Mutagenic effects of a single and an exact number of alpha particles in mammalian cells. Proc Natl Acad Sci U S A 94:3765-3770, 1997.

9. Jones C, Wuthier P, Puck TT: Genetics of somatic cell surface antigens. III. Further analysis of the AL marker. Somatic Cell Genet 1:235-246, 1975.

10. Kraemer SM, Vannais DB, Kronenberg A, Ueno A, Waldren CA: Gamma-ray mutagenesis studies in a new human-hamster hybrid, A(L)CD59(+/-), which has two human chromosomes 11 but is hemizygous for the CD59 gene. Radiat Res 156:10-19, 2001.

11. Kraemer SM, Waldren CA: Chromosomal mutations and chromosome loss measured in a new human-hamster hybrid cell line, ALC: studies with colcemid, ultraviolet irradiation, and 137Cs gamma-rays. Mutat Res 379:151-166, 1997.

12. Li AP, Aaron CS, Auletta AE, Dearfield KL, Riddle JC, Slesinski RS, Stankowski LF, Jr.: An evaluation of the roles of mammalian cell mutation assays in the testing of chemical genotoxicity. Regul Toxicol Pharmacol 14:24-40, 1991.

13. Matsukura N, Willey J, Miyashita M, Taffe B, Hoffmann D, Waldren C, Puck TT, Harris CC: Detection of direct mutagenicity of cigarette smoke condensate in mammalian cells. Carcinogenesis 12:685-689, 1991.

14. McGuinness SM, Shibuya ML, Ueno AM, Vannais DB, Waldren CA: Mutant quantity and quality in mammalian cells (AL) exposed to cesium-137 gamma radiation: effect of caffeine. Radiat Res 142:247-255, 1995.

15. Moore MM, Amtower A, Strauss GH, Doerr C: Genotoxicity of gamma-irradiation in L5178Y mouse lymphoma cells. Mutat Res 174:149-154, 1986.

16. Moore MM, Clive D, Howard BE, Batson AG, Turner NT: In situ analysis of trifluorothymidine-resistant (TFTr) mutants of L5178Y/TK+/- mouse lymphoma cells. Mutat Res 151:147-159, 1985.

17. Parker R, Waldren C, Hei TK, Wong DF, Puck TT: Analysis of mutant frequency curves and survival curves applied to the AL hybrid cell system. J Theor Biol 132:113-117, 1988.

18. Puck TT, Waldren CA: Mutation in mammalian cells: theory and implications. Somat Cell Mol Genet 13:405-409, 1987.

19. Puck TT, Wuthier P, Jones C, Kao FT: Genetics of somatic mammalian cells: lethal antigens as genetic markers for study of human linkage groups. Proc Natl Acad Sci U S A 68:3102-3106, 1971.

20. Qin S, Nowak NJ, Zhang J, Sait SN, Mayers PG, Higgins MJ, Cheng Y, Li L, Munroe DJ, Gerhard DS, Weber BH, Bric E, Housman DE, Evans GA, Shows TB: A high-resolution physical map of human chromosome 11. Proc Natl Acad Sci U S A 93:3149-3154, 1996.

21. Thacker J: The nature of mutants induced by ionising radiation in cultured hamster cells. III. Molecular characterization of HPRT-deficient mutants induced by gamma-rays or alpha-particles showing that the majority have deletions of all or part of the hprt gene. Mutat Res 160:267-275, 1986.

22. Thacker J, Stretch A: Recovery from lethal and mutagenic damage during postirradiation holding and low-dose-rate irradiations of cultured hamster cells. Radiat Res 96:380-392, 1983.

23. Thacker J, Stretch A, Stephens MA: Th induction of thioguanine-resistant mutants of Chinese hamster cells by gamma-rays. Mutat Res 42:313-326, 1977.

24. Ueno AM, Vannais DB, Gustafson DL, Wong JC, Waldren CA: A low, adaptive dose of gamma-rays reduced the number and altered the spectrum of S1-mutants in human-hamster hybrid AL cells. Mutat Res 358:161-169, 1996.

25. Waldren C, Correll L, Sognier MA, Puck TT: Measurement of low levels of x-ray mutagenesis in relation to human disease. Proc Natl Acad Sci U S A 83:4839-4843, 1986.

26. Waldren C, Jones C, Puck TT: Measurement of mutagenesis in mammalian cells. Proc Natl Acad Sci U S A 76:1358-1362, 1979.

27. Waldren C, Vannais D, Drabek R, Gustafson D, Kraemer S, Lenarczyk M, Kronenberg A, Hei T, Ueno A: Analysis of mutant quantity and quality in human-hamster hybrid AL and AL-179 cells exposed to 137Cs-gamma or HZE-Fe ions. Adv Space Res 22:579-585, 1998.

28. Waldren CA, Puck TT: Steps toward experimental measurement of total mutations relevant to human disease. Somat Cell Mol Genet 13:411-414, 1987.

29. Wedemeyer N, Greve B, Uthe D, Potter T, Denklau D, Severin E, Hacker-Klom U, Kohnlein W, Gohde W: Frequency of CD59 mutations induced in human-hamster hybrid A(L) cells by low-dose X-irradiation. Mutat Res 473:73-84, 2001.

30. Wilson AB, Seilly D, Willers C, Vannais DB, McGraw M, Waldren CA, Hei TK, Davies A: Antigen S1, encoded by the MIC1 gene, is characterized as an epitope of human CD59, enabling measurement of mutagen-induced intragenic deletions in the AL cell system. Somat Cell Mol Genet 25:147-157, 1999.

CHAPTER 4

KINETICS OF CD59 EXPRESSION IN CHO A_L CELLS ALTERED WITH PHOSPHOLIPASE C AND RNAi

Abstract

The expression of the human cell surface antigen, CD59, on Chinese hamster ovary A_L cells is well characterized as an effective tool to measure mutations in human chromosomes using the Flow Cytometry Mutation Assay. However, the temporal expression of CD59 mutants varies substantially between different mutagens such as lead acetate and N-methyl-N'-nitro-N-nitrosoguanidine (MNNG). This observation led me to analyze the kinetics of expression and loss of CD59 on the cell surface.

To confirm that CD59 is attached via a glycosylphosphotidyl inositol linkage, A_L cells were treated with 0.1% Triton-X; those cells that were resistant to detergent are located within the lipid rafts. Both CD59 and CD81, a transmembrane protein, were analyzed by detecting fluorescence of directly conjugated monoclonal antibodies, CD59-phycoerytherin and CD81-Alexa 647. CD81 had an 84% reduction in fluorescence intensity whereas CD59 fluorescence did not decrease, indicating that CD59 is located within the lipid raft. I then analyzed the CD59 protein turnover by cleaving the CD59 protein using phosphatidyl inositol phospholipase C (PI-PLC). After staining wild-type cells with phycoerythrin-conjugated monoclonal antibodies to CD59, I measured the temporal protein expression on a

Dako CyAn flow cytometer. PI-PLC reduced the protein expression by 90% by 2 hr and cells recovered within 8 hr and returned to control fluorescence by 24 hr after treatment. I then silenced the CD59 mRNA using Dharmacon Smart Pool siRNA for CD59. The protein expression decreased to background levels beginning at 5 hr post treatment and continued to about 15% of the control expression at 48 hr. After using RNAi to determine that CD59 protein turnover is less than 48 hr, I then analyzed cell cycle changes between cells treated with lead acetate and MNNG. Cells were stained with propidium iodide and then analyzed on the EPICs Coulter V flow cytometer. Cells treated with lead acetate had alterations lasting one day, whereas cells treated with MNNG had a prolonged G2 block of 4 days.

These results suggest that the temporal expression of CD59 is more likely dependent on the cell cycle modulation and not the lifetime of the surface protein or the mRNA of CD59.

Introduction

Mammalian mutagenesis assays are a requirement of the Food and Drug Administration (FDA) for all new pharmaceutical and chemicals being introduced to the market. Previously, I (19) and other researchers (33,29) have demonstrated that the Flow Cytometry Mutation Assay (FCMA) system effectively detects mutations caused by numerous chemicals with a higher degree of sensitivity and with less time required than the Mouse Lymphoma Assay (10) and the A_L clonogenic assay (29,32). Briefly, the cells are treated with a suspect mutagen and 7-10 days later are analyzed for the loss of CD59, a GPI (glycosyl phosphatidyl inositol)-linked cell surface marker.

As shown in Chapter 3, the mutant yield peaks at different times depending on the type of mutagen. For example, a standardized treatment of lead acetate (data courtesy of C. Tenley French) causes a maximum mutant yield by day 5 whereas MNNG (N-methyl-n-nitroso-

guanidine) takes approximately 9-12 days before a peak in mutant expression (Figure 4-1). Using a flow cytometry based assay, the CD59 mutant expression may be measured at any time point allowing the kinetics of CD59 to be measured and analyzed.

CD59 is located on chromosome 11 in the CHO A_L cells at 11p13.5 and in human erythrocytes is in charge of protecting the cell from complement mediated lysis. CD59 is a GPI-linked cell surface protein of about 18-20 kDa with various forms of glycylalation, giving three different conformations (21).

The GPI-anchor was first discovered in 1988 (4) and is found in diverse functioning proteins including enzymes, adhesion molecules, receptors, surface antigens and other proteins. Biosynthesis of the GPI-moiety takes place primarily in the endoplasmic reticulum (ER) (28). The GPI structure is fully assembled prior to attachment to the protein and requires sequential steps including many *PIG* gene products in mammalian cells (15). After the GPI moiety is created it is attached to the pre-protein on a hydrophobic stretch and is anchored in the lumen of the ER (28). Trafficking from the ER to the plasma membrane is determined by the trans-Golgi network (TGN) to segregate the molecules for different areas of the cell (24). Proteins are recognized by a particular sequence motif on the cytoplasmic domain by specific cytosolic sorter proteins. Using the placental alkaline phosphatase (PLAP) marker, researchers have located GPI-APs in mammalian cells at the cell surface, the ER, the Golgi and in exo- and endocytic structures (30).

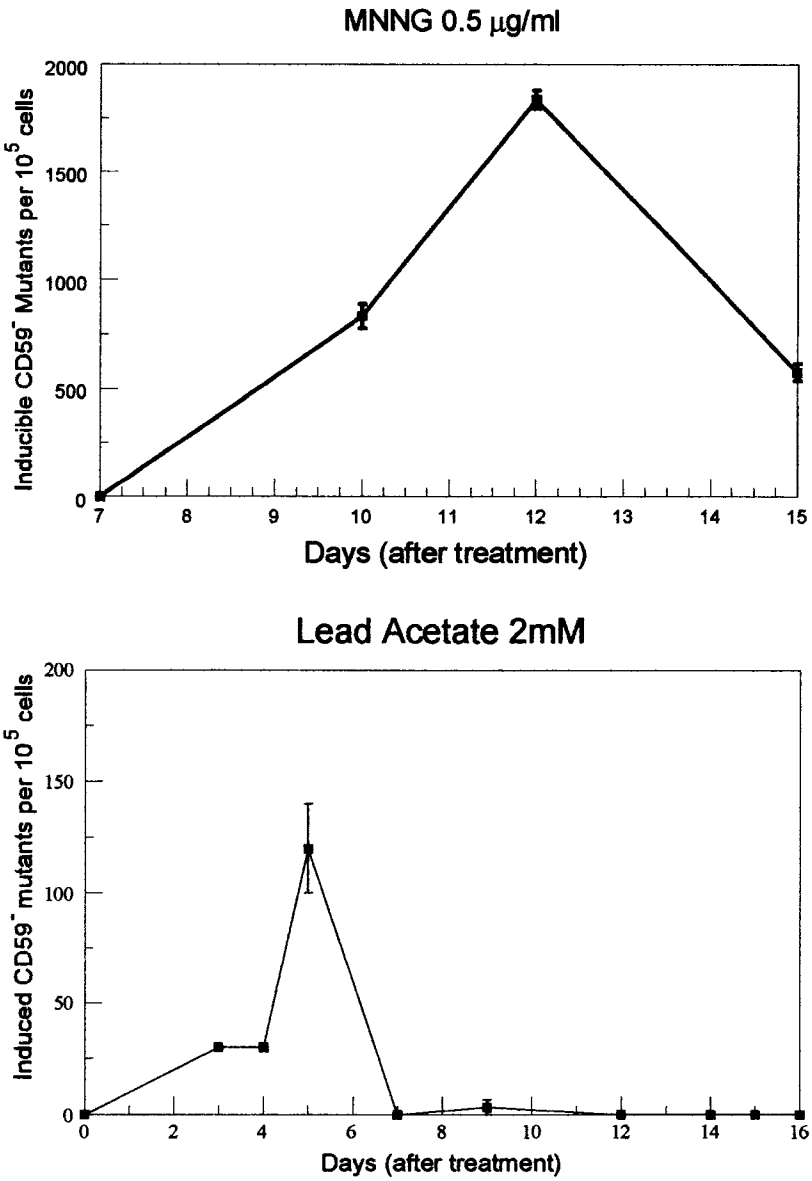

Figure 4-1. Temporal expression of CHO A_L cells treated with lead acetate and MNNG and assayed for CD59 mutant expression using the Flow Cytometry Mutation Assay (FCMA). Experiments done in triplicate with error bars representing the standard error of the mean. Mutant yield was measured by the number of $CD59^-$ cells per 10^5 over numerous days.

Packaging and presentation of the GPI-linked protein is essential in understanding the overall control of the CD59 protein kinetics. There is no general consensus explaining how CD59 and other GPI-associated proteins (GPI-APs) are endocytosed (22). Given their uniform, diffuse distribution at the cell surface, CD59 may be internalized by any number of routes of endocytosis available. CD59 may be endocytosed using dynamin and clathrin-independent means (12). Proteins that are associated with detergent resistant membranes (DRMs) may be endocytosed via a clathrin-independent RhoA-regulated pathway followed by DRM- associated interleukin receptors, IL2-R (11). Finally, Nichols *et al.* suggest that the CD59 proteins are endocytosed directly to the Golgi bodies and then recycled between the plasma membrane and the Golgi bodies at a rate of 8 min per cycle with a return rate to the plasma membrane of under 1 min (16). They also demonstrated that the CD59 protein is not newly synthesized, but instead is taken from an already translated pool of CD59 proteins within the Golgi Bodies. It may be possible that the mutant expression is delayed due to these existing populations. By removing all normal CD59 from the cell, I can measure how long it takes for the CD59 to be newly transcribed and presented on the outside of the cell. This information may then give us the minimum time required for mutant expression to occurs. I propose to deplete cells of CD59 by lysing the CD59 proteins with PI-PLC (phosphotidyl inositol phospholipase C) and then measuring the rate of CD59 recovery using the FCMA.

GPI-linked proteins are usually located within a lipid raft domain in the plasma membrane. Fivaz *et al.* (7) found that lipid raft association of GPI-APs modulates the location and kinetics of endocytosis, with GPI-APs sorted to different endosomes depending on how much time the GPI-AP was associated with the raft. A flow cytometry technique

termed Flow Cytometry Detergent Resistance (FCDR) (9) allows researchers to quickly determine if a cell surface protein is lipid-raft associated. By adding 0.1% Triton-X and measuring fluorescence intensity of fluorescent-labeled CD59 before and after the treatment, I can quickly determine if the CD59 antigen is lipid raft associated within the A_L cells.

Another possible rate limiting step is the lifetime of the mRNA for CD59. On average, the mRNA turnover is approximately 10 hr for cultured cells, but may range from 30 minutes to 24 hr depending on the type of protein (2). mRNA degradation is dependent on elements that stabilize or destabilize the mRNA and the mRNA binding proteins. Turnover of the CD59 mRNA may determine how rapidly the synthesis of the encoded protein can be shut down after transcription ceases (2). An effective method for shutting down the mRNA is using RNAi and measuring the rate of loss of CD59 using the FCMA. Through RNAi degradation of CD59 mRNA silencing, I may estimate the shortest time required for the loss of CD59 from the plasma membrane and thus of the mutant expression.

Another factor that may be important for the mutant expression time after treatment with a toxic agent is alterations in cell cycle traversal. Differing levels of damage could cause some treated cells to respond slower than others, giving a variation in the cell cycle and relative growth. Activation of DNA damage checkpoints that halt cell growth might explain the variation in mutation expression. I analyze the cell cycle for both the lead acetate and MNNG and measure cell cycle progression using flow cytometry.

The FCMA allows us to rapidly analyze cells for genotoxic effects by different mutagens without laborious processes. In this paper, I use flow cytometry to describe the kinetics of CD59 expression by analyzing the protein expression using mRNA silencing and CD59 lysis,

cell cycle alterations, and lipid raft association to clarify temporal differences in CD59$^-$ mutant expression.

Methods

Cell culture, antibody labeling and flow cytometry standard protocols are explained in Chapter 2.

Phosphotidyl Inositol Phospholipase C

To lyse the GPI-anchor of CD59, 4 x 10^6 CHO A_L cells were trypsinized and spun down in 15 ml conical tubes. The cells were then resuspended in phosphate buffer solution (PBS) at 4 x 10^6 cells per ml. One unit of PI-PLC (1-Phosphatidyl-D-*myo*-inositol inositol phosphohydrolase CAS Number 9001-86-9 (5)) was added to 1.2 ml microcentrifuge tubes and equivalent volume of PBS was added to the control. Cells were then incubated for 2 hr at 37° C, shaking every 15 minutes. After 2 hr, cells were washed two times with PBS and plated down into T25 tissue culture flasks and assayed using the FCMA protocol at differing time intervals.

CD59 Localization to lipid raft domains

Cells were grown until they reached a concentration of 4x10^6 cells per flask. They were then trypsinized and resuspended in staining buffer, and then stained with either PE conjugated CD59 antibodies(1:40 in 50 ul staining buffer) or Alexa-647-conjugated CD81 antibodies (1:2, 10 ul in 50 ul total volume, BD Pharmingen, San Jose, CA) for 30 min at 37°C. Cells were then washed and resuspended in 0.5 ml staining buffer and analyzed in the flow cytometer. The CyAn was set up to measure signals from both the 488 nm laser (PE-CD59) and the 635 nm laser (Alexa-647-CD81). Alexa 647 was detected using a 665/20 nm bandpass filter with 730nm dichroic long pass. After the fluorescence intensity of CD59 and

CD81 was measured initially, 0.1% Triton-X at was added to each sample and then incubated on ice for 5 min. Cells were then reanalyzed on the CyAn for the change in fluorescence intensity. I then calculated the detergent resistance of CD59 and CD81 using the following equation:

$FCDR = (FL_{det}-FL_{Bgdet})/(FL_{max}-FL_{bg})$ Equation 1 (9)

FL_{det} = fluorescence of cells treated with detergent; FL_{Bgdet}=autofluorescence of detergent; treated cells; FL_{max}=fluorescence of labeled untreated cells; FL_{bg} = autofluorescence of unlabeled cells.

RNAi

To analyze the loss of CD59 expression using siRNA requires a number of controls. All samples were run with untreated and mock transfected controls. To demonstrate effective transfection, positive fluorescence by Cy3 conjugated to cyclophilin b and RISC-free siRNA were measured using flow cytometry. To insure that the signals were targeting properly, I was using siCONTROL Non-targeting siRNA #1 and #2 and making sure that the CD59 signal did not decrease.

RNAi Transfection Optimization

Cells were plated into 6-well tissue culture plates at a cell density of both $1x10^5$ and $1.5X10^5$ cells per well and grown for one day. The F12 medium was replaced with exactly 1.8 ml of Opti-Mem I serum-free antibiotic-free medium. Lipofectamine (Invitrogen, Carlsbad, CA) was diluted in differing concentrations between 2.5 and 6 ul in Opti-Mem I serum-free medium and incubated for 5 min at room temperature. Each concentration was housed in a sterile 1.2 ml microcentrifuge tube to make the correct concentration for dosing into the 6-well plates, with 400 ul into each tube. Every tube received 200 ul of each

concentration of lipofectamine and siGLO RISC-free siRNA (Dharmacon, Denver, CO) in concentrations between 10-40 nM. Mixtures were incubated for 20 min at room temperature and then 200 ul of each mixture was added to 6-well plates and then incubated for 4 hr. After that time, 2 ml of F12 medium with 20% FBS was added to each well. The next day, cells were trypsinized and split into two equal aliquots to allow one sample to run on the flow cytometer and one for cell passage.

Cells were washed with PBS and resuspended in 0.5 ml of PBS and passed through a 40 μm nylon mesh filter into flow cytometry analysis tubes. The EPICS Coulter V was used with a 514 nm laser to measure the Cy3 stain conjugated to the siGLO RISC-free siRNA. Cy3 maximally excites at 550 nm with a peak fluorescence near 570 nm, but may be excited to about 50% of the maximum with the 514 nm laser. A 530nm long pass filter followed by a 575nm band pass filter were used to measure the Cy3 fluorescence. Cells were gated on forward angle light scatter (FALS) and fluorescence intensity was measured on a 3-decade log scale.

RNAi dose response

siRNA were obtained from Dharmacon (Denver, CO) including: siGENOME Smart Pool CD59, siGLO Cyclophilin b siRNA Human/Mouse, siCONTROL Non-targeting siRNA #1, siCONTROL Non-targeting siRNA#2. All siRNA were diluted in 1X RNAi buffer and aliquoted into 25 μl samples and frozen. The day prior to treatment, $1X10^5$ A_L cells were plated down into 6-well culture plates. On the day of treatment, F12 medium was removed and 1.8 ml of Opti-Mem I Reduced serum medium was added to each well. Lipofectamine was then diluted to give a total volume of 100 ul with 2.5 ul of lipofectamine for each well according to the transfection optimization. siRNA was diluted with 10 nM for controls and

CD59 siRNA was diluted in concentrations of 1 nM, 10 nM, 20 nM, 40 nM, 80 nM and 100 nM. After lipofectamine was added to each concentration, they were incubated at room temperature for 20 min. After incubation, 200 ul of lipofectamine-siRNA oligomer was added to each well drop wise and incubated 4 hr. F12 medium with 20% FBS was added to each well and they were incubated for another 24 hr.

At 28 hr after beginning siRNA treatment, cells were analyzed by flow cytometry for CD59 expression and control expression. Cells were trypsinized and split for analysis and cell passage. Untreated, mock transfected, CD59 samples, non-targeting siRNA #1 and #2 were stained as the FCMA protocol with CD59 and the cyclophilin b and RISC-free control were rinsed, filtered and prepped for flow cytometry analysis.

Cell Cycle Analysis

Stock solutions were made of both MNNG and lead acetate. MNNG stock was 1 mg/ml in H_2O and lead acetate stock was 50 mM in H_2O. Cells were treated with gentamycin 800 μM four days prior to treatment. In T75 tissue culture flasks (ISC Bioexpress) $1.5X10^6$ cells were plated for controls and $4x10^5$ cells for cell cycle analysis and cell passage. Cells were then treated with 2 mM lead acetate for 24 hr using 400 μl of 50 mM stock in 9.6 ml of F12 medium or with 0.5 μg/ml MNNG for 3 hr. After the treatment time, cells were washed and then fresh F12 medium was added. On the day of analysis, cells were trypsinized, washed with staining buffer and then stained with 5 μg/ml propidium iodide (CAS Number: 25535-16-4) for 20 min at room temperature in the dark. Cells were then analyzed on the EPICs Coulter V flow cytometer gating on forward angle light scatter and side scatter histograms and measuring $1X10^5$ cells. Histograms were analyzed using Multicycle (Phoenix Flow Cytometry, AZ) for percentages in G1, G2 and S phase.

Results

Lipid raft localization of CD59

Lipid raft localization causes cell surface antigens to be resistant to detergent treatment (9). The CD59 fluorescence intensity did not decrease when treated with 0.1% Triton-X (Figure 4-2); it was 101% of the control sample as calculated by equation 1. On the other hand, CD81, a transmembrane cell surface protein not located in lipid rafts (27), decreased fluorescence by about 84%. Thus the CD59 cell surface antigen is mostly likely located in lipid rafts of the CHO A_L cells.

CD59 protein turnover

A 2 hr treatment with PI-PLC caused a 90% decrease in CD59 by 1 hr, as measured by fluorescence intensity (Figure 4-3). CD59 expression gradually recovered at a later time. Detailed kinetics of the loss and recovery are shown in Figure 4-4. The rate of CD59 loss could be fitted by the linear equation $y=-270x+574$ with an $r^2=0.939$. After the treatment was removed by 2 hr, the cells recovered at a rate described by the linear equation $y=41.6x-103$ with $r^2=0.945$. The cells recovered CD59 expression by 24 hr with expression equal to control cells.

CD59 mRNA knockdown

To demonstrate that the RNAi technology was functioning properly, I analyzed the transfection and dose response as well as the temporal protein expression to determine the lifetime of the CD59 protein.

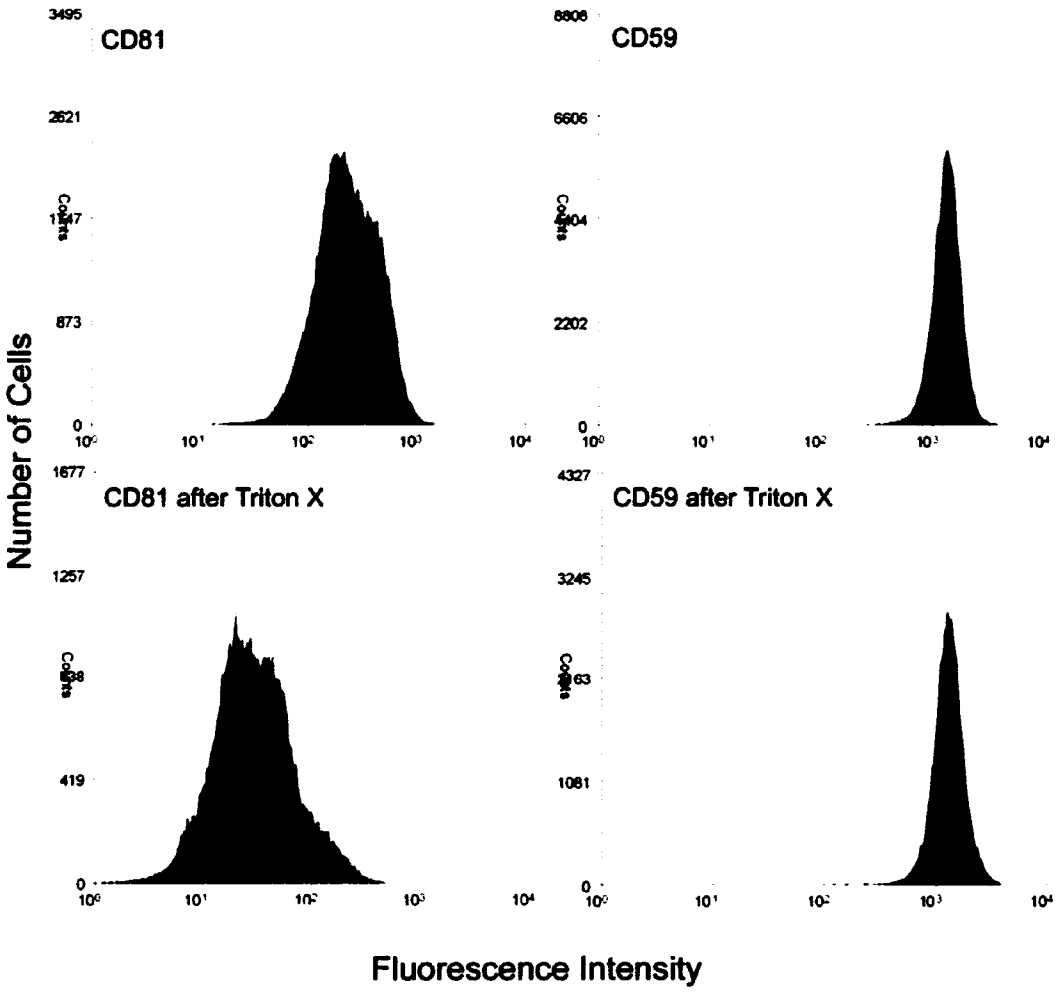

Figure 4-2. Localization of CD59 to the lipid raft using the Flow Cytometry Detergent Resistant (FCDR) protocol. Cells treated with 0.1% Triton-X were analyzed for both GPI-anchored CD59 and transmembrane CD81 using fluorescent antibodies. CD81 had a 84% decrease in fluorescence intensity after treatment with Triton-X indicating that it is not located in the lipid raft, whereas CD59 had no decrease in fluorescence intensity.

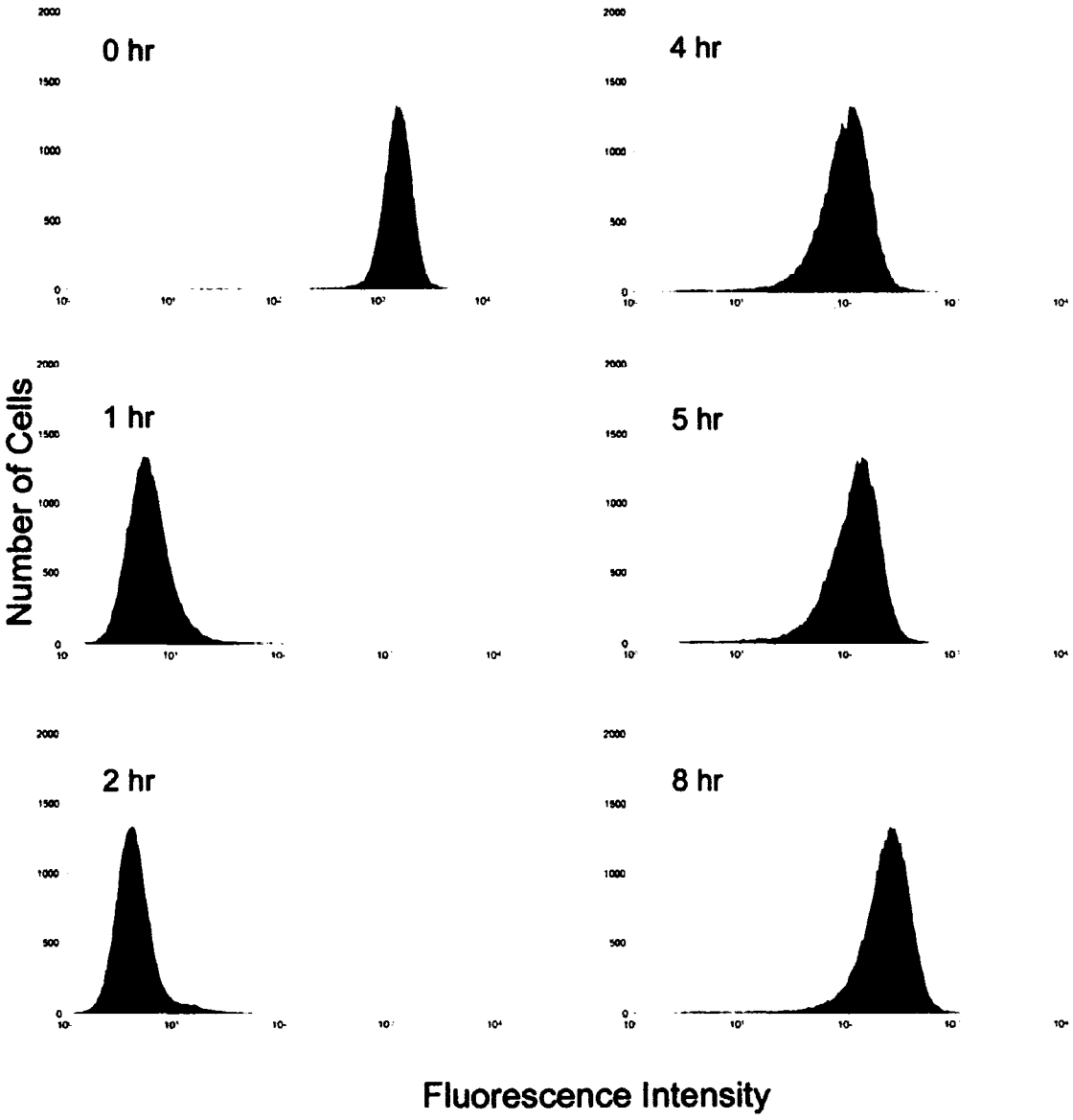

Figure 4-3. CHO A_L cells treated with phosphotidyl inositol phospholipase C (PI-PLC). Fluorescence intensity indicates CD59 cell surface protein expression at varying time points after treatment with PI-PLC.

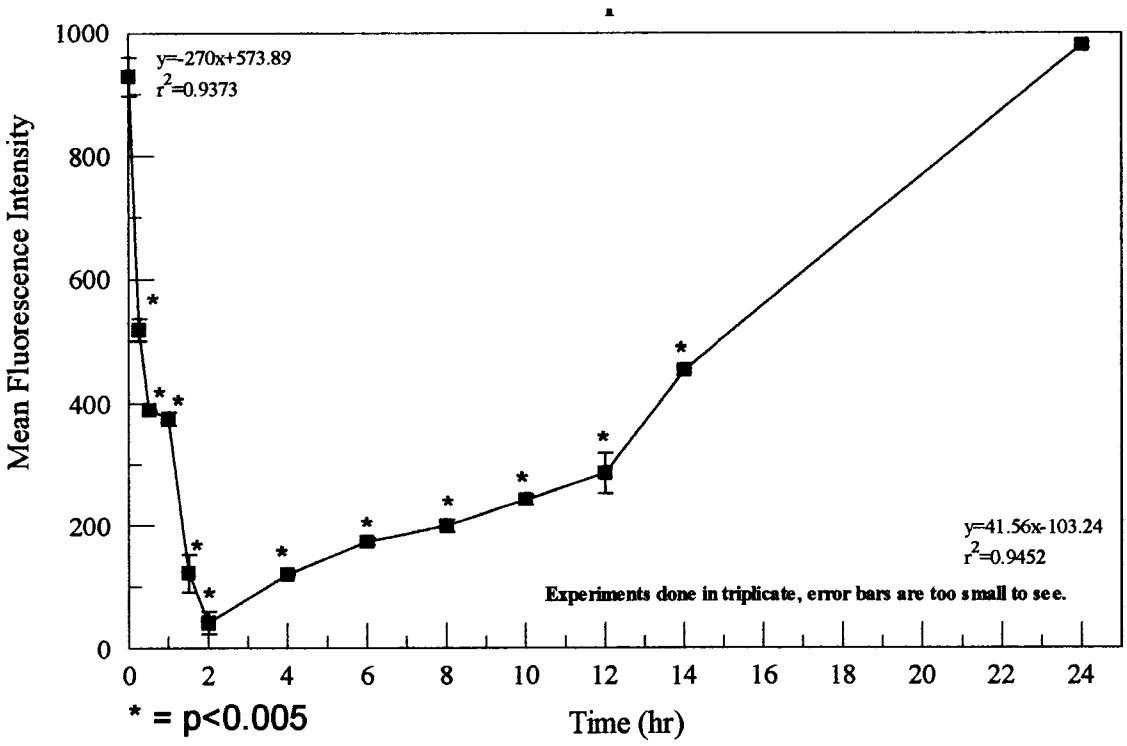

Figure 4-4. Graphical representation of PI-PLC treatment and resultant CD59 protein expression. Line represents experiments done in triplicate with error bars indicating standard error of the mean and (*) demonstrating p<0.005.

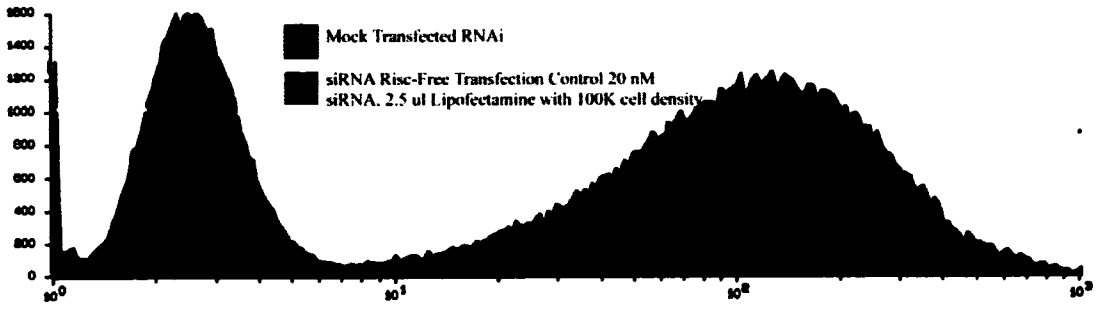

Figure 4-5. Optimization of RNAi transfection using lipofectamine. Fluorescence intensity is indicated for the siGLO RISC-free control which directly correlates with the transfection efficiency of over 95% at 24 hr.

The transfection optimization was measured as fluorescence of Cy3 caused by effective transfection of RISC-free siRNA siGLO. I chose a combination of lipofectamine, siRNA and cell density that would have the most fluorescence with the least amount of supplies required and still give sufficient transfection and silencing (Figure 4-5).

As shown in the gray sections on Table 4-1, 2.5 ul lipofectamine per sample with various concentrations of siRNA gave very high transfection rates (93-99%). Cell density of 100K gave slightly higher transfection than 200 K (93% vs 91%). The 40 nM siRNA gave the most silencing activity at (96-99%), but required twice as much siRNA as 20 nM with little difference in activity (91-93%). The optimal conditions for transfection in A_L cells were 100K cell density, 20 nM siRNA and 2.5 μl lipofectamine. All following work utilized 20 nM concentration of siRNA.

The longevity of the siRNA activity could be measured by the fluorescence of two positive controls: RISC-free siRNA and Cyclophilin B siRNA. Through a 4 day time course, the fluorescence was measured for both siRNAs. According to Table 4-2, the mean fluorescence did not decrease substantially until day 3 with both RISC-free and Cyclophilin B. This indicates that the siRNA should function through at least day 2, but has been known to continue until day 7 (18).

The next step was to determine if the siRNA knocked down the CD59 mRNA expression in a linear dose dependent manner. Using flow cytometry, there was a rapid decrease in CD59 expression as CD59 siRNA increased to 100 nM. CD59 control fluorescence had a lower CD59 fluorescence (580 fluorescence), possibly due to the toxic effects of lipofectamine. One nM CD59 siRNA only decreased the fluorescence slightly,

Lipofectamine (ul)	siRNA mM	Cell Density	Positive
0	0	100	1%
0	0	200	0%
0	20	100	0%
0	20	200	0%
2.5	10	100	84%
2.5	10	200	74%
2.5	20	100	93%
2.5	20	200	91%
2.5	40	100	98%
2.5	40	200	96%
4.25	0	100	0%
4.25	0	200	0%
4.25	10	100	87%
4.25	10	200	76%
4.25	20	100	92%
4.25	20	200	89%
4.25	40	100	95%
4.25	40	200	94%
6	10	100	79%
6	10	200	73%
6	20	100	89%
6	20	200	88%
6	40	100	97%
6	40	200	94%

Table 4-1. Transfection optimization using various concentrations of lipofectamine, RISC-free siGLO siRNA, and cell density. Optimization was measured as a percentage of cells in the positive peak. Cells highlighted in gray were the optimal concentrations.

	RISC-free siRNA *Cy3		Cyclophilin B siRNA Cy3	
	Mean Fluorescence	Percentage Positive	Mean Fluorescence	Percentage Positive
Day 1	128.6	96.50%	147.1	98.73%
Day 2	89.1	91.88%	84.6	94.42%
Day 3	20.11	60.75%	30.25	80.97%
Day 4	8.32	32.38%	10.87	47.92%

Table 4-2. Transfection optimization using RISC-free and Cyclophilin B siGLO conjugated to Cy3. There is a direct correlation to the fluorescence of Cy3 and siRNA transfection.

from 570 to 530 mean channel number, whereas doses of 10 nM-100nM decreased the CD59 expression significantly ($p<0.005$) (Figure 4-6).

With the optimal dose and transfection conditions established, a time course of CD59 knockdown was done. Examining the flow cytometry histograms (Figure 4-7), there were two distinct peaks, indicating populations that continued to be CD59 negative and positive. By day 4, that peak had disappeared and all cells were located near the control fluorescence intensity peak. Time points were taken over six days (Figure 4-8); by 20 hr post-treatment, CD59 fluorescence intensity decreased significantly over control. Loss of CD59 expression peaked at 48 hr and remained low for 2 more days before beginning to recover.

Cell Cycle Alterations by MNNG and Lead Acetate

Cells were treated with MNNG or lead acetate and the cell cycle was analyzed at various times using flow cytometry (Figure 4-9, Table 4-3). MNNG caused a block in G2 that lasted for 3 days and began to resolve by day 5. By day 7, MNNG-treated cells returned to a normal cell cycle. Lead acetate caused an increase by day 1 with no G1 or G2 block. The cell cycle was nearly normal by day 2. Clearly, the two agents modulate the cell cycle differently and this phenomenon may explain at least partially explain the temporal expression of CD59.

Discussion

The purpose of this study was to determine the kinetics of CD59 cell surface expression to pinpoint the possible rate limiting step in mutagen-induced mutant expression. Through these studies I determined that it takes less than 48 hours for CD59

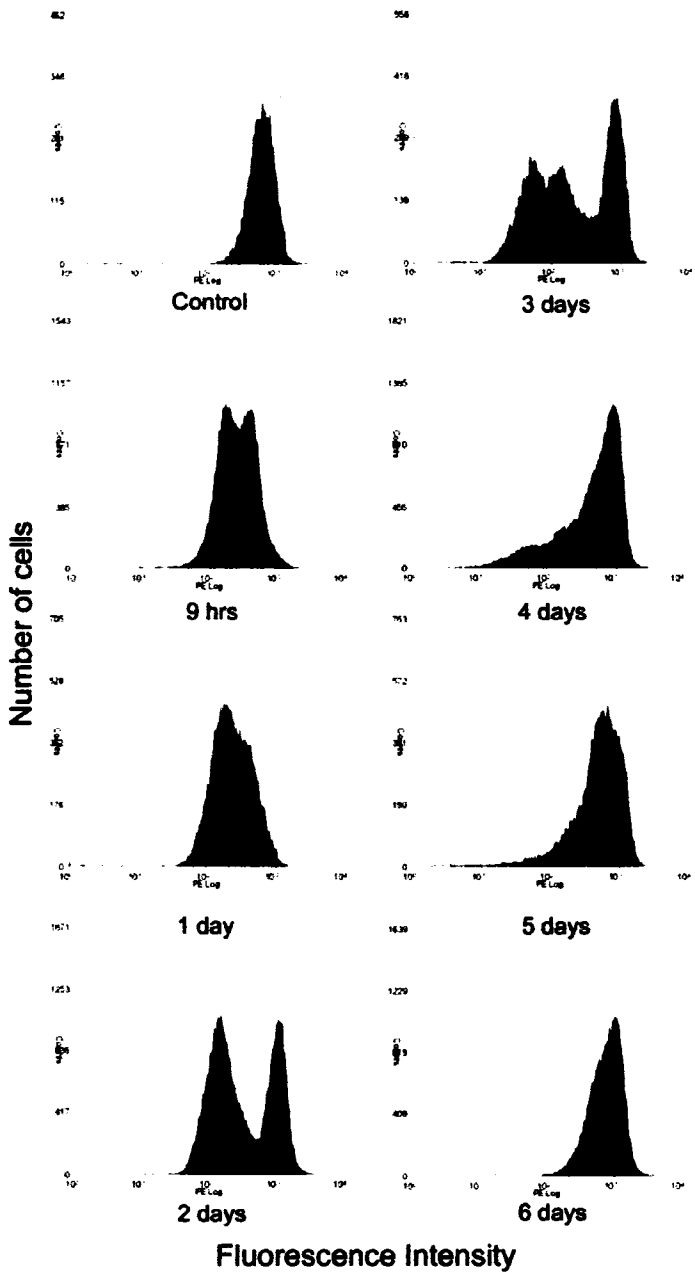

Figure 4-6. Kinetics of CD59 knockdown using RNAi. CD59 fluorescence intensity decreases until reaching its lowest level at 48 hr and continues for 2 days until it returns to control levels by day 6. Error bars indicate triplicate experiments with standard error of the mean and significance is indicated by (*) as $p<0.005$.

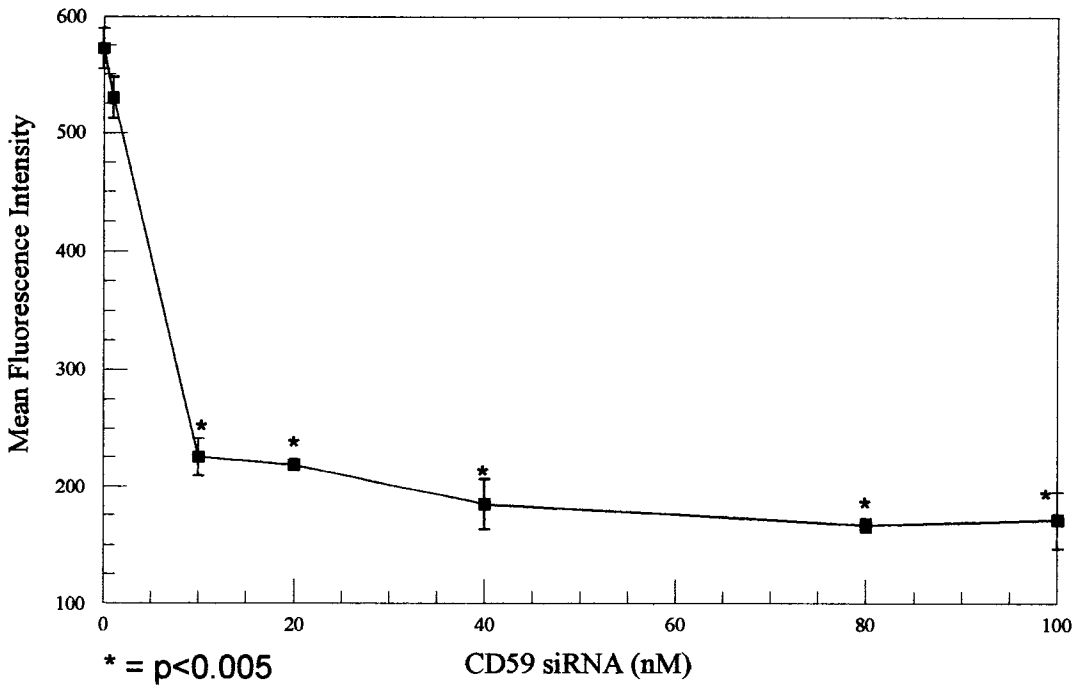

Figure 4-7. CD59 knockdown using CD59 siRNA at 1, 10, 20, 40, 80, 100 nM concentration. Error bars represent triplicate experiments with standard error and (*) indicate significance at p<0.005.

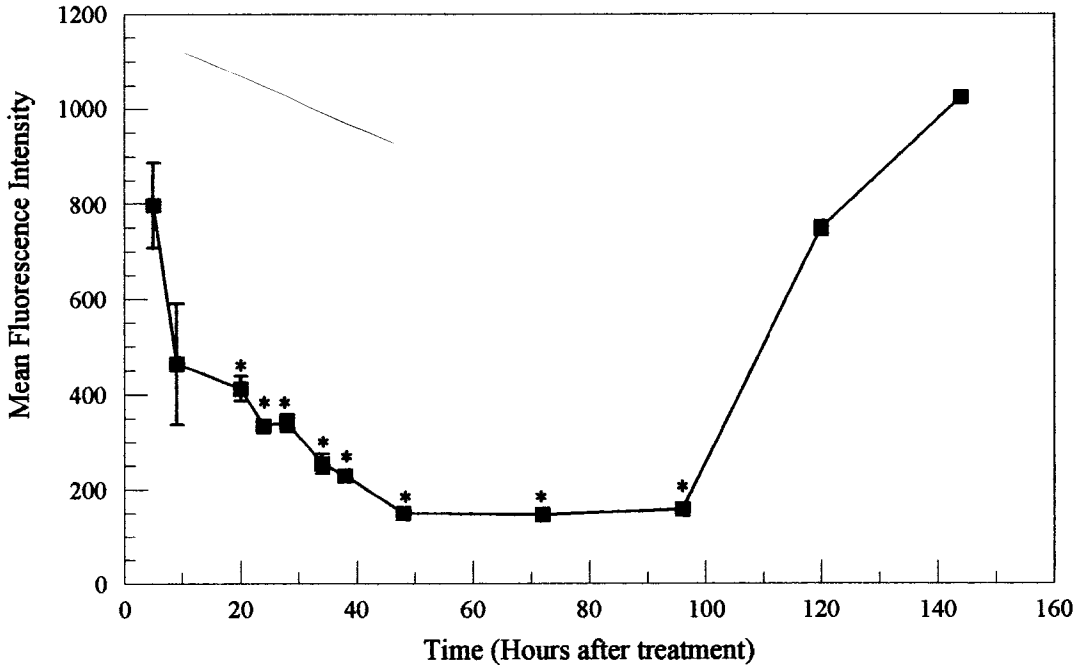

Figure 4-8. Flow cytometry histograms of CD59 knockdown using RNAi at different time points.

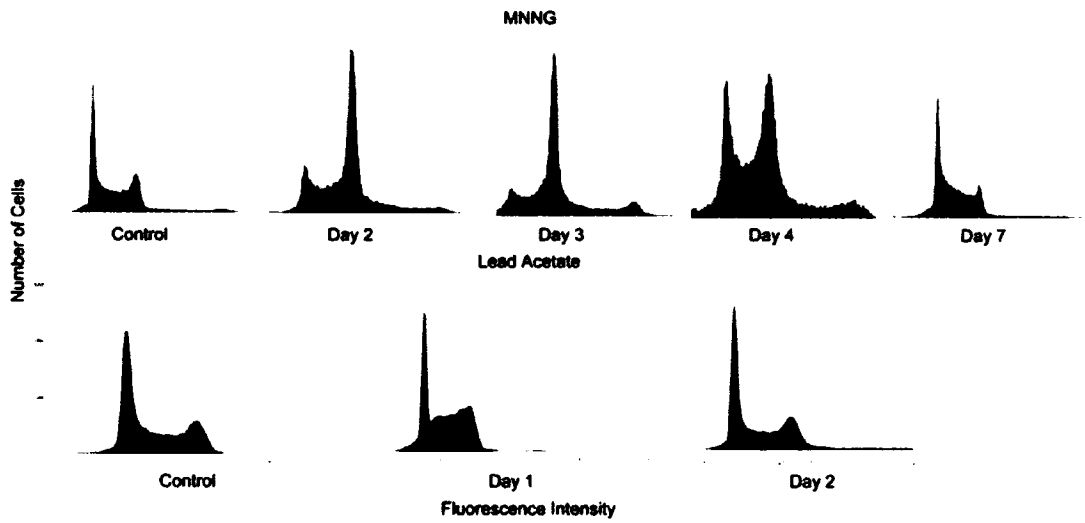

Figure 4-9. Cell cycle comparison of CHO A_L cells treated with both lead acetate and MNNG and then the cell cycle was analyzed at different time points. Propidium iodide was used to determine DNA contents of cells.

		%G1		%G2		%S		G2/G1		A%G1		A%G2		A%S		G2/G1		Chi Sq	
Day	Dose	Mean	STE	Mean	STE	Mean	STE	Mean	STE	Mean	STE	Mean	STE	Mean	STE	Mean	STE	Mean	STE
0	0	27.8	1.6	9.3	0.4	62.9	1.4	2.0	0.0									9.0	2.4
1		30.3	2.0	10.9	0.8	57.9	2.8	2.0	0.0									5.6	1.4
2		24.5	0.5	9.6	0.6	65.9	0.7	1.9	0.0									2.6	0.6
3		25.8	0.8	7.9	0.9	66.3	1.6	2.0	0.0									12.5	2.4
4		27.7	1.3	15.5	3.6	56.9	4.6	2.0	0.0									8.0	3.0
5		28.5	0.8	18.4	2.5	52.8	3.5	2.0	0.0									4.4	0.8
1	0.5 ug/ml MNNG	19.8	3.0	24.8	4.1	55.4	3.5	2.0	0.0									5.2	0.9
2		18.0	0.3	32.5	9.1	66.3	8.4	2.1	0.1	47.2	4.3	9.6	3.2	43.1	2.7	1.9	0.0	2.5	0.9
3		19.0	1.4	25.7	1.1	55.3	1.1	2.0	0.0	49.5	5.7	11.6	1.4	138.9	103.7	2.0	0.0	3.0	0.8
4		21.8	1.2	19.9	3.7	58.2	2.6	2.1	0.0	39.7	1.8	15.1	1.3	45.2	2.0	2.0	0.0	2.1	0.1
5		24.4	0.7	25.1	0.4	50.6	0.3	2.0	0.0	43.4	3.8	18.3	0.2	38.3	3.6	1.9	0.0	3.1	0.6
7		28.5		17.6		53.9		2.0											
0	2 mM LA	36.0		12.8		51.2		2.0										4.0	
1		26.1		6.8		67.0		2.0										14.3	
2		39.1		19.4		41.5		2.0										8.2	

Table 4-3. Cell cycle analysis of control, MNNG and lead acetate treated samples determined by Multicycle analysis. A = tetraploid populations.

to be lost from the plasma membrane. On the other hand, CD59 recovered within about 8 hr after lysis by PI-PLC.

The CD59 is located within cholesterol and sphingolipid enriched areas which float within a more fluid phospholipid area (23) termed lipid rafts. The appearance of the GPI-anchor on the protein seems to direct the protein to the lipid raft domains. Lipid rafts have been indicated as "hot spots" for signaling receptors acting as signaling platforms whereparticipating molecules are concentrated together (8). The GPI-anchor affects protein conformation and function and importantly seems to delay the protein turnover rate (13), essential information when studying the CD59 kinetics. Treatment with detergent (Figure 4-2) demonstrated that CD59 is located within the lipid rafts and therefore exo- and endocytosis may be modulated by this association.

The PI-PLC targets the GPI anchor point at the phosphodiester linkage in the phosphatidyl portion of the GPI anchor. The CD59 was successfully removed by 2 hr of treatment with PI-PLC and then recovered as a population, gradually increasing until it reached control levels. The enzymatic activity differed between PI-PLC, but the loss of CD59 was still significant and measurable in all experiments. The earliest we can measure mutants with the FCMA is 5 days post-treatment, so the antigen exocytosis may not be the main controlling factor.

The CD59 mRNA also controls the rate of CD59 exocytosis. Using RNAi, I successfully knocked the CD59 expression down to 15% of control levels within 48 hr of treatment. This signifies that the CD59 mRNA was silenced and affected the CD59 protein expression within 1 day. Given that transcription and translation takes nearly 1 hr, the CD59 protein turnover

Further work analyzing the cell cycle distribution for other genotoxic agents clarify the relationship between cell cycle retardation and temporal mutant expression. A comparisons of the mutant expression of CD59 and a transmembrane protein such as CD44 would also clarify the role of the GPI anchor in the temporal expression.

Reference List

1. Bonacker D, Stoiber T, Bohm KJ, Prots I, Wang M, Unger E, Thier R, Bolt HM, Degen GH: Genotoxicity of inorganic lead salts and disturbance of microtubule function. Environ Mol Mutagen 45:346-353, 2005.

2. Cao D, Parker R: Computational modeling of eukaryotic mRNA turnover. RNA 7:1192-1212, 2001.

3. Carethers JM, Hawn MT, Chauhan DP, Luce MC, Marra G, Koi M, Boland CR: Competency in mismatch repair prohibits clonal expansion of cancer cells treated with N-methyl-N'-nitro-N-nitrosoguanidine. J Clin Invest 98:199-206, 1996.

4. Chatterjee S, Smith ER, Hanada K, Stevens VL, Mayor S: GPI anchoring leads to sphingolipid-dependent retention of endocytosed proteins in the recycling endosomal compartment. EMBO J 20:1583-1592, 2001.

5. Coonrod S, Naaby-Hansen S, Shetty J, Herr J: PI-PLC releases a 25-40 kDa protein cluster from the hamster oolemma and affects the sperm penetration assay. Mol Hum Reprod 5:1027-1033, 1999.

6. Doniger J, O'Neill R, Noguchi P, DiPaolo JA: Initiation of carcinogenesis dependence upon MNNG-induced release of the G1 block of density-inhibited Syrian hamster cells. Teratog Carcinog Mutagen 3:123-131, 1983.

7. Fivaz M, Vilbois F, Thurnheer S, Pasquali C, Abrami L, Bickel PE, Parton RG, van der Goot FG: Differential sorting and fate of endocytosed GPI-anchored proteins. EMBO J 21:3989-4000, 2002.

8. Galbiati F, Razani B, Lisanti MP: Emerging themes in lipid rafts and caveolae. Cell 106:403-411, 2001.

9. Gombos I, Bacso Z, Detre C, Nagy H, Goda K, Andrasfalvy M, Szabo G, Matko J: Cholesterol sensitivity of detergent resistance: a rapid flow cytometric test for detecting constitutive or induced raft association of membrane proteins. Cytometry 61A:117-126, 2004.

10. Kirkland DJ, Clements J: Response by the authors of 'Recommendations for spacing of test chemical concentrations in the mouse lymphoma tk mutation essay (MLA)'. Mutat Res 419:181-182, 1998.

11. Lamaze C, Dujeancourt A, Baba T, Lo CG, Benmerah A, Dautry-Varsat A: Interleukin 2 receptors and detergent-resistant membrane domains define a clathrin-independent endocytic pathway. Mol Cell 7:661-671, 2001.

12. Lamaze C, Schmid SL: The emergence of clathrin-independent pinocytic pathways. Curr Opin Cell Biol 7:573-580, 1995.

13. Lehto MT, Sharom FJ: PI-specific phospholipase C cleavage of a reconstituted GPI-anchored protein: modulation by the lipid bilayer. Biochemistry 41:1398-1408, 2002.

14. Lips J, Kaina B: Repair of O(6)-methylguanine is not affected by thymine base pairing and the presence of MMR proteins. Mutat Res 487:59-66, 2001.

15. McConville MJ, Menon AK: Recent developments in the cell biology and biochemistry of glycosylphosphatidylinositol lipids (review). Mol Membr Biol 17:1-16, 2000.

16. Nichols BJ, Kenworthy AK, Polishchuk RS, Lodge R, Roberts TH, Hirschberg K, Phair RD, Lippincott-Schwartz J: Rapid cycling of lipid raft markers between the cell surface and Golgi complex. J Cell Biol 153:529-541, 2001.

17. Nikaido O, Fox BW: The time course of DNA repair following methyl nitro-nitrosoguanidine (MNNG) treatment of p388f lymphoma cells in culture. II. DNA repair synthesis and its correlation with strand breakage. Chem Biol Interact 14:47-55, 1976.

18. Paddison PJ, Caudy AA, Hannon GJ: Stable suppression of gene expression by RNAi in mammalian cells. Proc Natl Acad Sci U S A 99:1443-1448, 2002.

19. Ross CD, Lim CU, Fox MH: Assay to measure CD59 mutations in CHO A(L) cells using flow cytometry. Cytometry A 66:85-90, 2005.

20. Roy NK, Rossman TG: Mutagenesis and comutagenesis by lead compounds. Mutat Res 298:97-103, 1992.

21. Rudd PM, Morgan BP, Wormald MR, Harvey DJ, van den Berg CW, Davis SJ, Ferguson MA, Dwek RA: The glycosylation of the complement regulatory protein, human erythrocyte CD59. J Biol Chem 272:7229-7244, 1997.

22. Sabharanjak S, Sharma P, Parton RG, Mayor S: GPI-anchored proteins are delivered to recycling endosomes via a distinct cdc42-regulated, clathrin-independent pinocytic pathway. Dev Cell 2:411-423, 2002.

23. Sharom FJ, Lehto MT: Glycosylphosphatidylinositol-anchored proteins: structure, function, and cleavage by phosphatidylinositol-specific phospholipase C. Biochem Cell Biol 80:535-549, 2002.

24. Simons K, van Meer G: Lipid sorting in epithelial cells. Biochemistry 27:6197-6202, 1988.

25. Slamenova D, Gabelova A, Ruzekova L, Chalupa I, Horvathova E, Farkasova T, Bozsakyova E, Stetina R: Detection of MNNG-induced DNA lesions in mammalian cells; validation of comet assay against DNA unwinding technique, alkaline elution of DNA and chromosomal aberrations. Mutat Res 383:243-252, 1997.

26. Tomita-Mitchell A, Kat AG, Marcelino LA, Li-Sucholeiki XC, Goodluck-Griffith J, Thilly WG: Mismatch repair deficient human cells: spontaneous and MNNG-induced mutational spectra in the HPRT gene. Mutat Res 450:125-138, 2000.

27. Tsuji K, Feng MA, Wang D: Development of human lymphohematopoiesis defined by CD34 and CD81 expression. Leuk Lymphoma 43:2269-2273, 2002.

28. Udenfriend S, Kodukula K: How glycosylphosphatidylinositol-anchored membrane proteins are made. Annu Rev Biochem 64:563-591, 1995.

29. Wedemeyer N, Greve B, Uthe D, Potter T, Denklau D, Severin E, Hacker-Klom U, Kohnlein W, Gohde W: Frequency of CD59 mutations induced in human-hamster hybrid A(L) cells by low-dose X-irradiation. Mutat Res 473:73-84, 2001.

30. Weise F, Stierhof YD, Kuhn C, Wiese M, Overath P: Distribution of GPI-anchored proteins in the protozoan parasite Leishmania, based on an improved ultrastructural description using high-pressure frozen cells. J Cell Sci 113 Pt 24:4587-4603, 2000.

31. Wozniak K, Blasiak J: In vitro genotoxicity of lead acetate: induction of single and double DNA strand breaks and DNA-protein cross-links. Mutat Res 535:127-139, 2003.

32. Zhou H, Xu A, Gillispie JA, Waldren CA, Hei TK: Quantification of. Mutat Res 594:113-119, 2006.

CHAPTER 5

MULTIPARAMETER ANALYSIS OF MUTANT POPULATIONS SORTED ON CD59 EXPRESSION

Abstract

Background: A flow cytometry mutation assay was developed previously using a Chinese hamster ovary cell line (CHO A_L) that stably incorporates human chromosome 11. The assay measures mutations in the *CD59* gene on chromosome 11 by the loss of fluorescence of antibodies CD59 directly conjugated to phycoerythrin. An essential issue that needs to be addressed is why there is a peak in mutant expression after radiation-induced damage which is not detected by other mammalian mutation assays.

Methods: *CHO AL* cells were irradiated with 0-4 Gy and analyzed by the FCMA protocol. On day 6, the maximum day of expression for irradiated cells, treated cells were labeled with antibodies against CD59. The FCMA mutant region and intermediate region were separated into 6 equal regions and then 1000 cells were sorted. Fourteen days after sorting, the cells were analyzed for CD59 as well as CD90 and CD44. The CD59 mutant spectra were determined by analyzing the percentage of cells in each of four regions found in a bivariate histogram for CD44 and CD90.

Results: The radiation-induced mutant fraction peaked at day 6, dropped until day 10, and then was stable until day 17, after which it was reduced to almost background levels on day

20. The mutant and intermediate regions were divided into 6 gated regions and cells were sorted on day 6 after a dose of 4 Gy. Regions 1-3 corresponded to the normal mutant region and 4-6 corresponded to the intermediate region. The majority of the CD59 mutant population was contained in regions 1-4, with region 5 and 6 at nearly background levels for CD59 expression. The growth rate was similar between all regions and the surviving fraction dropped to 50% of control cells. The multiparameter analysis of CD59/CD44/CD90 indicated that region 1-3 and 4 have similar phenotypes and region 5 and 6 were quite similar. The change in phenotypic expression of CD59/CD44/CD90 over time indicated that the loss of mutant expression could partially be explained by the loss of triple mutants from the sorted populations from 48% on day 6 to 5% on day 24.

Conclusions: To give a more accurate measurement of the mutant frequency, the FCMA mutant region was redefined to incorporate a larger portion of the mutant peak on the CD59 histogram. The reduction in mutant frequency from the peak expression may be explained by the inclusion of triple mutants which are mostly lethal. Radiation-induced $CD59^-$ mutants have an unstable intermediate mutant expression that is lost after extended culturing. The FCMA gives researchers the tools to measure mutant yield and mutant spectra rapidly and efficiently and provides new insights into the mechanisms of action of mutagenic agents.

Introduction

In the previous chapters, I have developed and quantified a flow cytometry mutation assay (FCMA) that utilizes the A_L cell line to measure mutations in *CD59*. One puzzling aspect of the data is that all mutagens have a mutant expression period with a peak at different time points. As addressed in Chapter 4, it may be likely that the time for mutant

expression is modulated by cell cycle regulation. An essential component that needs to be addressed is why there is a peak in mutant expression after radiation-induced damage which is not detected by other mammalian mutation assays.

The Mouse Lymphoma Assay (MLA) and the A_L clonogenic assay use trifluorothymidine or rabbit complement to kill cells that lack either the *tk* or *CD59* gene, respectively. The number of clones determines the mutant fraction after treatment. The cells used in the MLA may form either small or large colonies, reflecting clastogenic (chromosomal) damage or mutational events involving the *tk* locus, respectively (1). Outside of this simple small/large colony detection, both the MLA and the A_L clonogenic assay are unable to characterize the type of mutants without further genetic work using PCR. The FCMA, on the other hand, is able to measure the kinetics of CD59 mutant expression at any time point after irradiation or other treatment.

Unlike the MLA and the CHO A_L clonogenic assay, the FCMA mutant measurement is defined by cells that fall into a gated region on a histogram (Figure 5-1). The CD59 mutant region (CD59 negative cells) is located on the left of the histogram, with the CD59 positive cells on the right. The "intermediate region" is located in between the two peaks. This histogram, taken from radiation induced damage on day 6 from a previous chapter, shows that the mutant peak is located within the gated mutant region. However, where to set the boundary of the mutant region is a somewhat difficult and complicated issue.

In flow cytometry, a specific region or gating determines what statistics are measured. In Chapter 3, I set the CD59 mutant region so that it included 97% of the unstained

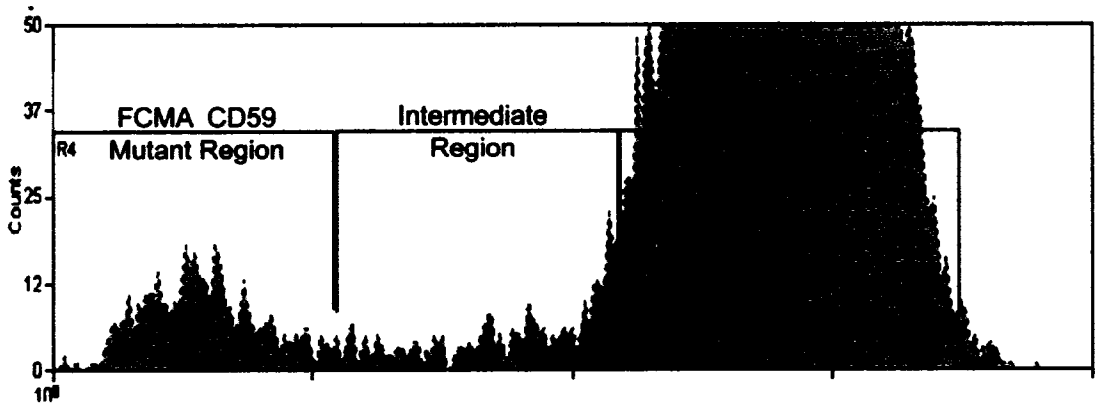

Figure 5-1. A typical flow cytometry histogram from A_L cells treated with radiation and grown for six days. The CD59 mutant region is set at 1% of the mean positive peak; the intermediate region is between the positive and negative peaks.

population. After analyzing several mutagens, I found that the mutant region was bisecting some of the mutant peak, possibly causing an underestimation of the mutant yield. By setting the region on the unstained mutants, however, did not take into account possible staining variability. The positive peak fluorescence shifts slightly with each experiment and could affect the fluorescence of the mutant population.

In 2001, Wedemeyer *et al.* (13) used a similar flow cytometry mutation assay utilizing the CHO A_L cell line and gated on 10% of the positive mutant peak. They estimated the CD59 mutant fraction for X-ray mutagenesis (4 Gy) as 2% or 2000 mutants per 10^5 cells analyzed. In comparison, Waldren *et al.*(11), using the same cell line but using the clonogenic assay, measured only 400 mutants, or 0.4% mutant yield after the same dose. Although there might be some variation in the experiments between laboratories, such a discrepancy leads me to believe that 10% of the mean positive peak may overestimate the mutant yield due to an increase in spontaneous $CD59^-$ background.

In this chapter, I examine the kinetics of mutant yield, the mutant spectra, cell survival and relative growth of cells from both the CD59 mutant and intermediate regions, in hopes of defining the most accurate mutant region and the underlying cause of the peak during mutant expression.

Methods

General methods of the FCMA are described in Chapter 2. The mutant region was set at 1% of the mean positive peak.

Radiation Extended Time Course

CHO A_L cells were irradiated with 0-4 Gy doses as described in Chapter 2, then plated into flasks for mutation analysis on various days after treatment. Cells were trypsinized and

triplicate samples were analyzed over a period of 20 days using the FCMA protocol. Statistical significance was determined by the Students T-test measuring control versus treated populations.

Radiation-Induced sorted cell survival and growth curve

On day 6, the maximum day of expression for irradiated cells, treated cells were labeled with antibodies against CD59 under aseptic conditions and then sorted using either the EPICS Coulter V cell sorter (early experiments) or the Dako High Performance MoFlo™ cell sorter (later experiments after it was available). The FCMA mutant region and intermediate region (Figure 5-1) were separated into 6 equal regions and then 1000 cells were sorted for each region. Concurrently, 300 cells were sorted into 35 mm tissue culture plates in triplicate, then grown into colonies for survival analysis. After sorting, cells were analyzed for their rate of growth by using an electronic cell counter (Particle Data) to count cell populations at varying time intervals. The cells used for survival analysis were grown for 7 days and colonies were counted to give the surviving fraction, after correcting for plating efficiency. The sorted populations were allowed to grow for 8 days and then were analyzed using the FCMA protocol and also passed for continued analysis. At that time, from at least $1x10^4$ cells, the entire negative peak of each region was again sorted to ensure that the normal population would not outgrow the negative population. Fourteen days after sorting, the cells were analyzed for CD59 as well as CD90 and CD44.

Multicolor Staining

To stain cells simultaneously with CD59, CD44 and CD90 antibodies, CD59-PE (Caltag, Burlingame, CA 1:40 dilution), CD44 biotin (Serotec, Raleigh, NC, 1:5 dilution), and CD90-Alexa 647 (Serotec, Raleigh, NC, 1:5 dilution) directly-conjugated monoclonal antibodies

were added to a total volume of 50 µl in staining buffer. The cells were incubated for 30 min on ice and then 1 ml staining buffer was added. After centrifugation and aspiration, cells were resuspended in 99 µl staining buffer and 1 µl Alexa 488 Streptavidin (Molecular Probes, Invitrogen, Carlsbad, CA, 1:100) and stained for 30 min on ice. All buffers and staining solutions were kept on ice throughout the experiment.

Mutant Spectra Analysis

The CD59 mutant spectra were determined by analyzing the percentage of cells in each of four regions found in a bivariate histogram for CD44 and CD90. On the day of peak mutant expression, $5x10^5$ cells were analyzed for the presence or absence of CD59, CD44, and CD90. Eighteen days later, the sorted populations were evaluated again for their mutant spectra. At that time, only $CD59^-$ cells were analyzed for CD44 and CD90 using bivariate histograms.

Results

The overall focus of this chapter is to determine the most accurate mutant yield defined by the FCMA CD59 mutant region and to explain the kinetics of CD59 expression. I separated the CD59 mutant and intermediate regions into six regions and then used flow cytometry to characterize the CD59/CD44/CD90 mutant spectra, survival, and relative growth. In the process, I also detected the CD59 mutant kinetics over time.

Radiation Time Course

The expression of CD59 negative cells after gamma radiation was measured over a time period of 20 days (Figure 5-2), longer than the 15-day time course done previously (Ross *et al.* 2005 (7), Chapter 3). The radiation-induced mutant fraction peaked at day 6, dropped until day 10, and then was stable until day 17, after which it was reduced to almost

background levels on day 20. There was a linear dose response from 0-4 Gy for the induction of CD59 mutants on day 6 (Chapter 3), with continued CD59 mutants until at least day 17. The mutant yield for all doses was significantly above background on day 3 and continued through day 20.

Flow cytometry histograms (Figure 5-3) show the kinetics of CD59 expression from day 0-10 of the radiation time course. There was an increased population of cells in both the mutant and intermediate CD59 regions by day 3. As time passed, the population grew into a definable mutant peak by day 5 and by day 6 was a clear peak in the mutant region. On day 7, the mutant peak broadened and only half of the mutant peak was measured by the mutant region. The mutant peak diminished by day 10, although it was still visible.

Characterization of Sorted Regions

The mutant and intermediate regions were divided into 6 gated regions and cells were sorted on day 6 after a dose of 4 Gy. Regions 1-3 (Figure 5-4) corresponded to the normal mutant region and 4-6 corresponded to the intermediate region. The majority of the CD59 mutant population was contained in regions 1-4, with region 5 and 6 at nearly background levels for CD59 expression.

After a growth period, the sorted regions were analyzed for the expression of CD59 using flow cytometry. The histograms (Figure 5-5A) show the CD59 expression 8 days post-sort and 14 days post-radiation treatment. Region 1 was mostly negative for CD59, with only 10% $CD59^+$ cells. Regions 2-5 had approximately 50% $CD59^-$ cells with varying intermediate expression within the peak. Region 6 was no different from control as 99% of the population was $CD59^+$. The entire $CD59^-$ peak was then sorted to prevent the positive

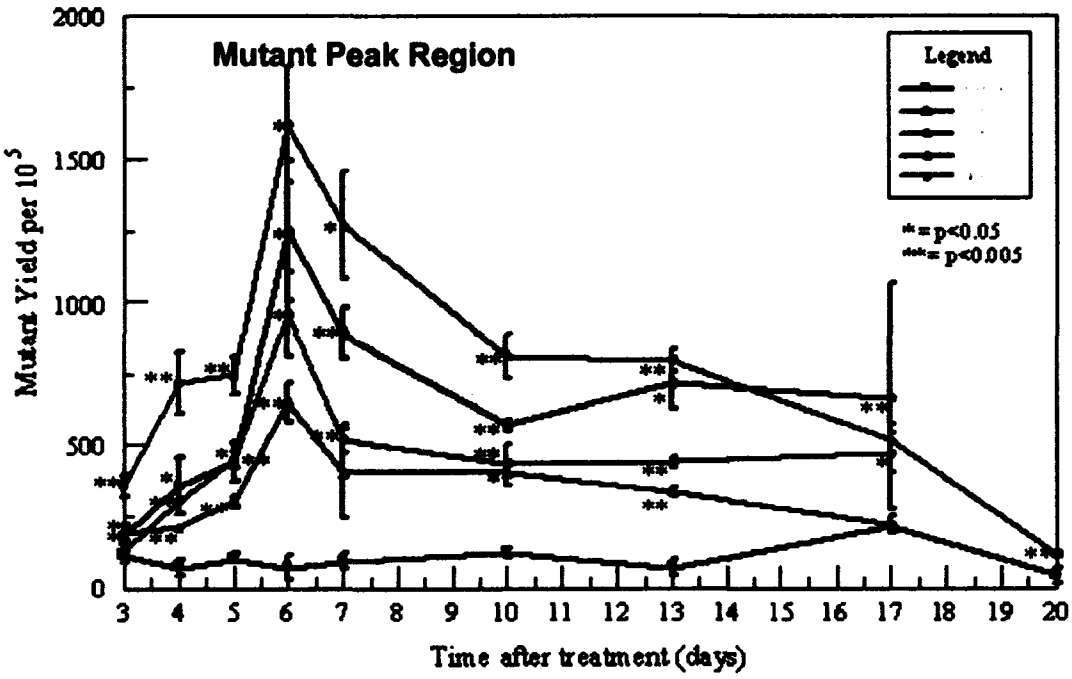

Figure 5-2. CHO A_L mutant yield induced by gamma radiation and CD59 expression measured at various time points after irradiation. CD59 expression was measured in triplicate after doses of 0-4 Gy. The "mutant peak region" is defined by the shaded area. Statistically significant differences were determined using the Student's T test.

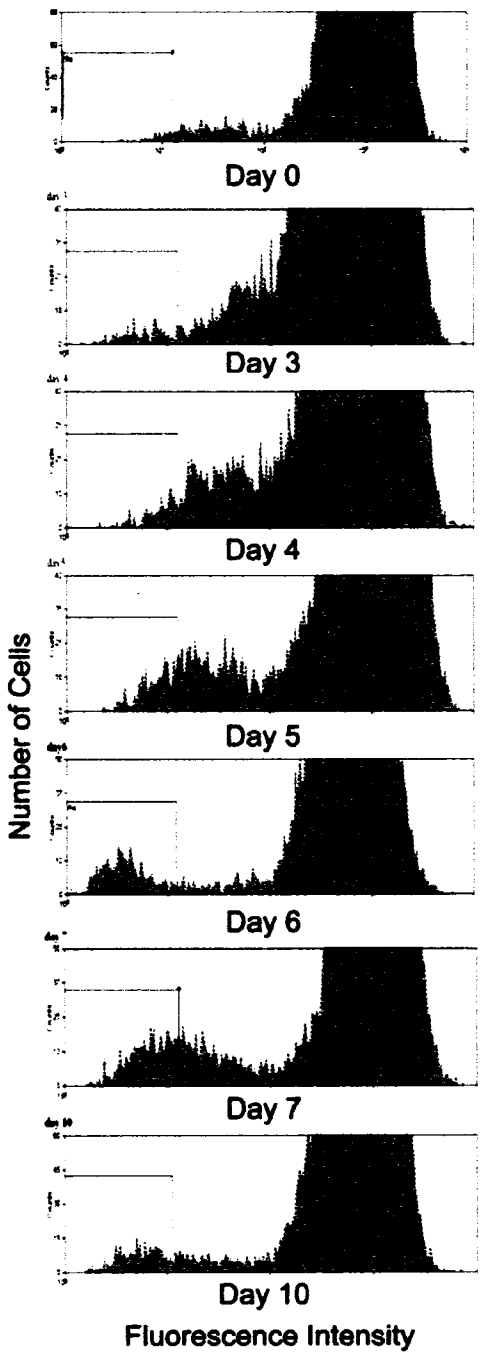

Figure 5-3. Flow cytometry histograms of CD59 expression after a dose of 4 Gy. The mutant peak shifts from the intermediate region into the CD59 mutant region by day 6. Histograms such as these were used for data in Figure 5-2.

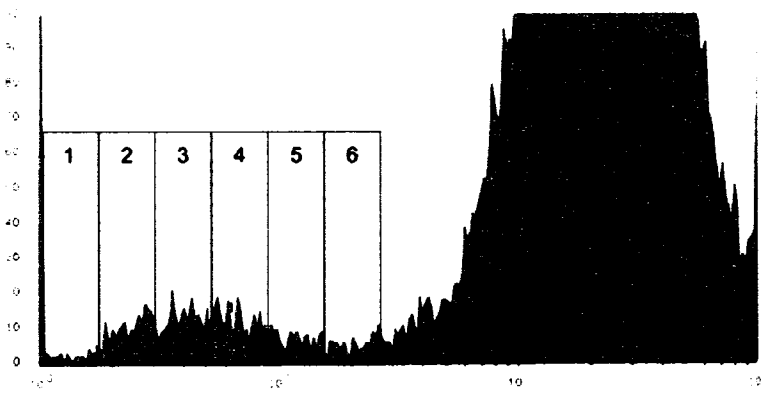

Figure 5-4. Flow cytometry histogram of day 6 CD59 expression after gamma irradiation of 4 Gy. The mutant peak and intermediate regions were sorted into regions 1-6. Sorting was done with an EPICS V cell sorter.

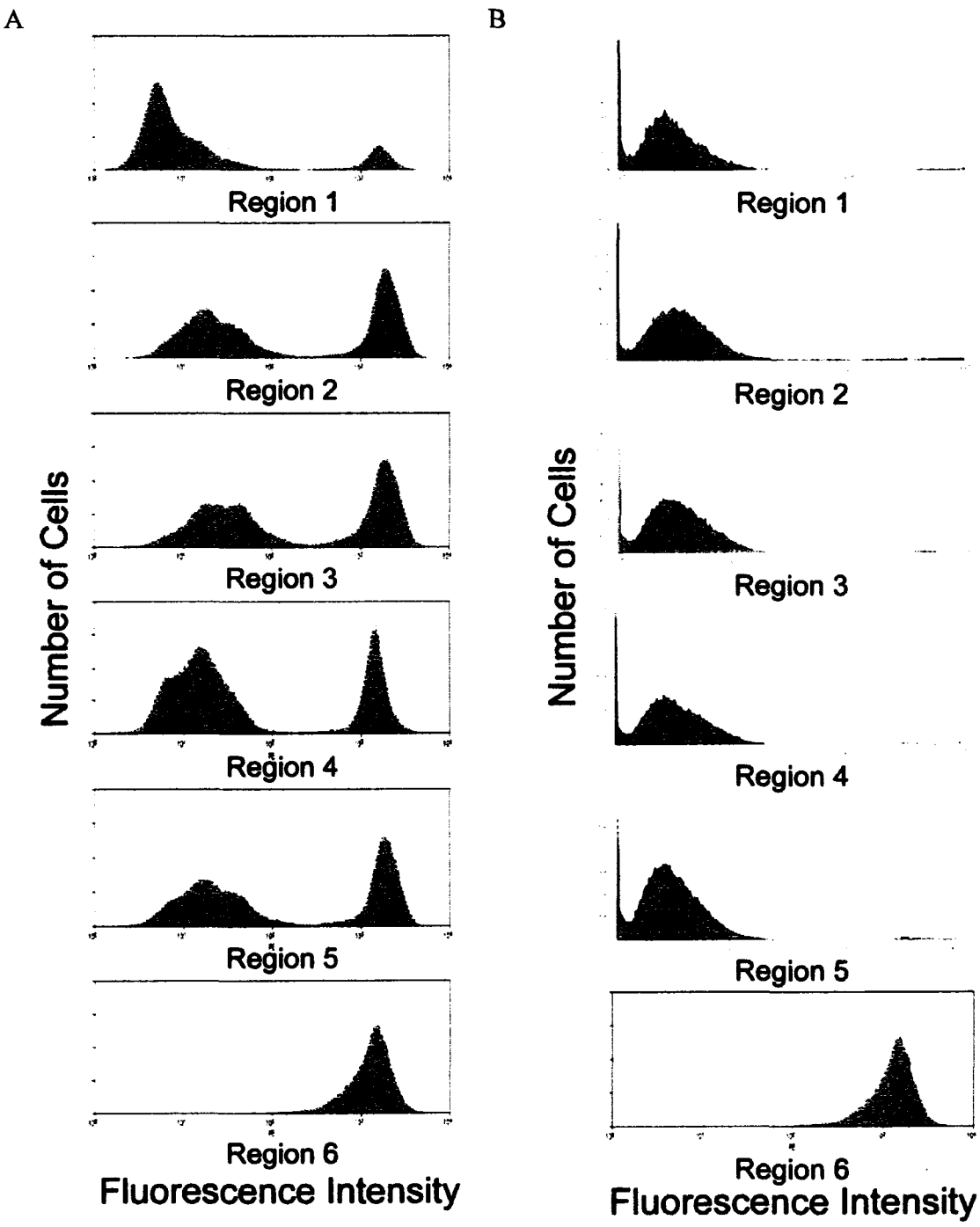

Figure 5-5. A. Flow cytometry histograms of CD59 expression 8 days after sorting from Regions 1-6 of Figure 5-4 (14 days post-irradiation). B. Flow cytometry histograms of CD59 expression from sorted regions, 14 days post-sort and 20 days post-irradiation. At least $1x10^4$ cells from the entire lower populations in Figure 5-5a were sorted, then grown and analyzed for CD59 expression.

cells from outgrowing the mutants. On day 14 post-sort and 20 days post treatment, the cells were analyzed again for CD59 expression (Figure 5-5B). Regions 1-5 after the resort were completely negative for CD59. The intermediate $CD59^-$ expression present 14 days post-treatment had disappeared. Region 6 remained entirely $CD59^+$ cells.

The growth rate and survival of cells from the sorted regions were also determined. Each of the populations started with the same number of cells and they were counted at various time points (Figure 5-6). There was little difference between the growth in all regions.

Three hundred cells from each region in Figure 5-4 were sorted into 35 mm tissue culture plates and allowed to grow until colonies formed (Figure 5-7). Cells sorted from the $CD59^+$ peak (Region 0), had a survival of 100% after correcting for plating efficiency. Cells from Regions 1-6 had decreased survival compared to Region 0. Cells from Region 1 had the lowest survival (20%). Cells from the remaining regions had about 50-60% survival.

Using the same regions, irradiated cells (4 Gy), were sorted into four regions, 1-3 corresponding to the CD59 mutant region and 4-6 dividing the intermediate region defined in Figure 5-1. Six days after irradiation, cells were stained with antibodies against CD59, CD44 and CD90. The mutant peak (Figure 5-8) was localized to regions 1-3 and 4 with region 5 and 6 containing a shoulder of the positive CD59 peak. Each of the regions is color coded for analysis in Figure 5-9.

Table 5-1 describes the phenotypic expression of CD59, CD44 and CD90 found in Regions 1-3, 4, 5 and 6. Spontaneous mutants were determined from untreated control samples analyzed for $CD59^-$. The background levels increased from 0.6% corresponding to 60 in $1x10^5$ cells to 1.22%. Region 1-3 contained 0.80% $CD59^-$ cells, corresponding to data measured in Chapter 3. The 0.80% CD59 mutant region was further analyzed for CD44 and

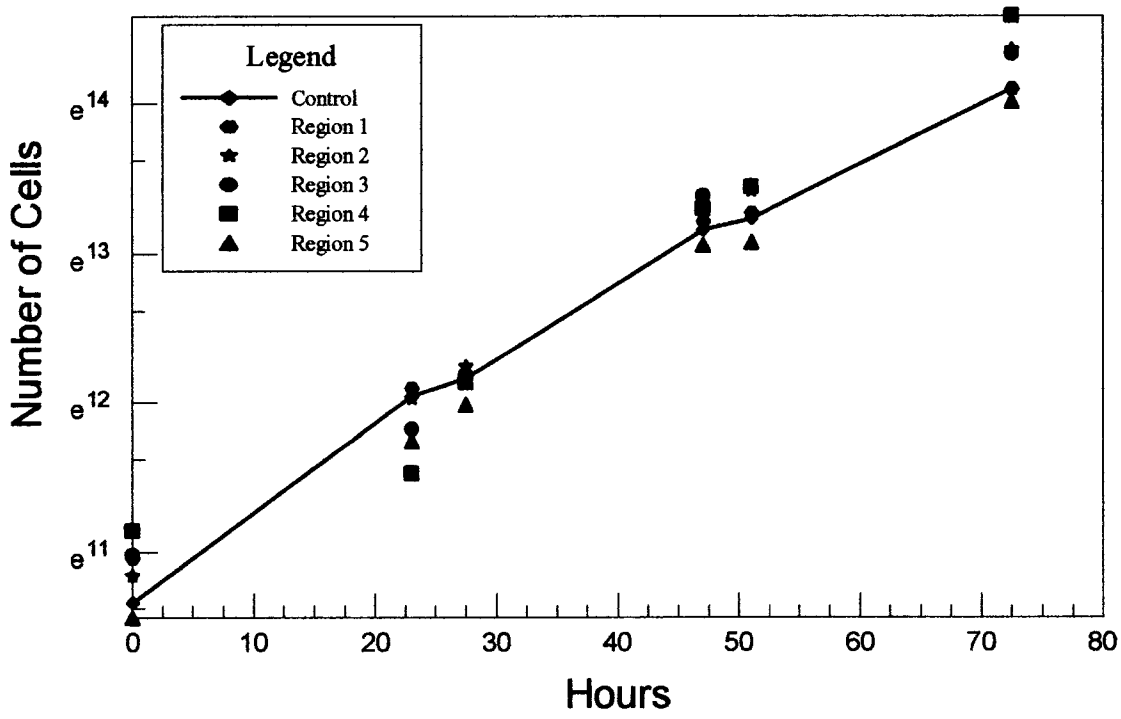

Figure 5-6. Relative growth of sorted regions in comparison to control. After sorting the cells from regions shown in Fig. 5-4, cells were counted at various times.

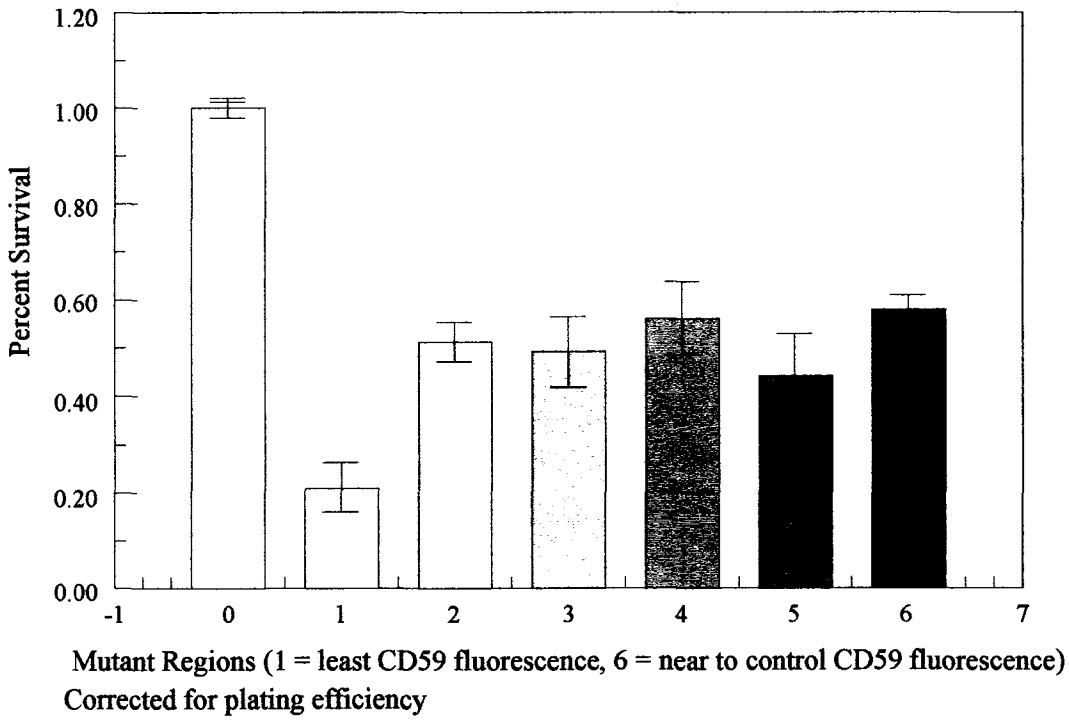

Figure 5-7. Survival of irradiated A_L cells sorted from regions shown in Figure 5-4. X-axis is the Region number. 300 cells were sorted per each region and survival determined after a 7 day growth period. Control cells (Region 0) were sorted from CD59 positive peak. Experiments were done in triplicate with proper controls. Error bars are the standard error of the mean from 3 independent experiments.

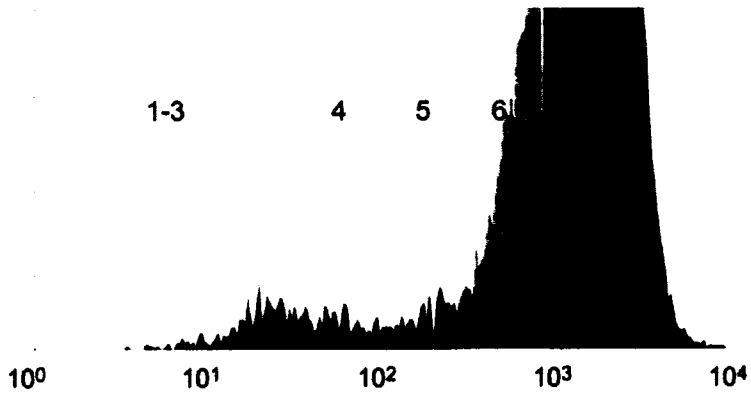

Figure 5-8. Flow cytometry histogram of CD59 expression 6 days after irradiation with 4 Gy. Regions 1-3 of Figure 5-4 were combined to represent the CD59 mutant region. Cells were sorted from each region and simultaneously analyzed for CD44 and CD90.

CD90 phenotypes. Almost all of the $CD59^-$ cells were also negative for CD44 (94%) but only 50% were negative for CD90 in region 1-3. Since CD44 is also negative, the triple mutants were mainly two phenotypes: $CD59^-CD44^-CD90^+$ (48%) and $CD59^-CD44^-CD90^-$ (48%). Region 4 reflected similar phenotypic trends as Region 1-3. Region 5, however, only contained 65% $CD44^-$ and 43% $CD90^-$ cells. Of those cells that were $CD44^-$, 54% were also negative for CD90. Region 6 contained 67% that were negative for CD44 and 61% were $CD90^-$ and only 44% were both $CD90^-$ and $CD44^-$. The overall trend is that region 1-3 and 4 have similar phenotypes and region 5 and 6 were quite similar. Even though region 4-6 were outside the normal CD59 mutant region, they still contained a large portion of CD59, CD44 and CD90 mutants. Triple phenotypes could only be determined for region 1-3 because CD59, according to the FCMA protocol, would be $CD59^+$ for regions 4-6.

Eighteen days after the initial sort, cells were again analyzed for their mutant phenotypes using CD59, CD44 and CD90 antibodies (Figure 5-9). The color coding relates to the regions sorted in Figure 5-8, where purple is region 1-3, pink is region 4, dark blue is region 5 and light blue is region 6. The bivariate histograms represent $CD59^-$ populations grown up for 24 days post-irradiation and 18 days post-sort where the CD44 and CD90 phenotypes were simultaneously measured. The positive and negative CD44 populations were separated at least 40 fold and the CD90 populations have a 10-fold separation. Clearly there are distinct mutant populations represented by circular groupings in each of the four quadrants. Similar to results in Figure 5-5, cells lost intermediate CD59- expression between day 6 and day 24. CD59/CD44/CD90 staining effectively separated mutant regions into distinct, measurable phenotypes by multiparameter flow cytometry. Very few cells were CD59- in region 6.

Table 5-1. CD44/CD59/CD90 expression measured by flow cytometry on sorted regions on day 6 after irradiation with 4 Gy. Mutant fractions for CD44 and CD90 were determined for the sorted regions. Cells were analyzed for all three CD proteins only in Regions 1-3.

	Region 1-3	Region 4	Region 5	Region 6
Control (68384)	0.06%	0.18%	0.26%	1.22%
CD59-	0.80% (3281)	0.72% (3137)	0.66% (2860)	0.77% (3332)
CD44-	94% (3084)	96% (3014)	65% (1867)	67% (2235)
CD90-	50% (1664)	51% (1601)	43% (1241)	61% (2041)
CD44-CD90+	44% (1444)	45% (1399)	34% (972)	20% (664)
CD44-CD90-	50% (1645)	51% (1612)	54% (1548)	44% (1479)
CD59-CD44+CD90+	1% (25)			
CD59-CD44-CD90+	48% (1560)			
CD59-CD44+CD90-	1% (33)			
CD59-CD44-CD90-	48% (1575)			

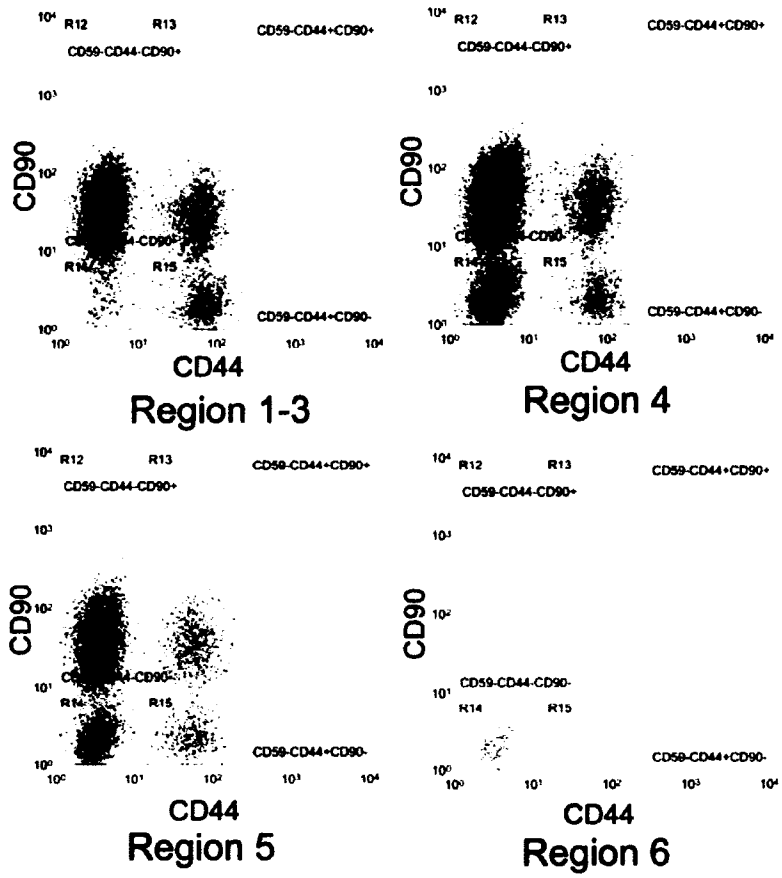

Figure 5-9. Bivariate flow cytometry histograms of sorted populations from Figure 5-8 grown for 24 days post treatment and gated only on CD59- populations so all cells analyzed were CD59$^-$. Quantification of region phenotypes is listed in Table 5-2.

Triple marker phenotypes were analyzed by flow cytometry and statistics were gathered for control, Region 1-3, 4, 5, and 6 (Table 5-2). In the control, $6.9x10^4$ cells were measured and only 68 were found in the FCMA CD59 mutant region. The majority of the control cells were $CD59^-CD44^-CD90^-$ (69%). Region 6 mirrored control cells with 61% of cells being triple mutants. On the other hand, after 18 days post-sort, $5x10^5$ cells were analyzed from Region 1-3, 4, and 5 and most of the $CD90^-$ mutants were lost, with 10%, 16% and 11%, respectively, of the populations being $CD90^-$. This also occurred with $CD44^-$, which dropped to 32%, 47%, and 27% for regions 1-3, 4, and 5.

Combining the data from the last two experiments, the loss of mutant expression is clear (Table 5-3). On day 6, 94% of $CD59^-$ mutants were also $CD44^-$, but by 24 days that value had reduced by two-thirds. CD90 also demonstrated a loss of 40% from day 6 to day 24. These values were also reflected in the triple mutant phenotype $CD59^-CD44^-CD90^-$ dropping from 48% of the mutants to 5%.

Discussion

The current mammalian mutation assays, MLA and A_L clonogenic assay, rely upon colony growth for detection of mutants. Although the results are clear cut for gene expression, neither of the assays are able to measure the gene expression over time. Also, since the assays both require colony counting, the amount of data generated is limited. The flow cytometer, on the other hand, is able to analyze 100,000 cells per minute with multiple parameters simultaneously, decreasing laborious processes to mere minutes. The one challenge, though, is deciding where to set the regions for flow cytometry detection.

Table 5-2. Phenotypes of sorted mutant regions 24 days post-radiation treatment measured by multiparameter flow cytometry, as shown in Figure 5-9. CD59/CD44/CD90 markers were simultaneously analyzed and quantified. The total number of cells in each region out of $5X10^5$ are given in parentheses.

	Control (68)	Region 1-3 (14179)	Region 4 (23688)	Region 5 (12141)	Region 6 (2220)
CD44-	5%	32%	47%	27%	3%
CD90-	7%	10%	16%	11%	7%
CD59-CD44+CD90+	7%	19%	12%	11%	17%
CD59-CD44-CD90+	9%	64%	65%	63%	16%
CD59-CD44+CD90-	15%	12%	5%	7%	6%
CD59-CD44-CD90-	69%	5%	18%	19%	61%

Table 5-3. CD marker expression measured by flow cytometry on day 6 and day 24 after irradiation with 4 Gy. Only cells in Regions 1-3 are compared.

Phenotype	day 6	day 24
CD44-	94%	32%
CD90-	50%	10%
CD59-CD44+CD90+	1%	19%
CD59-CD44-CD90+	48%	64%
CD59-CD44+CD90-	1%	12%
CD59-CD44-CD90-	48%	5%

Mutant Peak Region

Using 1% of the mean positive peak as the criteria for the CD59 mutant region, I measured CD59 mutants in irradiated cell populations. After an extended time course, the mutant yield peaked in a dose-dependent fashion on day 6 (Figure 5-2) and then was reduced to a plateau between days 10 and 17, and was nearly gone by day 20. If the mutant peak regions were ignored and the lines from day 5 to day 10 were connected, there would be a stable plateau expression of CD59 from days 5 to 17. Additionally, the mutant yield would be about half as high (750 mutants per 10^5 cells for 4 Gy) but it still would be considerably higher than the A_L clonogenic assay (approximately 300 mutants per 10^5 cells at 4 Gy) (4)) The rationale for considering this is discussed below.

According to Waldren *et al.* (12,10,5), there are two types of A_L mutants that occur after irradiation - simple or complex, as described in Chapter 1. Simple mutations lost *CD59* and other contiguous markers, whereas complex mutations had a mixture of markers present or absent throughout the chromosome. With radiation, 97% of the mutants measured by the clonogenic assay were simple deletions. It may be that the mutant peak region contains complex deletions that cause lethality. In the case of the FCMA, there is a mixture of mutants, mutant and non-mutant cells that are going to die, and viable cells that changes over time.

By analyzing the survival of cells in the FCMA mutant regions (Figure 5-7), I determined that 50% of the mutants die after sorting (corrected for death caused by sorting and plating). In contrast, the relative growth was very similar to control. In Chapter 4 I showed that the cell cycle returns to normal before mutant expression occurs. Therefore, when the cells were sorted, they were already actively growing. It may be that the cells destined for death after

the peak of mutant expression still contribute to population growth for a time. Either way, the reduction of the mutant peak is most likely caused by cell death.

According to Table 5-3, the triple mutant population was reduced from 48% to 5% within 20 days of analysis. Considering the cell survival, the mutant peak region and the kinetics of $CD59^-CD44^-CD90^-$ triple mutants, I conclude that for gamma radiation-induced mutations, the peak in mutant yield is skewed upward by measuring triple mutants that, over time, will be lethal to the cell. It is important to note that these mutants could not be measured by other mutagenesis assays because they would likely not form colonies. Thus, the FCMA gives additional important information about the actual chromosomal lesions caused by gamma radiation.

FCMA CD59 Mutant Region

However, if the FCMA CD59 mutant region is set at 1% of the mean positive peak, the mutant yield for CD59 may be underestimated. After sorting the cells from different regions and analyzing their mutant spectra (Figures 5-9, Tables 5-1 to 5-3), the phenotypes found in regions 1-3 and 4 were very similar. The only reason not to include region 4 would be the increase in spontaneous $CD59^-$ mutant background. Without region 4, the background level was 0.06% (196 mutants) whereas with region 4 it would be 0.24% (1540 mutants). The mutant yield would also increase to 1.57% (6418 $CD59^-$ cells/410000). Removing the background gives a mutant yield of 1.33% or an increase of about 166% over previously measured results above. Other researchers using the CHO A_L flow cytometry mutation assay have tackled this same issue. Wedemeyer *et al.* (13) set the mutant region at 10% of the CD59 positive peak and had a 20% mutant background before their method of background reduction. These results seem clearly too high. Zhou *et al.* (14), on the other hand, set their

mutant region to 99.9% of the unstained control cells giving a background level of 0.15%. Even though the background levels would be higher, I suggest that increasing the FCMA mutant region to include region 4 would more accurately measure CD59$^-$ mutant yield. Having the larger region would also reduce the variability of the mutant yield due to the shift in the mutant peak as shown in Figure 5-3.

Unlike other mammalian mutation assays, the FCMA is able to measure multiple markers simultaneously and track the expression of CD59 over time after treatment with mutagens. This is a powerful tool which could be used determine how new mutagens damage cells. By measuring multiple markers without a laborious PCR process, I can quickly determine the size of the genetic lesion as well as categorize the mutant as simple or complex. In approximately 2 weeks, cells may be analyzed for not only their CD59 phenotype, but numerous other cell surface antigens discussed in Chapter 6, including CD98 and CD151.

CD59$^-$ kinetics with gamma radiation-induced damage

Measuring the CD59 mutant expression at several time points also helps explain how mutagens affect the cell. Figure 5A and B show how radiation-induced mutants lose the expression of CD59 over time. The intermediate CD59 expression present in 5A is completely absent after 6 days of cell culture, or 20 days post treatment. This was reflected in at least three experiments. McGuinness *et al.* (6) have shown that radiation-induced damage causes large deletions. Therefore it is possible that the intermediate expression of CD59 is not stable and either the cells lose the expression entirely or die, reducing the population to only cells that survive with CD59 mutations.

A moderate CD59 expression is also indicated in the intermediate region. According to Rudd (9,8), the glycosylation of the CD59 protein may also determine the conformation on

the outside of the cell. Extensive molecular modeling of the heterogeneity of N- and O-linked glycans suggests that the glycans influence the geometry of the CD59 packing, and it is unlikely that CD59 molecules will form a regular array on the cell surface. This, in turn, could modulate the attachment of the CD59 antibody giving a reduced but not completely negative CD59 expression.

It may be that the deletions caused by IR radiation cause an accumulation of errors within the GPI-anchor genes (there are more than 11 involved (2)) or in the method of endocytosis which causes this strange phenomenon. These issues are explored more fully in Chapter 4 Ethyl methyl sulfonate (EMS), on the other hand, causes a stable intermediate region (unpublished data by Steve Keysar) but also mainly causes point mutations(3) instead of large deletions such as IR. The FCMA allows researchers to analyze the kinetics of mutagenesis giving insight into mutagen's mode of action.

Spontaneous Mutants

Through the multiple marker analysis, I found that almost all (96%) spontaneous mutants were mutated in all three markers, $CD59^{-}CD44^{-}CD90^{-}$ (Table 5-2) indicating that possibly the entire chromosome has been lost. A portion of the chromosome at 11p15.5 is required for cell survival (5), so those cells that are missing such a large portion of the chromosome may be non-viable, reducing the spontaneous background. With the multiple marker analysis and kinetics studies, it took 20 days for the loss of 40% of the triple mutants in radiation-induced mutant cells and spontaneous mutants may also have this delay.

Conclusion

In the course of this study I have redefined the FCMA mutant region to incorporate a larger portion of the mutant peak. The mutant peak region may be explained by cell lethality

of triple mutants. Radiation-induced $CD59^-$ mutants have an unstable intermediate mutant expression that is lost after extended culturing. Overall, the FCMA gives researchers the tools to measure mutant yield and mutant spectra rapidly and efficiently and provides new insights into the mechanisms of action of mutagenic agents such as ionizing radiation.

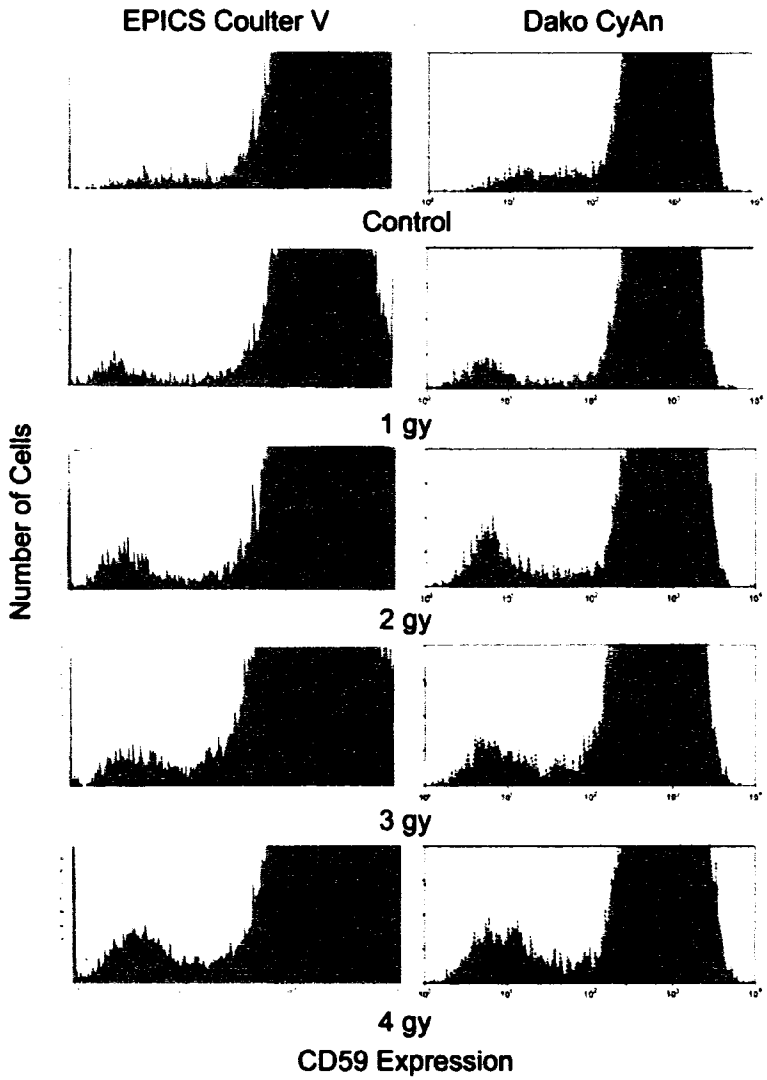

Figure 5-10. Flow cytometry histograms of A_L cells treated with radiation and CD59 expression analyzed on day 6, post-treatment. The Epics Coulter V and Dako CyAn measured A_L treated cells with various radiation doses. By setting the mutant region on both machines, I was able to compare mutant yield between machines. The Dako CyAn detected slightly fewer spontaneous mutants (0.02% versus 0.12%) possibly due to electronic noise on the EPICS Coulter V.

Cells were treated with ^{137}Cs γ radiation (J.L. Shepherd and Associates, Glendale, CA). The day before treatment, $4x10^5$ cells were plated in a T75 flask, giving $8x10^5$ at time of treatment. Cells were then irradiated with doses of 0-4 Gy (dose rate of 0.93 Gy/min at 22° C) and returned to the incubator for 2 days. Cells were passed with a minimum of $1.5x10^5$ cells per T75 flask. During the day of maximum mutant expression, day 6, cells were analyzed using the FCMA protocol. Regions were set identical on both the EPICS Coulter V and Dako CyAn machines and samples were simultaneously analyzed for doses 0-4 Gy.

Reference List

1. el Tarras A, Dubins JS, Warner J, Hoffman C, Cobb RR: Molecular analysis of the TK locus in L5178Y large and small colony mouse lymphoma cell mutants induced by hycanthone methanesulfonate. Mutat Res 332:89-95, 1995.

2. Fivaz M, Vilbois F, Thurnheer S, Pasquali C, Abrami L, Bickel PE, Parton RG, van der Goot FG: Differential sorting and fate of endocytosed GPI-anchored proteins. EMBO J 21:3989-4000, 2002.

3. Horikawa M, Suzuki F, Ban S: Mammalian cell mutagenesis: comparison of the sensitivity in assay systems of mutations induced by radiations and chemicals [proceedings]. Mutat Res 38:3371976.

4. Kraemer SM, Vannais DB, Kronenberg A, Ueno A, Waldren CA: Gamma-ray mutagenesis studies in a new human-hamster hybrid, A(L)CD59(+/-), which has two human chromosomes 11 but is hemizygous for the CD59 gene. Radiat Res 156:10-19, 2001.

5. Kraemer SM, Waldren CA: Chromosomal mutations and chromosome loss measured in a new human-hamster hybrid cell line, ALC: studies with colcemid, ultraviolet irradiation, and 137Cs gamma-rays. Mutat Res 379:151-166, 1997.

6. McGuinness SM, Shibuya ML, Ueno AM, Vannais DB, Waldren CA: Mutant quantity and quality in mammalian cells (AL) exposed to cesium-137 gamma radiation: effect of caffeine. Radiat Res 142:247-255, 1995.

7. Ross CD, Lim CU, Fox MH: Assay to measure CD59 mutations in CHO A(L) cells using flow cytometry. Cytometry A 66:85-90, 2005.

8. Rudd PM, Dwek RA: Glycosylation: heterogeneity and the 3D structure of proteins. Crit Rev Biochem Mol Biol 32:1-100, 1997.

9. Rudd PM, Morgan BP, Wormald MR, Harvey DJ, van den Berg CW, Davis SJ, Ferguson MA, Dwek RA: The glycosylation of the complement regulatory protein, human erythrocyte CD59. J Biol Chem 272:7229-7244, 1997.

10. Ueno AM, Vannais DB, Gustafson DL, Wong JC, Waldren CA: A low, adaptive dose of gamma-rays reduced the number and altered the spectrum of S1-mutants in human-hamster hybrid AL cells. Mutat Res 358:161-169, 1996.

11. Waldren C, Correll L, Sognier MA, Puck TT: Measurement of low levels of x-ray mutagenesis in relation to human disease. Proc Natl Acad Sci U S A 83:4839-4843, 1986.

12. Waldren C, Jones C, Puck TT: Measurement of mutagenesis in mammalian cells. Proc Natl Acad Sci U S A 76:1358-1362, 1979.

13. Wedemeyer N, Greve B, Uthe D, Potter T, Denklau D, Severin E, Hacker-Klom U, Kohnlein W, Gohde W: Frequency of CD59 mutations induced in human-hamster hybrid A(L) cells by low-dose X-irradiation. Mutat Res 473:73-84, 2001.

14. Zhou H, Xu A, Gillispie JA, Waldren CA, Hei TK: Quantification of. Mutat Res 594:113-119, 2006.

CHAPTER 6

MUTANT SPECTRA DETERMINED FOR RADIATION-INDUCED MUTATIONS IN CHO A_L CELLS USING MULTIPLE MARKERS WITH THE FLOW CYTOMETRY MUTATION ASSAY

Abstract

Background: A sensitive mammalian cell mutation assay was developed previously using a Chinese hamster ovary cell line that stably incorporates human chromosome 11 (CHO A_L) using flow cytometry (143,110,154). Currently, all mutant spectra are determined either through molecular techniques such as PCR or on a global scale with microarrays. Both of these techniques are costly and laborious. We show that multiparameter flow cytometry may be used to analyze mutagenized CHO A_L cells for mutations in 5 markers along chromosome 11 and also the GPI anchor, yielding a mutant spectrum within two weeks of mutant induction.

Methods: Directly-conjugated monoclonal antibodies to CD59, CD44, CD90, CD98 and CD151 were used to detect mutations not only at the CD59 locus but also in four other genes along chromosome 11, and thus to determine the mutant spectra of irradiated cells. Cells were irradiated with 4 Gy ^{137}Cs gamma radiation. After a seven day expression period, they were analyzed for the expression of CD59, CD44, CD90, CD98 and CD151 by multiparameter flow cytometry. Cells were also analyzed for the presence of a glycosylphosphatidylinositol (GPI) anchor using fluorescent proaerolysin (FLAER). Mutant

populations were sorted and then cloned for individual analysis. Clones were stained and scored for protein expression. To confirm phenotypic results, PCR was done on all 4 exons of *CD59* as well as 5 other flanking genes on chromosome 11: *RAS, LDHA, CAT, WT,* and *APO-1.*

Results: There was clear separation between the stained and unstained control samples for CD59, CD44, CD90, CD98, CD151 and the GPI anchor, varying from a 400-fold to 15-fold difference. CD59-negative irradiated populations were sorted, cultured and analyzed for all markers. The resulting mutant cell populations had a mixture of phenotypes, with CD59, CD44 and CD90 the most frequently mutated (at 88%, 56%, 44% respectively), CD98 and CD151 less frequently mutated (2% for both) and about 6% mutated for GPI anchor expression. Individual cells were sorted from these mixed populations and clones were analyzed for their phenotypes and confirmed via PCR. All clones analyzed were negative for CD59 expression and PCR confirmed that at least *CD59* exon 4 was also absent. Different combinations of expression of CD genes and other genes were apparent, reflecting mutations ranging from intragenic to large deletions involving nearly the entire chromosome. The mutant spectrum analysis by flow cytometry was substantiated by PCR analysis of the loss of flanking genes.

Conclusions: The FCMA multiple marker analysis substantially reduces the time and resources required for mutant spectrum development from 1-2 months for conventional methods to 14-21 days for the FCMA. With this multi-gene mutation analysis system, researchers could quickly ascertain the mutagenic potential of novel chemicals and pharmaceuticals as well as clarify the method of mutagenesis without large expense.

Additionally, the FCMA would be able to quickly analyze mutated populations during extended time periods to evaluate the evolution of phenotypic expression.

Introduction

DNA damage and mutagenesis are essential aspects of understanding the toxicology of chemical and pharmaceutical products. The Food and Drug Administration (FDA) currently requires that all new drugs be tested by a battery of mutation assays to determine the chemical's mutagenic potential (75). Although not required by the FDA, mutant spectra may also determine the extent of the DNA damage by the chemical along an entire chromosome. Mutant spectra may be defined as a sequence-dependent distribution of the different types of mutations induced by a mutagen along a gene (101). Until now, mutation assays have heavily relied upon PCR or Southern blot of DNA isolated from single mutants to determine the mutant spectrum (28,101,126,136). Even though these methods are effective, they are not very efficient as it takes at least 2 months for analysis, including the time to isolate individual clones. Thus mutant spectrum analysis is not routinely done. We propose to use a flow cytometry mutation assay (FCMA) to rapidly determine the mutant spectrum of mutagenic agents within a two week period for populations and one month for individual clones.

We have previously developed the FCMA (110), which measures the mutation rate in *CD59* on human chromosome 11 in a Chinese hamster ovary hybrid cell line (A_L) developed originally by C. A. Waldren and colleagues(134,133,105,51,53,135). The assay measures the presence or absence of CD59, a GPI-linked cell-surface protein that is encoded by *CD59* on human chromosome 11. We and others have demonstrated that the FCMA effectively measures mutations from a wide range of mutagens (110,143,154) and we now propose to use this system to measure mutations in 4 other genes located on chromosome 11 using flow

cytometry. The CHO A_L cell line expresses four additional human cell surface proteins: CD44 (transmembrane cell surface receptor for hyaluron located adjacent to CD59 (129)), CD90 (GPI-anchored membrane protein involved in cell to cell or cell to ligand interactions (115,144)), CD98 (type II membrane protein involved in cell growth (24,31,136)) and CD151 (member of the tetraspanin family of cell membrane proteins (41,65)). Using available directly-conjugated monoclonal antibodies, we can simultaneously analyze CD59, CD44 and CD90 using multicolor fluorochromes and other combinations of antigens using CD98 and CD151 antibodies. These proteins vary in their attachment in the plasma membrane and the genes are located in widely different regions of chromosome 11. As shown in Figure 6-4, CD59 and CD44 are adjacent to each other (1.4 Mbp), but differ in that CD44 is a transmembrane protein whereas CD59 is a GPI-linked, lipid raft-associated protein. CD151, an integral membrane protein, is on the distal end of the p-arm near a gene required for CHO survival (70). CD98 is on the q-arm of chromosome 11 close to the centromere and is a transmembrane protein. CD90 is located on the distal end of the q-arm and is a GPI-linked protein. Mutational spectra within these five markers may indicate the mutant specificity and/or size of mutation.

Since two of the markers (CD59 and CD90) are GPI-linked, it is possible that some putative mutations in these genes are actually mutations in one of the ten different genes for GPI anchor formation. The most likely candidate is *Pig-A*, a gene located on the X-chromosome, that is well known to cause GPI defects in paroxymal nocturnal haemoglobinuria (PNH) (11,55,67). A specific bacterial toxin, aerolysin, has been developed to detect the presence of GPI anchors (22,21,23,32,94,119). Aerolysin binds to the GPI anchor and then lyses cells by enzymatic activity. A particular mutant variant, proaerolysin,

conjugated to Alexa-488 (FLAER)(17), lacks the lytic capability but still binds to the anchor. FLAER can be used to rule out false negative results due to a mutation in the GPI genes.

Using these markers together, the FCMA may determine the mutant spectra for various mutagens rapidly without compromising cell survival or requiring laborious, time consuming and sensitive techniques such as PCR. In this paper we show the feasibility of using flow cytometry to measure mutations in 5 genes as well as the GPI anchor and compare the mutant spectrum obtained with flow cytometry to that obtained by PCR.

Methods

General cell culture, FCMA, monoclonal antibody labeling are described in Chapter 2.

Monoclonal antibody labeling

To stain cells simultaneously with CD59, CD44 and CD90 antibodies, CD59-PE (Caltag, Burlingame, CA 1:40 dilution), CD44 biotin (Serotec, Raleigh, NC, 1:5 dilution), and CD90-Alexa 647 (Serotec, Raleigh, NC, 1:5 dilution) directly-conjugated monoclonal antibodies were added to a total volume of 50 µl in staining buffer. The cells were incubated for 30 min on ice and then 1 ml staining buffer was added. After centrifugation and aspiration, cells were resuspended in 99 µl staining buffer and 1 µl Alexa 488 Streptavidin (Molecular Probes, Invitrogen, Carlsbad, CA, 1:100) and stained for 30 min on ice. All buffers and staining solutions were kept on ice throughout the experiment.

Cells were similarly stained with CD151 and CD98 antibodies using 10 µl CD151-PE (BD Pharmingen, San Jose, CA 1:2 dilution) and CD98-FITC (BD Pharmingen, San Jose, CA 1:2 dilution) in a total volume of 50 µl staining solution.

The GPI-anchor was detected using the bacterial toxin aerolysin conjugated to Alexa-488 at a concentration of 10nM per sample. Cells were resuspended in 225 µl staining buffer and

then 25 µl of 0.1 nM FLAER (Protox Biotech, Victoria, Canada) was added and gently mixed. Cells were then incubated for 30 min on ice.

After incubation, all samples were washed in cold staining buffer and resuspended in 0.5 ml cold buffer, filtered through a 40 µm nylon mesh and kept on ice prior to analysis by flow cytometry.

Flow Cytometry

A CyAn™ flow cytometer (Dako, Ft. Collins, CO) was used with 488 and 635 nm lasers for excitation. FITC was detected using a 530/40 nm bandpass filter with a 545 nm dichroic long pass, PE was detected using a 575/25 nm bandpass filter with a 595 nm dichroic long pass, and Alexa 647 was excited using the 635 nm laser and detected using a 665/20 nm bandpass filter with a 730 nm dichroic long pass. A total of $1x10^5$ cells were analyzed for each sample. Gating on forward scatter vs. side scatter eliminated cellular debris, thus reducing false negatives. The photomultiplier voltages were set so that the unstained populations with each marker had the same mean value on the histogram with the mutant region gated on 99% of the negative parental cells which lacked chromosome 11. Compensation was required between the PE and FITC/Alexa 488 stains and was done with the Summit Software v4.2 (Dako, Ft. Collins, CO). Within the PE histogram, the mutant region was defined as those cells with fluorescence intensity less than 1% of the mean fluorescence intensity of the $CD59^+$ population of control cells. This enabled quantification of $CD59^-$ (mutant) cells for subsequent calculation of the mutant fraction.

Mutation Assay

Radiation Treatment

Cells were treated with G418 (800 μM) for 5 days prior to treatment. The day before treatment, $4x10^5$ cells were plated in a T75 flask, giving $8x10^5$ cells at time of treatment. The cells were then irradiated with doses of 0-4 Gy ^{137}Cs γ radiation, a well-known clastogen (57,133) (J.L. Shepherd and Associates, Glendale, CA), at a dose rate of 0.93 Gy/min at 22° C, to test the response of multiple markers on chromosome 11. Treatment and control flasks were passed with a minimum of $1.5x10^5$ cells per T75 flask and assayed using the FCMA protocol with multiple markers on day 6, the maximum day for CD59 mutation expression. The spontaneous background was subtracted to determine the corrected mutant fraction for each marker.

Mutant Region Sorting

The mutant region was isolated by sorting the population on CD59, CD44 and CD90 markers using a Dako MoFlo™ High-Performance Cell Sorter (Dako, Fort Collins, CO) and filter set-up similar to the CyAn™ mentioned above. Populations were selected by their phenotypes (i.e. $CD59^-CD44^+CD90^+$) and 1000 cells were sorted into 15 ml sterile conical tubes and later transferred into T75 tissue culture flasks. Compensation was carried out before sorting began using control samples. Individual cells that were primarily $CD59^-$ were sorted using the MoFlo CyCLONE™ into 96-well tissue culture plates for clonal analysis. Phenotypes included in the single cell sort were: $CD59^-CD44^+CD90^+$, $CD59^-CD44^-CD90^+$, $CD59^-CD44^+CD90^-$ and $CD59^-CD44^-CD90^-$.

Cells cultures were expanded 14 days or until enough cells were available for analysis using the FCMA. At that time, clones were screened for CD59 phenotypes and subsequent study of the other markers.

PCR Analysis

The mutant spectrum of sorted mutant clones was determined by PCR analysis of nine separate genetic loci spanning the length of chromosome 11. After expanding the individual clones, the DNA was extracted and analyzed for the presence or absence of different markers through multiplex PCR. The primer sequences and PCR conditions were adapted from the work of Charles A. Waldren and Diane B. Vannais (82,68,69,76,130). The primers were synthesized by Macro Molecular Resources, Ft. Collins, CO and all the PCR components obtained from Invitrogen (Carlsbad, CA).

The four exons of the *CD59* gene were examined via multiplex PCR for exons 1-3 and an independent PCR reaction for exon 4 because of difficulties running all 4 exons simultaneously. The 20 µl reaction volume contained 200 µM dNTPs, 0.01% gelatin, 1xPCR Buffer, 1.5 mM $MgCl_2$, 0.5 U Taq DNA Polymerase and the following primer pair concentrations: 4 µM exon 1, 0.5 µM exon 2, 0.2 µM exon 3 and 10 µM exon 4. The PCR program consisted of an initial denaturation at 95°C for 5 min followed by 30 cycles of 94°C, 45 s; 52°C, 45 s; 72°C, 45 s for denaturation, annealing and extension, respectively and then a final incubation at 72°C for 20 min. Samples were electrophoresed on a 3% agarose gel, stained with SYBR® Gold Nucleic Acid Gel Stain (Invitrogen – Molecular Probes, Eugene, OR) and visualized on a dark reader transilluminator. The PCR product sizes were as follows: 87, 205, 350 and 401 bp for exons 1, 2, 3 and 4, respectively. Exon 4 encodes the majority of the translated sequence, including the GPI anchor binding site (100,16).

Five additional chromosome 11 markers were analyzed in two separate multiplex PCR reactions. These markers were chosen based on their proximity to relevant *CD* genes and the availability of optimized primer sequences used successfully by other laboratories

(136,130). Lactate dehydrogenase A (LDHA), Wilms tumor 1 (WT) and catalase (CAT) were optimal at 3 mM $MgCl_2$ while v-Ha-ras Harvey rat sarcoma viral oncogene homolog (RAS) and apolipoprotein A-1 (APO-A1) were optimal at 1.5 mM $MgCl_2$. The 20 μL reaction volume contained 200 μM dNTPs, 1xPCR Buffer, 1 U Taq DNA Polymerase and the following primer pair concentrations: 0.5 μM for LDHA, WT and CAT, 12.5 μM for RAS and 1 μM for APO-A1. The PCR cycle consisted of an initial denaturation at 95°C for 5 min followed by 30 cycles of 94°C, 1 min; 55°C, 1 min; 72°C, 1 min, and then a final incubation at 72°C for 20 min. As with the CD59 amplicon products, samples were electrophoresed on a 3% agarose gel and stained with SYBR® Gold Nucleic Acid Gel Stain. PCR product sizes were 400 bp for LDHA, 252 for WT, 207 bp for CAT, 63 bp for RAS and 109 bp for APO-A1.

Results

Separation between negative and positive populations for all markers

To clearly identify the positive and negative phenotypes of the mutagenized CHO A_L cells, it was necessary to optimize the staining procedure to give the greatest distance between the unstained and stained control populations. One method of determining the staining efficacy is to measure the mean fluorescence peak intensity of the positive population in comparison to an unstained or negative population. The most outstanding separation was our primary mutagenesis marker, CD59, with about a 400-fold separation between $CD59^+$ and $CD59^-$ (Figure 6-1). CD90, CD98 and CD151 were also well resolved with 100-, 72- and 60-fold separations between negative and positive populations. CD44 and FLAER, although were not as well resolved, but still had clear positive and negative populations with 20- and 15- fold separations between the populations. These procedures

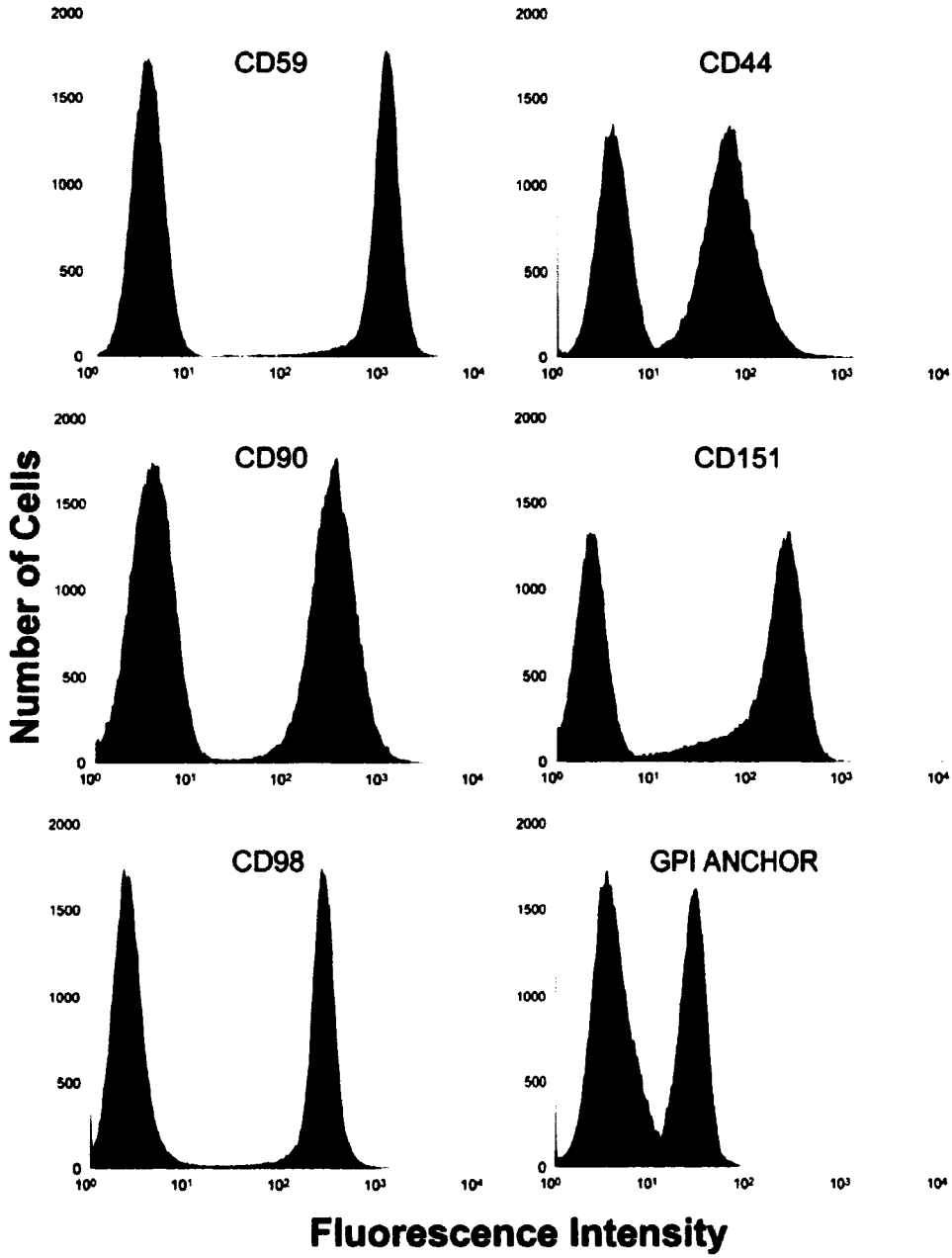

Figure 6-9. Flow cytometry histograms showing separation between positive and unstained control cells for CD59, CD44, CD90, CD151, CD98 and GPI Anchor.

have been optimized utilizing the best combinations of antibodies and stains commercially available to allow simultaneous phenotyping of both mutant populations and clones, though not all antibodies can be run at the same time because of similar fluorochromes in some cases.

Radiation-induced mutant spectra

Analysis of multiple markers in sorted populations

Cells were irradiated and analyzed 6 days later for mutations in *CD59*. Out of 500,000 cells, about 4000 mutants were detected after a dose of 4 Gy, giving a mutant yield of 0.8%, similar to our previous results(110). One thousand cells in this mutant region were then sorted and cultured to allow for multiple marker analysis of the mutant population.

Subsequent analysis of the sorted cell populations showed that the mutant region contained 88% $CD59^-$ mutants (Figure 6-2). Since sorting purity is never 100%, a few positive cells were likely included in the sorted region, giving a small positive population. CD59 mutants were also analyzed for CD44 and CD90 phenotypes. Univariate and bivariate histograms clearly show that the majority of the $CD59^-$ mutants were also negative for CD44, and about half of the $CD59^-$ mutants were also negative for CD90.

A detailed analysis of these populations is given in Table 1. Cells in the CD59 mutant region were 88% negative for CD59, 56% negative for CD44 and 44% negative for CD90. The other three markers had a much lower mutant yield at 6%, 2% and 2% for GPI-anchor, CD98 and CD151 respectively. There was good agreement between the analysis of univariate and bivariate histograms. $CD59^-/CD44^-/CD90^-$ triple mutants were about 22% of the entire population. When $CD59^-/CD90^-$ mutants were analyzed for the GPI-anchor control, 33% of those were negative for the GPI-anchor marker. The bivariate histograms demonstrated clear clustering of mutant populations into distinct groups. Using these

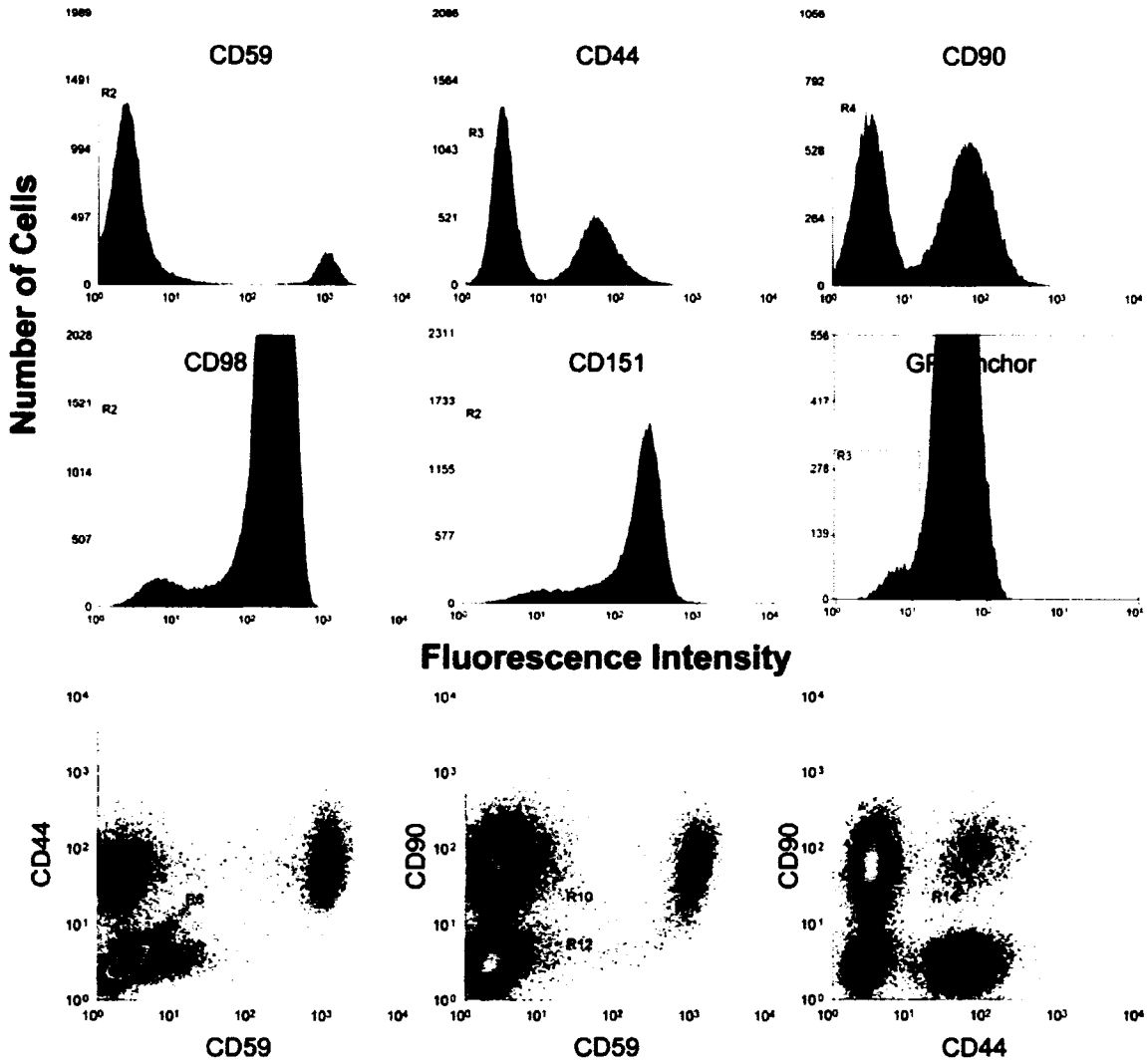

Figure 6-10. Irradiated (4 Gy) A_L cells sorted on the FCMA CD59 mutant region, grown for 14 days and then analyzed for CD59, CD44, CD90, CD98, CD151, GPI-Anchor. The red in the CD151 and GPI-Anchor indicate CD98- and CD151+/- and CD90- and FLAER+/-. Simultaneous analysis of CD59, CD44 and CD90 occurred in the bivariate histograms at the bottom.

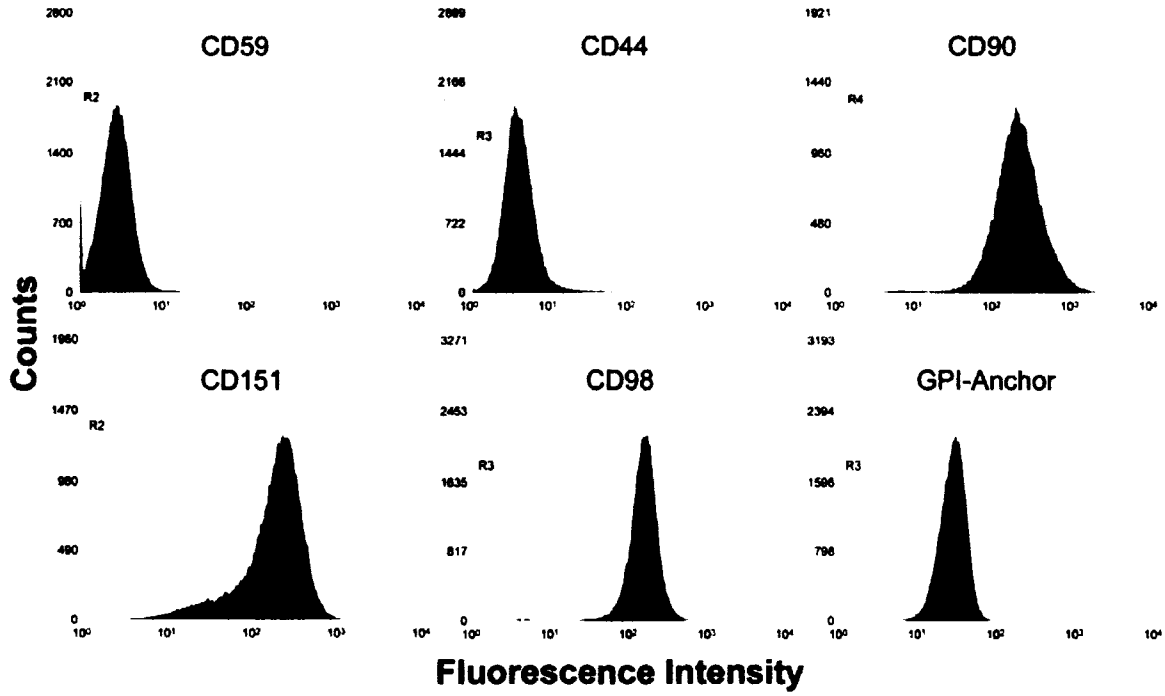

Figure 6-3. Mutant spectra of irradiated A_L cell clone measuring phenotypes at CD59, CD44, CD90, CD151, CD98 and GPI-Anchor.

Table 6-1. Irradiated A_L cells (a dose of 4 Gy) sorted by the FCMA CD59 mutant region and analyzed for mutant spectra in CD59, CD44, CD90, CD151, and GPI Anchor.

Phenotype	Percent of Cells
$CD59^-$	88%
$CD44^-$	56%
$CD90^-$	44%
GPI $Anchor^-$	6%
$CD98^-$	2%
$CD151^-$	2%
$CD59^-/CD44^-$	57%
$CD59^-/CD90^-$	46%
$CD59^-/CD44^-/CD90^-$	22%
$CD59^-/CD90^-$/GPI $Anchor^-$	33%

histograms, single cells with varying phenotypic expression were sorted and grown up for phenotypic analysis using all six markers.

FCMA Mutant Spectra

The clones were then analyzed for the expression of the 6 different markers. A representative sample of one clone with a $CD59^-/CD44^-/CD90^+/CD151^+/CD98^+/GPI\text{-}Anchor^+$ phenotype is shown in Figure 6-3.

The region outlined in each histogram delineates 99% of the unstained population; those cells that fall into that region are negative for the particular marker. Control cells and 19 different sorted clonal populations were analyzed by this methodology (Figure 6-4).

PCR Mutant Spectra

PCR was also done on the same clones analyzed by flow cytometry and demonstrated similar mutant spectra. The relative locations of the genes along chromosome 11, as well as the PCR and flow cytometry results, are shown in Figure 6-4. All of the clones that were analyzed as $CD59^-$ by flow cytometry were also negative in at least 1 of the four exons for *CD59* (exon 4 was negative in all cases). CAT, which is located in between both CD59 and CD44, was missing from all clones that were negative for CD59 and CD44 by flow cytometry. WT and LDHA were distal to CD59 and had a varied expression. Three clones show the loss of CD59 and CD90 but with no intervening genes missing though they were all negative for GPI. APO-A1 was only missing in those clones that had a $CD90^-GPI^+$ phenotype according to FCMA analysis. RAS was utilized as a positive control because of an unknown gene at the tip of the p arm that is essential for survival, and was present in all samples.

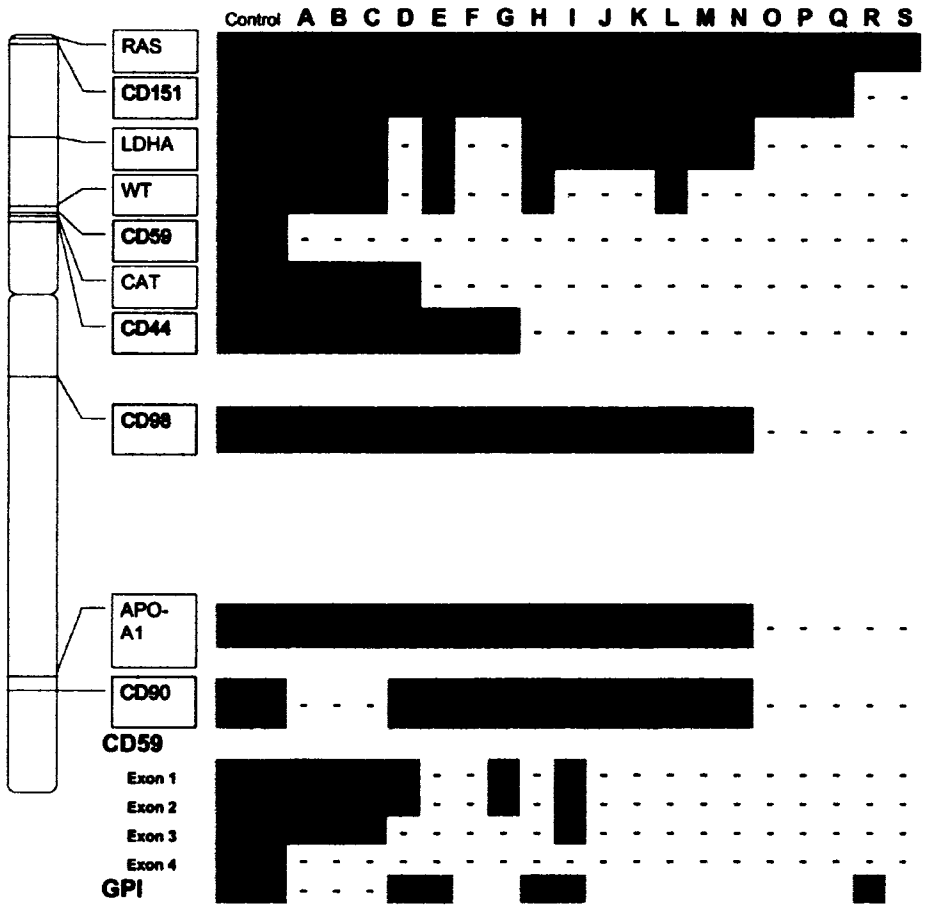

Figure 6-4. Mutant spectra of 4 Gy irradiated A_L clones analyzed both by PCR (indicated by white labels) and flow cytometry markers (indicated by the aqua labels). Exons for CD59 and GPI-anchor were also analyzed. Presence or absence of markers is indicated by (+) and (-).

Discussion

Effectiveness of FCMA multiple marker analysis

The conventional methods for determining mutant spectra require PCR or Southern blotting to determine the change in gene expression. Both of these methods require cloning individual mutant cells, which is very laborious, and interpretation at times may be difficult. We have shown here that CHO A_L cells can be analyzed for multiple mutations by flow cytometry to obtain a mutant spectrum in a much faster and less laborious process.

To demonstrate that there was adequate separation between the negative and positive populations for each of these markers, we analyzed both stained and unstained cells. All of the markers were clearly resolved with very little overlap between the negative and positive populations. Our primary mutagenesis marker, CD59, had the largest separation between $CD59^+$ and $CD59^-$ cells (400-fold). This large separation and corresponding very low background of mutants is sufficient to accurately and sensitively measure dose-dependent mutant yield after treating with genotoxic agents, as we have previously shown (110). The other markers are not as accurate for primary mutant analysis, but can analyzed in combination with the loss of CD59 to give additional information. The smallest difference was the GPI-anchor marker with a 15-fold difference, but that was sufficient to resolve a positive and negative peak clearly. According to these results, it is possible to determine mutations in these genes by measuring the loss of protein expression by multivariate flow cytometry. This demonstrates that the FCMA multiple marker analysis, in principle, can determine mutant spectra.

After we analyzed the control cells and optimized the FCMA multiple marker methods, irradiated samples were evaluated for mutants in all six markers. As with the control, we

were able to clearly analyze the populations for expression of all six markers (Figure 6-2) and even utilized this method to sort out individual clones for continued study (Figure 6-3). After 14 days we then examined the phenotype of each individual clone to determine the mutant spectrum in different clones (Figure 6-4, Table 6-1).

Radiation Mutant Spectra Analysis

The mutant spectrum induced by a given agent is independent of the mutation system used but is instead dependent on the specific mutagen's mode of action (101). Gamma radiation is known to cause large deletions as shown by analysis, not only with the *CHO AL* clonogenic assay (82), but also the mouse lymphoma *tk* gene assay (148,10) and the *hprt* mutation assay (26,128). Other assays are limited in scoring large deletions because they frequently lead to the loss of essential genes and the cells die. Because human chromosome 11 is not essential for CHO A_L cell survival, almost the entire chromosome may be lost without cell death occurring (134). Thus much larger deletions can be measured and the mutant spectra would be more comprehensive. Waldren *et al.* have shown the mutant spectra after ionizing radiation using PCR on clones of mutated CHO A_L cells and found large and complex mutations (82).

FCMA Mutant Spectra Analysis

We used multiparameter analysis to measure the loss of multiple CD markers along chromosome 11 to analyze the mutant spectrum with flow cytometry. When 1000 CD59 mutant cells were sorted and cultured, the resulting population was subsequently analyzed for 6 markers. The proportion of double and triple mutants ($CD59^-/CD44^-$ and $CD59^-/CD44^-/CD90^-$) was much higher than if they were random independent mutational events (Table 6-

1). In the case of CD44 and CD59, the proximity of the markers (only a 1.4 Mbp separation) would suggest that a mutant in both genes indicates that the entire region has been deleted.

This hypothesis, however, cannot explain the high frequency of mutants at CD59 and CD90 (44%). CD90 and CD59 are farther apart than CD44 with about 85 Mbp separating the two genes. Analyzing the bivariate mutant populations, in addition, gave a frequency of 50% for the double mutants, $CD59^-/CD90^-$. Similarities between the physical properties of these cell surface proteins may clarify why the expression of CD90 was also lost at such a high frequency. Both of these markers are anchored into the plasma membrane via a GPI anchor and are localized to lipid-rafts in the plasma membrane. It is highly probable that one of the ten genes required for GPI-linkage, most likely the X-linked *pigA* gene, was mutated causing a loss of expression of CD59 and CD90. We investigated this problem by labeling the $CD59^-/CD90^-$ mutants with fluorescent aerolysin (FLAER) which detects the presence of a GPI-anchor. Thirty-three percent of the $CD59^-$ cells were also negative for CD59 and GPI expression, indicating that GPI-anchor mutagenesis may explain a portion of the elevated mutant yield.

CD98, in contrast to CD90, only had a mutant frequency of about 6% in the $CD59^-$ population. There are several possible reasons including location, size of coding region, and available isoforms. CD90 is located at the end of the q-arm of chromosome 11 which may make it more available for translocations and truncations, whereas CD98 is located near the centromere. Given that the centromere is required for chromosome segregation, mutants in the CD98 gene may be less likely to survive. Also, CD90 is a small glycoprotein 25-28 kDa in size with a short sequence (~2 kbp) in comparison to CD98 which is a 120 kDa protein with ~33 kbp sequence. CD98, in addition, has 6 isoforms that may function to express the

cell surface protein, protecting the cell from complete loss of CD98. Even though CD98 has a low mutant yield in comparison to CD44, CD59 and CD90, it functions as an excellent marker for total chromosome loss with its proximity to the centromere.

The frequency of CD151 mutants is low most likely because of its proximity to other essential gene(s). It has been determined that the CHO A_L hybrid cells have an essential gene at the tip of the p-arm of chromosome 11 (11p15.5) that is required for CHO survival (70). Since CD151 is located near 11p15.5, those cells lacking the CD151 marker most likely also have mutations in this area and do not survive for mutant analysis (82).

PCR Mutant Spectra

The PCR results demonstrate that putative CD59 mutants measured by flow cytometry also correspond directly to a loss of at least one of the *CD59* exons (Figure 6-4). The majority of clones analyzed were also missing some or all of the *WT*, *CAT* and *LDHA* markers and CD44, showing that radiation frequently causes large deletions of entire sections of the chromosome. Ten percent of the clones were missing all markers (Clones R and S), but the entire chromosome was not lost as *RAS* was still present. *APO-A1* and *CD90* reflected the same expression except in clones A, B, and C. These three clones lost expression of only CD59 and CD90 but no intervening genes, demonstrating that these clones are more likely to be mutant for the *pigA* GPI anchor gene and not the CD90 coding region. Overall, these results show that the FCMA mutant spectra directly reflect the genotypic mutant spectra based on PCR. Our results support previous research using the clonogenic CHO A_L assay which suggested that 97% of the mutations caused by radiation were simple deletions with very few complex mutations.

The FCMA multiple marker analysis drastically reduces the time and resources required for mutant spectrum development from 1-2 months for conventional methods to a week to 10 days for the FCMA. Clonal populations were used here, but it is possible to do the initial analysis of mutants screening for all markers and determine the yield of mutants for all markers. Because of overlapping fluorochromes, we could not analyze all 5 markers and GPI simultaneously. However, in principle this is quite possible given appropriate tagged antibodies. Using this system, researchers could quickly ascertain the mutagenic potential of novel chemicals and pharmaceuticals as well as clarify the method of mutagenesis without large expense. Additionally, the FCMA would be able to quickly analyze mutated populations during extended time periods to evaluate the evolution of phenotypic expression.

Reference List

1. Amundson SA, Liber HL: A comparison of induced mutation at homologous alleles of the tk locus in human cells. Mutat Res 247:19-27, 1991.

2. Araten DJ, Luzzatto L: The mutation rate in PIG-A is normal in patients with Paroxysmal Nocturnal Hemoglobinuria (PNH). Blood 2006.

3. Bodian DL, Davis SJ, Morgan BP, Rushmere NK: Mutational analysis of the active site and antibody epitopes of the complement-inhibitory glycoprotein, CD59. J Exp Med 185:507-516, 1997.

4. Brodsky RA, Mukhina GL, Li S, Nelson KL, Chiurazzi PL, Buckley JT, Borowitz MJ: Improved detection and characterization of paroxysmal nocturnal hemoglobinuria using fluorescent aerolysin. Am J Clin Pathol 114:459-466, 2000.

5. Buckley JT: Purification of cloned proaerolysin released by a low protease mutant of Aeromonas salmonicida. Biochem Cell Biol 68:221-224, 1990.

6. Buckley JT: Secretion and mechanism of action of the hole-forming toxin aerolysin. Experientia 47:418-419, 1991.

7. Buckley JT, Howard SP: Aerolysin from Aeromonas hydrophila. Methods Enzymol 165:193-199, 1988.

8. Cai S, Bulus N, Fonseca-Siesser PM, Chen D, Hanks SK, Pozzi A, Zent R: CD98 modulates integrin beta1 function in polarized epithelial cells. J Cell Sci 118:889-899, 2005.

9. Clive D, Johnson KO, Spector JF, Batson AG, Brown MM: Validation and characterization of the L5178Y/TK+/- mouse lymphoma mutagen assay system. Mutat Res 59:61-108, 1979.

10. Costes S, Sachs R, Hlatky L, Vannais D, Waldren C, Fouladi B: Large-mutation spectra induced at hemizygous loci by low-LET radiation: evidence for intrachromosomal proximity effects. Radiat Res 156:545-557, 2001.

11. Diaz LA, Jr., Fox DA: A role for CD98 in cellular activation. J Biol Regul Homeost Agents 12:25-32, 1998.

12. Diep DB, Nelson KL, Raja SM, Pleshak EN, Buckley JT: Glycosylphosphatidylinositol anchors of membrane glycoproteins are binding determinants for the channel-forming toxin aerolysin. J Biol Chem 273:2355-2360, 1998.

13. Geary SM, Cambareri AC, Sincock PM, Fitter S, Ashman LK: Differential tissue expression of epitopes of the tetraspanin CD151 recognised by monoclonal antibodies. Tissue Antigens 58:141-153, 2001.

14. Hei TK, Hall EJ, Waldren CA: Mutation induction and relative biological effectiveness of neutrons in mammalian cells. Experimental observations. Radiat Res 115:281-291, 1988.

15. Hei TK, Piao CQ, He ZY, Vannais D, Waldren CA: Chrysotile fiber is a strong mutagen in mammalian cells. Cancer Res 52:6305-6309, 1992.

16. Hernandez-Campo PM, Almeida J, Sanchez ML, Malvezzi M, Orfao A: Normal patterns of expression of glycosylphosphatidylinositol-anchored proteins on different subsets of peripheral blood cells: a frame of reference for the diagnosis of paroxysmal nocturnal hemoglobinuria. Cytometry B Clin Cytom 70:71-81, 2006.

17. Horikawa M, Suzuki F, Ban S: Mammalian cell mutagenesis: comparison of the sensitivity in assay systems of mutations induced by radiations and chemicals [proceedings]. Mutat Res 38:3371976.

18. Karamatic C, V, Burton N, Kagan A, Green CA, Levene C, Flinter F, Brady RL, Daniels G, Anstee DJ: CD151, the first member of the tetraspanin (TM4) superfamily detected on erythrocytes, is essential for the correct assembly of human basement membranes in kidney and skin. Blood 104:2217-2223, 2004.

19. Korte W, Heijnen IA: [Paroxysmal nocturnal hemoglobinuria--consequences of a missing anchor]. Ther Umsch 63:71-77, 2006.

20. Kraemer SM, Kronenberg A, Ueno A, Waldren CA: Measuring the spectrum of mutation induced by nitrogen ions and protons in the human-hamster hybrid cell line A(L)C. Radiat Res 153:743-751, 2000.

21. Kraemer SM, Vannais DB, Kronenberg A, Ueno A, Waldren CA: Gamma-ray mutagenesis studies in a new human-hamster hybrid, A(L)CD59(+/-), which has two human chromosomes 11 but is hemizygous for the CD59 gene. Radiat Res 156:10-19, 2001.

22. Kraemer SM, Waldren CA: Chromosomal mutations and chromosome loss measured in a new human-hamster hybrid cell line, ALC: studies with colcemid, ultraviolet irradiation, and 137Cs gamma-rays. Mutat Res 379:151-166, 1997.

23. Li AP, Aaron CS, Auletta AE, Dearfield KL, Riddle JC, Slesinski RS, Stankowski LF, Jr.: An evaluation of the roles of mammalian cell mutation assays in the testing of chemical genotoxicity. Regul Toxicol Pharmacol 14:24-40, 1991.

24. Liu SX, Athar M, Lippai I, Waldren C, Hei TK: Induction of oxyradicals by arsenic: implication for mechanism of genotoxicity. Proc Natl Acad Sci U S A 98:1643-1648, 2001.

25. McGuinness SM, Shibuya ML, Ueno AM, Vannais DB, Waldren CA: Mutant quantity and quality in mammalian cells (AL) exposed to cesium-137 gamma radiation: effect of caffeine. Radiat Res 142:247-255, 1995.

26. Nelson KL, Raja SM, Buckley JT: The glycosylphosphatidylinositol-anchored surface glycoprotein Thy-1 is a receptor for the channel-forming toxin aerolysin. J Biol Chem 272:12170-12174, 1997.

27. Petranka JG, Fleenor DE, Sykes K, Kaufman RE, Rosse WF: Structure of the CD59-encoding gene: further evidence of a relationship to murine lymphocyte antigen Ly-6 protein. Proc Natl Acad Sci U S A 89:7876-7879, 1992.

28. Pfeifer GP: Involvement of DNA damage and repair in mutational spectra. Mutat Res 450:1-3, 2000.

29. Puck TT, Waldren CA: Mutation in mammalian cells: theory and implications. Somat Cell Mol Genet 13:405-409, 1987.

30. Ross CD, Lim CU, Fox MH: Assay to measure CD59 mutations in CHO A(L) cells using flow cytometry. Cytometry A 66:85-90, 2005.

31. Schafer H, Bartels T, Hahn G, Otto A, Burger R: T-cell-activating monoclonal antibodies, reacting with both leukocytes and erythrocytes, recognize the guinea pig Thy-1 differentiation antigen: characterization and cloning of guinea pig CD90. Cell Immunol 197:116-128, 1999.

32. Sowdhamini R, Mitchell TJ, Andrew PW, Morgan PJ: Structural and functional analogy between pneumolysin and proaerolysin. Protein Eng 10:207-215, 1997.

33. Tomita-Mitchell A, Kat AG, Marcelino LA, Li-Sucholeiki XC, Goodluck-Griffith J, Thilly WG: Mismatch repair deficient human cells: spontaneous and MNNG-induced mutational spectra in the HPRT gene. Mutat Res 450:125-138, 2000.

34. Turker MS, Pieretti M, Kumar S: Molecular evidence for the induction of large interstitial deletions on mouse chromosome 8 by ionizing radiation. Mutat Res 374:201-208, 1997.

35. Tzircotis G, Thorne RF, Isacke CM: Chemotaxis towards hyaluronan is dependent on CD44 expression and modulated by cell type variation in CD44-hyaluronan binding. J Cell Sci 118:5119-5128, 2005.

36. Ueno A, Vannais D, Lenarczyk M, Waldren CA: Ascorbate, added after irradiation, reduces the mutant yield and alters the spectrum of. J Radiat Res (Tokyo) 43 Suppl:S245-S2492002.

37. Waldren C, Correll L, Sognier MA, Puck TT: Measurement of low levels of x-ray mutagenesis in relation to human disease. Proc Natl Acad Sci U S A 83:4839-4843, 1986.

38. Waldren C, Jones C, Puck TT: Measurement of mutagenesis in mammalian cells. Proc Natl Acad Sci U S A 76:1358-1362, 1979.

39. Waldren C, Vannais D, Drabek R, Gustafson D, Kraemer S, Lenarczyk M, Kronenberg A, Hei T, Ueno A: Analysis of mutant quantity and quality in human-hamster hybrid AL and AL-179 cells exposed to 137Cs-gamma or HZE-Fe ions. Adv Space Res 22:579-585, 1998.

40. Waldren CA, Ueno AM, Schaeffer BK, Wood SG, Sinclair PR, Doolittle DJ, Smith CJ, Harvey WF, Shibuya ML, Gustafson DL, Vannais DB, Puck TT, Sinclair JF: Mutant yields and mutational spectra of the heterocyclic amines MeIQ and PhIP at the S1 locus of human-hamster AL cells with activation by chick embryo liver (CELC) co-cultures. Mutat Res 425:29-46, 1999.

41. Wedemeyer N, Greve B, Uthe D, Potter T, Denklau D, Severin E, Hacker-Klom U, Kohnlein W, Gohde W: Frequency of CD59 mutations induced in human-hamster hybrid A(L) cells by low-dose X-irradiation. Mutat Res 473:73-84, 2001.

42. Wetzel A, Wetzig T, Haustein UF, Sticherling M, Anderegg U, Simon JC, Saalbach A: Increased neutrophil adherence in psoriasis: role of the human endothelial cell receptor Thy-1 (CD90). J Invest Dermatol 126:441-452, 2006.

43. Yandell DW, Dryja TP, Little JB: Molecular genetic analysis of recessive mutations at a heterozygous autosomal locus in human cells. Mutat Res 229:89-102, 1990.

44. Zhou H, Xu A, Gillispie JA, Waldren CA, Hei TK: Quantification of. Mutat Res 594:113-119, 2006.

CHAPTER 7

CONCLUSIONS

Overview of significant findings

In this dissertation, I described the development of the Flow Cytometry Mutation Assay (FCMA) that is more efficient, rapid and less expensive than the Mouse Lymphoma Assay and CHO A_L clonogenic assay. The use of this mutation system allowed me to describe the kinetics of CD59 inducible mutants caused by different mutagens, characterize the CD59 cell surface protein in the context of the protein turnover rate and cell cycle, and do extensive studies on radiation-induced mutant spectra in CHO A_L cells using multiple marker analysis.

In Chapter 3, I discussed the development of the FCMA to improve mammalian mutagenesis detection of novel pharmaceuticals. The separation between CD59 positive and negative CHO A_L cells was over 300-fold. The FCMA was calibrated properly by detecting $CD59^-$ CHO-K1 parental cells mixed in precise concentrations with $CD59^+$ A_L cells. The observational mutant yield corresponded to the experimental CHO-K1 and $CD59^+$ mixtures in a linear fashion. After calibration, I treated CHO A_L cells with ionizing radiation and N-methyl-n-nitrosoguanidine (MNNG) to determine if the FCMA could detect mutations induced by both a clastogen and point mutagen. The chemicals induced $CD59^-$ mutants in a linear dose-dependent manner with a higher mutant yield than the A_L clonogenic and MLA

mutation assays. I validated the hypothesis that flow cytometry could be used to develop a mammalian mutation assay that was rapid, robust and linear in detecting mutants at CD59.

Chapter 4 focused on the kinetics of CD59 protein turnover rate on the plasma membrane. As reported in Chapter 3, there was a peak in mutant expression at different times for different mutagens. The kinetics of CD59 expression could be dependent on many factors including lipid raft localization, rate of exocytosis and endocytosis or cellular processes such as the cell cycle. Primarily I wanted to address how long would it take for a mutation in *CD59* to affect the expression of CD59 protein on the cell surface. I showed that the CD59 protein was localized to the lipid raft by measuring its detergent resistance. Then I removed CD59 from the cell surface using PI-PLC and measured the rate of CD59 recovery using flow cytometry. By 8 hr, the CD59 expression had reached control values indicating that exocytosis of CD59 takes less than 8 hr. I then silenced the CD59 mRNA using RNAi technology and measured how long it would take for CD59 to be lost from the plasma membrane. By 48 hr, CD59 expression dropped to 15% of control values. By silencing *de novo* synthesis of CD59, I could measure the CD59 protein turnover rate as less than 2 days. Finally, I examined the cell cycle alterations caused by two mutagens, lead acetate and MNNG, that gave CD59 mutant peaks at 5 and 12 days, respectively. Lead acetate caused substantial alteration in the cell cycle by day 1 but the cell cycle was normal by day 2, whereas MNNG caused a G_2 block until day 4 and returned to normal by day 7. Through these experiments, I determined that the mutant peak expression was most likely controlled by cell cycle alterations and not limited to the exo- and endocytosis of CD59.

In Chapter 5 I investigated the CD59 mutant expression peak by analyzing sorted regions of the FCMA histogram and validated the gating regions on the CD59 histograms used to

define mutants. As discussed in Chapter 4, the cell cycle alterations may largely explain the temporal CD59 mutant expression. In the A_L clonogenic assay, Waldren *et al.* (25) never report a peak in mutant expression possibly because their assay requires clonogenic survival and growth. In contrast, the FCMA measures a mutant expression peak for all mutagens we have tested. I hypothesized that the peak in mutant expression was a measurement of mutations that, after numerous cell doublings, were lethal. I first irradiated A_L cells with ^{137}Cs γ radiation and then stained the population for CD59, CD44 and CD90 cell surface antigens. I then sorted the FCMA CD59 mutant and intermediate region into six populations of 1000 cells each and 300 cells from each region in triplicate for survival analysis. The phenotypic expression of CD44, CD59, and CD90 were analyzed for each region using multicolor flow cytometry on day 6 and day 24 after treatment. Cells from Region 1 had 20% survival and cells from regions 2-6 had 50% survival. Relative growth was similar for all regions. When multiple marker phenotypes were analyzed on days six and 24, 48% of the $CD59^-$ cells were also $CD44^-/CD90^-$ on day 6 but by day 24 this population was reduced to 5%. This indicates that approximately 40% of the mutants at peak expression were triple mutants that were subsequently lethal and were lost from the population. By analyzing the phenotypes of the sorted regions, I was also able to justify the placement of FCMA CD59 mutant region in the histogram. Regions 1-3 and 4 had similar mutant spectra and although the spontaneous CD59 mutant background would be higher, I suggested that cells in region 4 should be included in the mutant region. I also analyzed the kinetics of intermediate cell surface expression of CD59 after irradiation. There was a transient intermediate expression of CD59 present on day 14 which was absent on day 20. Ionizing radiation is known to cause large deletions (2) and it may be that the intermediate CD59 expression indicates a

lethal phenotype. Utilizing flow cytometry, I was able to measure kinetics of $CD59^-$ mutants and determine mutant spectra in the FCMA CD59 mutant and intermediate region.

Chapter 6 discussed how CHO A_L cells can be analyzed for multiple mutations by flow cytometry to obtain a mutant spectrum much faster than conventional PCR and Southern Blot techniques. I first analyzed unstained and stained populations for CD44, CD90, CD98, CD151 and a GPI-anchor control. All of the markers were clearly resolved with very little overlap between negative and positive populations. According to these results, it is possible to determine mutations in these genes by measuring the loss of protein expression by multiparameter flow cytometry. After I analyzed the control cells and optimized the FCMA multiple marker methods, irradiated samples were evaluated for mutants in all six markers. I was able to clearly analyze the populations for expression of all six markers and even utilized this method to sort out individual clones for continued study. I then examined the phenotype of each individual clone to determine the mutant spectrum. The proportion of double and triple mutants ($CD59^-/CD44^-$ and $CD59^-/CD44^-/CD90^-$) was much higher than if they were random independent events. In the case of CD44 and CD59, the proximity of the markers (only a 1.4 Mbp separation) would suggest that a mutatation in both genes indicates that the entire region has been deleted. This does not explain, however, the high frequency of mutants at CD59 and CD90 (44%). I investigated this problem by labeling the $CD59^-/CD90^-$ mutants with fluorescent aerolysin (FLAER), which detects the presence of a GPI-anchor. Thirty-three percent of the $CD59^-$ cells were also negative for CD59 and GPI expression, indicating that mutations in the GPI-anchor genes, presumably *PIGA*, may explain a portion of the elevated mutant yield. The frequency of the CD151 mutants was low most likely because of its proximity to an essential gene(s) of chromosome 11. The PCR results

demonstrated that putative CD59 mutants measured by flow cytometry also correspond directly to a loss of at least one of the *CD59* exons. These results show that the FCMA mutant spectra directly reflect the genotypic mutant spectra based on PCR. My results support previous research using the clonogenic CHO A_L assay which suggested that 97% of the mutations caused by radiation were simple deletions with very few complex mutations (17).

The FCMA multiple marker analysis drastically reduces the time and resources required for mutant spectrum development from 1-2 months for conventional analysis to a week to 10 days for the FCMA. It is possible to do an initial analysis of mutants screening for all markers and determine the yield of mutants for all markers. Using this system, researchers could quickly ascertain the mutagenic potential of novel chemicals and pharmaceuticals as well as clarify the mechanism of mutagenesis without large expense. Additionally, the FCMA would be able to quickly analyze mutated populations during extended time periods to evaluate the evolution of phenotypic expression.

Findings in light of existing research studies

An essential component to this work is the CHO AL cell line that contains a single, unrearranged copy of human chromosome 11. Only a portion of the chromosome is required for CHO survival (11p15.5) and therefore is an excellent target for mutagenesis. Waldren and Puck(25) utilized the CHO A_L cell line to develop the A_L clonogenic assay. CHO A_L cells were treated with a suspect mutagen and after a period of growth were then treated with antibodies to CD59 and rabbit complement. Those $CD59^+$ cells were lysed by rabbit complement whereas $CD59^-$ cells survived. Waldren and others then utilized the A_L cell line

to measure mutations in CD59 on chromosome 11 for a panel of different mutagens. Comparing the A_L clonogenic assay to *hprt* assay and Mouse Lymphoma Assay, the mutant yield was much higher with the A_L assay, indicating that the clonogenic assay was more sensitive to mutations (Figure 7-1). To improve upon the A_L clonogenic assay, I used fluorescent antibodies to CD59 and measured rates of mutagenesis using flow cytometry in the A_L cell line. The sensitivity of the flow cytometry measurement was much higher than all other mammalian mutation assays comparing ^{137}Cs γ radiation (Figure 7-1).

The ability of the FCMA to detect mutations across a diverse panel of agents exhibiting wide ranging modes of action (Table 7-1) demonstrates its reliability and widespread applicability. The Fox lab collaborated to test mutagens and measured mutations in CD59 in CHO A_L cells (Mutation Research, in press) (6). As shown by the variety of agents screened, both point mutations and large, multilocus deletions are quantifiable. The majority of agents had a dose response with an increase in the mutant fraction corresponding to an increase in dose (Table 7-2). In the case of the exceptions, such as lead acetate, benzo(a)pyrene and ethidium bromide it is possible that these chemicals exhibit a threshold effect as opposed to the linear dose response trend seen with other agents. The FCMA is also effective in correctly classifying non-mutagens such as chloropheniramine maleate and thalidomide. Furthermore, the FCMA could detect mutations induced by several known mutagens that were not mutagenic in the MLA including lead acetate, ethidium bromide and TTCE. The FCMA is also more sensitive than the MLA in that it is capable of detecting a higher mutant fraction for a given dose of an agent. Furthermore, the flow cytometry based assay is more sensitive than the traditional clonogenic assay using CHO A_L cells.

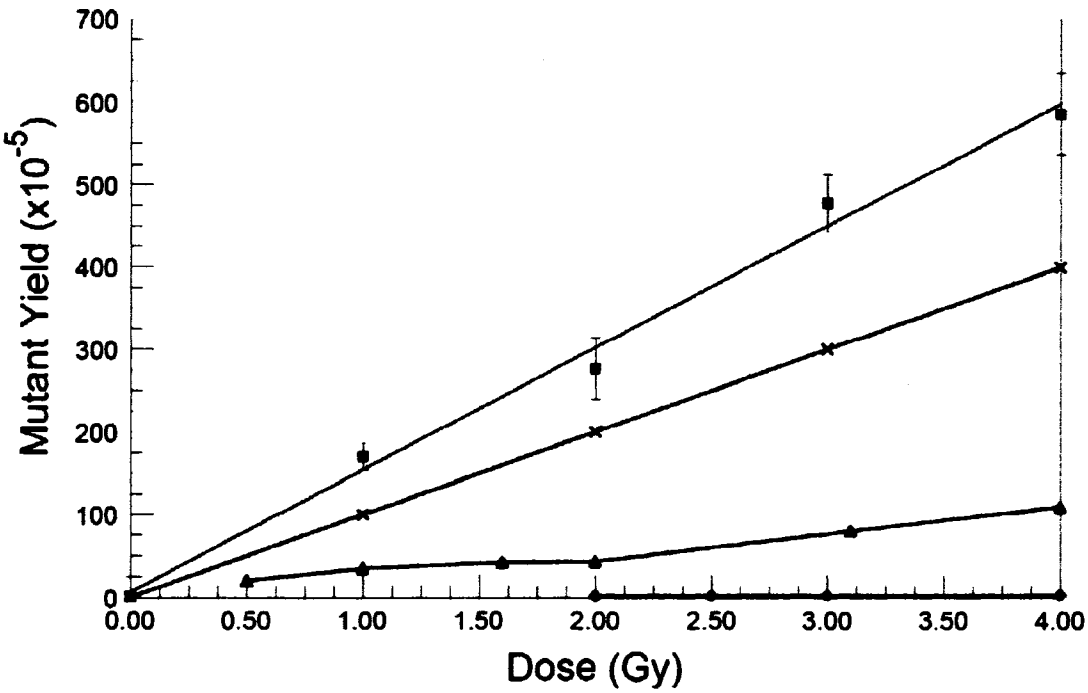

Figure 7-11. Dose response curve for 137Cs γ radiation with various mutation assays. Results are normalized to 0 at 0 Gy; () FCMA, data taken from Ross *et al.* (21) (x) Clonogenic A_L assay, data taken from Waldren 1998 (26); (▲) MLA assay, data taken from Moore 1985 (18); (♦) HPRT assay, data taken from Thacker (22).

Table 7-1. Comparison of mutagenesis results from various agents by type of assay. NT = not tested.

COMPOUND CLASS	COMPOUND	MLA	A_L	FCMA	Sources Cited
Clastogens	γ radiation	+	+	+	(5,25)
Heavy metals	Sodium arsenite	+	+	+	(9,19)
	Lead acetate (LA)	-	+	+	(8)
Alkylating agents & other direct acting mutagens	Ethyl methanesulfonate (EMS)	+	NT	+	(11)
	MNNG	+	+	+	(11,24)
	n-Nitroso n-ethylurea (ENU)	+	NT	+	(4)
	UV radiation	+	+	+	(24,5)
Oxidizing agents	Hydrogen peroxide (H_2O_2)	+	+	+	(11,7)
	Ascorbate	-	-	NT	(23,28, 1)
Cross linker	Mitomycin C (MMC)	+	+	+	(11,7)
DNA intercalater	Ethidium bromide (EtBr)	-	NT	+	(20)
Mutagens requiring S9 activation	3- Methyl cholanthrene	+	+	+	(11,27)
	Benzo(a)Pyrene (BaP)	+	+	+	(11,24)
MLA false negatives	Asbestos (chrysotile)	NT	+	+	(10)
	1,1,1,2-Tetrachloroethane	+/-	NT	+	(11,16)
	1,4 – Dioxane	-	NT	-	(11,16)
	Colchicine	+	+	+	(11,14)
	Benzene	+/-	NT	-	(11)
MLA false positives	Chlorpheniramine maleate (CM)	-	NT	-	(15)
Negative control	Thalidomide	-	-	-	(3)

Table 7-2. CD59 mutagenesis results for increasing doses of various agents done by Tenley French, Dhanashree Joshi, Steve Keysar, Chang Uk-Lim, Carley Ross and Mike Fox (Mutation Research, in press) (6). Categories correspond to the treatment concentration resulting in approximately 80%, 60%, 40% and 20% cell survival. Numerical values represent the average mutant frequency ± SEM in 1x105 cells from multiple experiments. The CD59 negative mutant region was defined as those cells exhibiting a florescence signal of less than 1% of the mean fluorescence value from the CD59-positive population of control cells. * indicates significance difference relative to control ($p < 0.05$). †indicates significant difference ($p < 0.1$). NT = not tested.

AGENT TESTED	CONTROL	80% CELL SURVIVAL	60% CELL SURVIVAL	40% CELL SURVIVAL	20% CELL SURVIVAL	DAY
Chrysotile Rhodesian Asbestos	65 ± 9	NT	70 ± 4	412 ± 151*	565 ± 155*	9
Benzo(a)Pyrene (BaP)	74 ± 38	NT	108 ± 40	197 ± 38†	212 ± 55†	9
Chlorpheniramine maleate (CM)	79 ± 49	91 ± 52	91 ± 55	NT	82 ± 54	12
Colchicine	75 ± 6	88 ± 11	93 ± 23	130 ± 11*	NT	9
Ethidium bromide (EtBr)	26 ± 7	NT	65 ± 5	141 ± 34*	190 ± 31*	9
Ethyl methanesulfonate (EMS)	97 ± 19	217 ± 30*	430 ± 78*	581 ± 67*	765 ± 94*	9
n-Nitroso n-ethylurea (ENU)	68 ± 19	NT	NT	363 ± 69*	721 ± 94*	14
γ radiation	70 ± 10	650 ± 70*	955 ± 145*	1245 ± 245*	1618 ± 202*	6
Hydrogen peroxide (H_2O_2)	77 ± 16	NT	70	80 ± 20	210 ± 34*	12
Lead acetate (LA)	68 ± 30	142 ± 58	148 ± 39	557 ± 95*	NT	6
Methyl cholanthrene	183 ± 9	220 ± 6*	243 ± 19*	227 ± 12*	NT	9
Methyl nitro nitrosoguanidine	62 ± 42	334 ± 108†	521 ± 116*	785 ± 95*	900 ± 60*	12
Mitomycin C (MMC)	78 ± 18	148 ± 17*	135 ± 21	297 ± 24*	532 ± 40*	10
Sodium arsenite (SA)	59 ± 15	69 ± 26	91 ± 32	192 ± 28*	320 ± 59*	12
Tetrachloroethane (TTCE)	94 ± 8	127 ± 16	146 ± 35*	162 ± 7†	168 ± 12*	13
Thalidomide	133 ± 6	163 ± 13	NT	NT	NT	12
UV radiation	108	NT	177 ± 21	281 ± 15	394 ± 16	10

While I developed the FCMA, Wedemeyer and coworkers (29) also used CHO A_L cells to measure mutation at CD59 using flow cytometry. Similar to my results, they measured a 3-fold increase in mutant yield over A_L clonogenic data when cells were irradiated with X-rays, even though they set the mutant yield to 10% of the mean positive peak (Figure 7-2). Fluorescence *in situ* hybridization (FISH) of hamster and human chromosomes was done to determine chromosomal aberrations caused by X-rays(Figure 7-3). They found, as I did, that the kinetics of CD59 could be measured at different time points with maximum expression on day 6, similar to my results with ^{137}Cs γ radiation. The mutant spectra was also determined using PCR of primer sequences along the entirety of chromosome 11. They determined that as the dose increased, the average size of the CD59 deletions measured in Mbp also increased (Figure 7-4).

The study by Wedemeyer *et al.* lacked in-depth analysis of several mutagens to demonstrate the robust nature of the flow cytometry mutation assay. Also, they only measured fluorescence for one marker and did not clearly show a calibration of their system for linear detection of CD59 mutants. Time course experiments were limited to measuring CD59 mutants until the day of maximum mutant expression, whereas my results continue for 20 days post-treatment. They did, however, set the CD59 mutant region to 10%, which corresponds with my findings in Chapter 5, to capture the mutant yield.

Zhou and coworkers (30) also used the CHO A_L cell line to measure mutations at CD59 using flow cytometry. Their results mirror Chapter 3 and Ross *et al.* (21) in the calibration curve, dose dependent CD59 mutant expression for N-methyl-N-nitrosourea (MNU) and ^{137}Cs γ radiation. Zhou *et al.* measured CD59 mutants using both the flow cytometry and clonogenic assay, similar to my results in Chapter 3, appendix. Their data indicated less

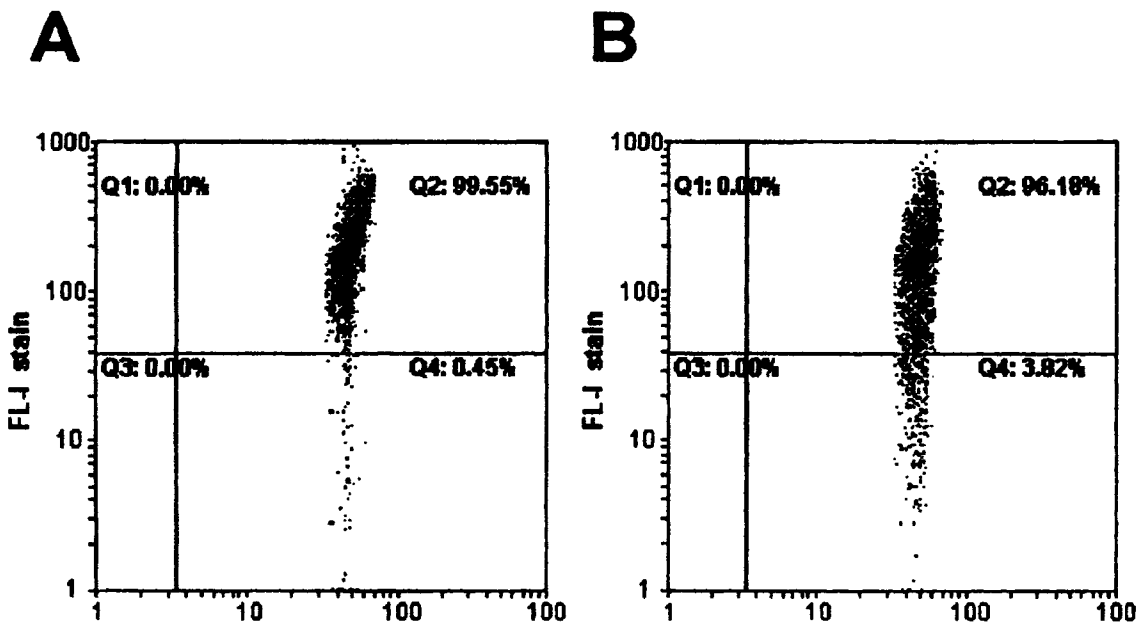

Figure 7-2. Flow cytometry histograms of a CHO AL mutation assay developed by Wedemeyer *et al.* (29) (A) Control cells. (B) 3 Gy irradiated CHO AL cells 3 days post treatment. Q4 in each histogram was the mutant yield.

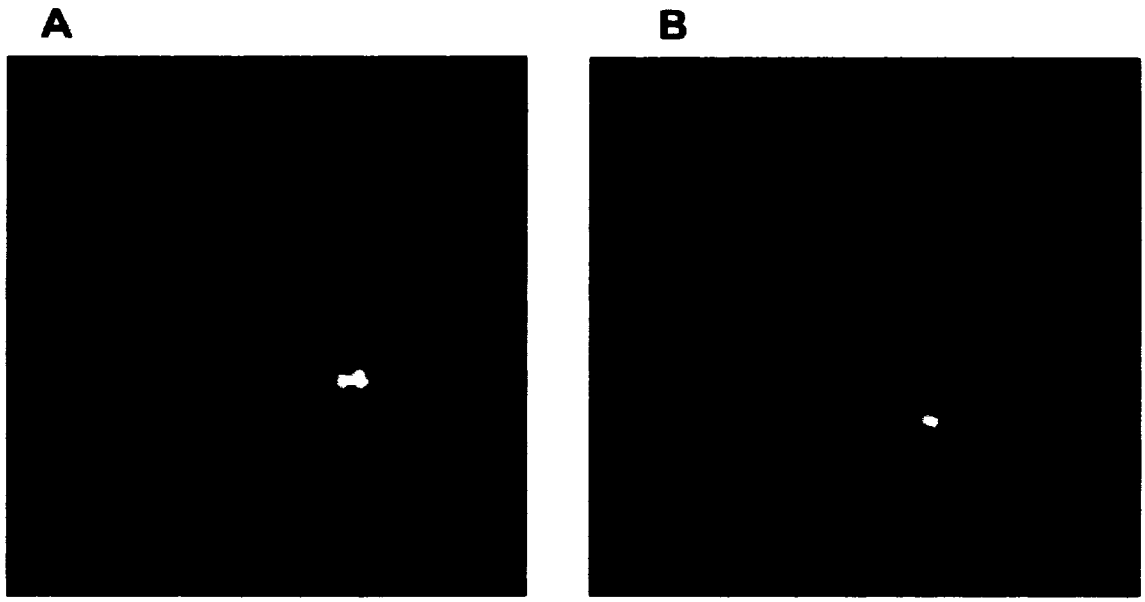

Figure 7-3 Fluorescence in situ hybridization (FISH) of metaphase chromosomes derived from (A) an AL wild type cell and (B) an AL cell irradiated with an X-ray dose of 5Gy (100 kV). For hybridization a digoxigenin-labeled total human genome probe was used, the hybridized probe was detected using an FITC-conjugated anti-digoxigenin antibody and the hamster chromosomes were counterstained with DAPI (29).

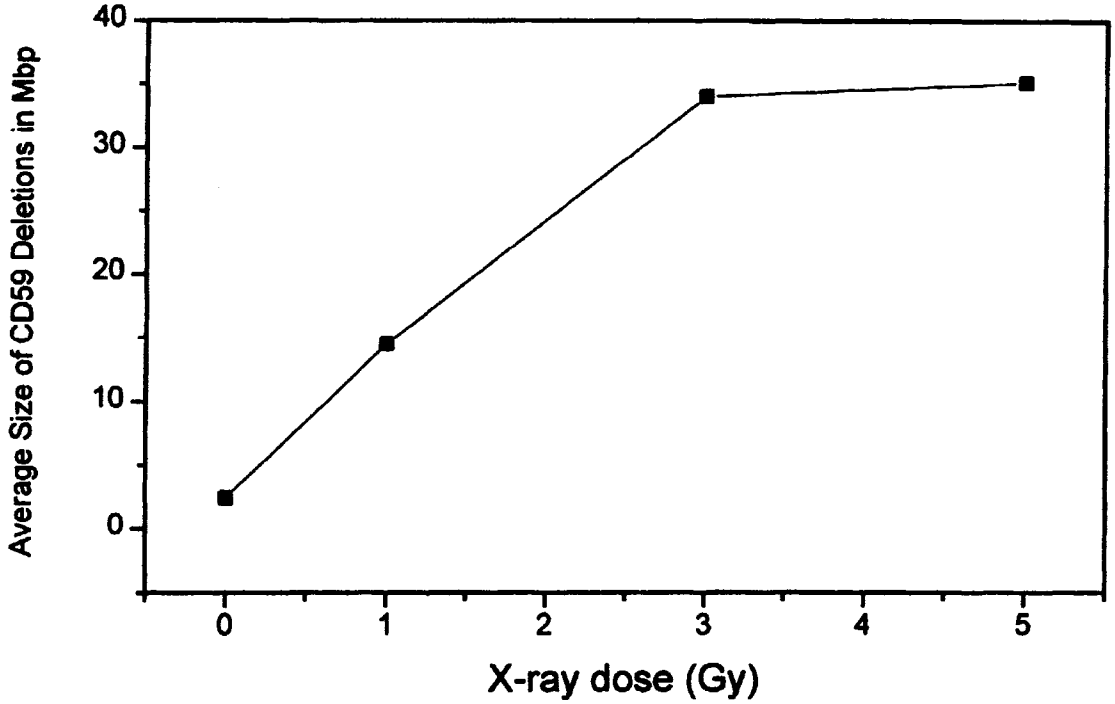

Figure 7-4. Average size of deletions in the CD59 gene region induced spontaneously or by various X-ray doses analyzed by Wedemeyer *et al.* (29).

Table 7-3. Zhou *et al.* comparison gamma ray-induced CD59$^-$ mutation in A_L cells using either flow cytometry or traditional complement/antibody assay (30).

Group	No. of experiments	S.F.*	Traditional complement/antibody assay					Flow cytometry assay		
			No. of cells	P.E.*	No. of mutants	M.F.* (10^{-5})	Means ± S.D.	Total no. of cells	M.F.* (10^{-5})	Means ± S.D.
Control	5	100	3×10^5	0.92	99	36	56 ± 18	1×10^5	60	120 ± 50
		100	3×10^5	0.90	157	58		1×10^5	130	
		100	3×10^5	0.94	118	42		1×10^5	100	
		100	3×10^5	0.81	199	82		1×10^5	190	
		100	3×10^5	0.88	164	62		1×10^5	120	
1Gy	5	86	3×10^5	0.85	260	102	125 ± 33	1×10^5	160	240 ± 60
		78	3×10^5	0.86	390	151		1×10^5	250	
		64	3×10^5	0.93	237	85		1×10^5	240	
		68	3×10^5	0.81	396	163		1×10^5	320	
		70	3×10^5	0.86	320	124		1×10^5	230	
3Gy	5	71	3×10^5	0.65	332	170	211 ± 47	1×10^5	360	430 ± 120
		60	3×10^5	0.68	530	260		1×10^5	600	
		50	3×10^5	0.61	287	157		1×10^5	300	
		61	3×10^5	0.58	444	255		1×10^5	480	
		42	3×10^5	0.60	383	213		1×10^5	410	
5Gy	5	30	3×10^5	0.45	346	256	334 ± 76	1×10^5	580	790 ± 170
		27	3×10^5	0.38	443	389		1×10^5	1000	
		12	3×10^5	0.40	328	273		1×10^5	730	
		18	3×10^5	0.42	538	427		1×10^5	920	
		15	3×10^5	0.36	362	335		1×10^5	720	

* S.F.: surviving fraction; P.E.: plating efficiency with complement in the medium; M.F.: mutation fraction.

precision with flow cytometry compared to the traditional assay based on the large standard deviations in mutant yields in experiments using gamma rays and MNU. They suggest that the difference is due to the inherent fluctuations in the fluorescence of CD59 measured by flow cytometry. I suggest, however, that their CD59 mutant region, set at 99.9% of the unstained control cells, may not capture the entire CD59 mutant peak and therefore slight variations in staining could explain less precise measurement of CD59 mutant yield.

Limitations of the study

One area of improvement to this study would be to utilize A_LC cells as described by Kraemer *et al.*(14,14,26,12,13). They fused CHO A_L hybrid cells with CHO cells to produce a new hybrid, A_LC in which the deletion of the 11p15.5 region is not lethal, allowing for detection of chromosome loss or other chromosomal mutations involving 11p15.5. After irradiating the cells with ^{137}Cs γ radiation, the survival of A_LC cells was much higher than for for A_L cells. The mutant fraction, in addition, was also much higher for the A_LC cell line with Colcemid and ^{137}Cs γ radiation but not UV(Table 7-3). The drawback to this cell line is that it has two copies of chromosome 11 with only one functioning CD59. I could use A_LC to measure CD59 mutations, but none in the other markers because the cell line would be hemizygous. Another challenge to this system is that the spontaneous mutant rate is much higher at 600 cells per 10^5 clonable cells.

Recommendations for future

Future work in this project could focus on three major findings that need further development. First, in Chapter 4, I determined that the cell cycle alterations possibly controlled the time for CD59 mutant expression. By analyzing the panel of chemicals in

Table 7-1 for alterations in cell cycle progression, more definitive conclusions could be drawn about the relationship between the time for mutant expression and the delay in cell cycle. Second, in Chapter 5 I elucidated the evolution of phenotypic expression in irradiated A_L cell using analysis of three genes (CD59, CD44 and CD90). If all six markers discussed in Chapter 6 were used, it would be possible to compare different mutagens and how multiple markers respond in a time and dose dependent manner. Third, the mutant spectra induced by several chemicals could be obtained using simultaneous analysis of multiple markers with the initial sample to analyze the variability in genotoxicity.

Table 7-4. Comparison between A_LC and A_L mutant yield for Colcemid, UV and ^{137}Cs γ radiation taken from Kraemer *et al.* 1997 (14).

A_LC and A_L mutation

Cell line	Colcemid[a]			UV 254			^{137}Cs γ-rays		
	$S1^-$ mutants per			$S1^-$ mutants per			$S1^-$ mutants per		
	μg/ml	D_o	LD_{50}	J/m^2	D_o	LD_{50}	cGy	D_o	LD_{50}
A_L	0	NA	0	15	60	255	0.5	100	110
A_LC	2700 [a]	NA	1200	20	200	540	6	1380	2160

All values are per 10^5 clonable cells.
[a] Based on initial slope.

Reference List

1. Amacher DE, Paillet SC: Ascorbate is detectably mutagenic in the L5178Y TK+/- cell mutation assay. Cancer Lett 14:151-158, 1981.

2. Amacher DE, Zelljadt I: Mutagenic activity of some clastogenic chemicals at the hypoxanthine guanine phosphoribosyl transferase locus of Chinese hamster ovary cells. Mutat Res 136:137-145, 1984.

3. Ashby J, Tinwell H, Callander RD, Kimber I, Clay P, Galloway SM, Hill RB, Greenwood SK, Gaulden ME, Ferguson MJ, Vogel E, Nivard M, Parry JM, Williamson J: Thalidomide: lack of mutagenic activity across phyla and genetic endpoints. Mutat Res 396:45-64, 1997.

4. Chen T, Harrington-Brock K, Moore MM: Mutant frequency and mutational spectra in the Tk and Hprt genes of N-ethyl-N-nitrosourea-treated mouse lymphoma cellsdagger. Environ Mol Mutagen 39:296-305, 2002.

5. Evans HH, Mencl J, Horng MF, Ricanati M, Sanchez C, Hozier J: Locus specificity in the mutability of L5178Y mouse lymphoma cells: the role of multilocus lesions. Proc Natl Acad Sci U S A 83:4379-4383, 1986.

6. French CTRCDKSBJDDLCUFMH: Comparison of the Mutagenic Potential of 14 Physical and Chemical Agents Analyzed by the Flow Cytometry Mutation Assay. Mutat Res 2006.(in press)

7. Gustafson DL, Franz HR, Ueno AM, Smith CJ, Doolittle DJ, Waldren CA: Vanillin (3-methoxy-4-hydroxybenzaldehyde) inhibits mutation induced by hydrogen peroxide, N-methyl-N-nitrosoguanidine and mitomycin C but not (137)Cs gamma-radiation at the CD59 locus in human-hamster hybrid A(L) cells. Mutagenesis 15:207-213, 2000.

8. Hartwig A, Schlepegrell R, Beyersmann D: Indirect mechanism of lead-induced genotoxicity in cultured mammalian cells. Mutat Res 241:75-82, 1990.

9. Hei TK, Liu SX, Waldren C: Mutagenicity of arsenic in mammalian cells: role of reactive oxygen species. Proc Natl Acad Sci U S A 95:8103-8107, 1998.

10. Hei TK, Piao CQ, He ZY, Vannais D, Waldren CA: Chrysotile fiber is a strong mutagen in mammalian cells. Cancer Res 52:6305-6309, 1992.

11. Kirkland D, Aardema M, Henderson L, Muller L: Evaluation of the ability of a battery of three in vitro genotoxicity tests to discriminate rodent carcinogens

and non-carcinogens I. Sensitivity, specificity and relative predictivity. Mutat Res 584:1-256, 2005.

12. Kraemer SM, Kronenberg A, Ueno A, Waldren CA: Measuring the spectrum of mutation induced by nitrogen ions and protons in the human-hamster hybrid cell line A(L)C. Radiat Res 153:743-751, 2000.

13. Kraemer SM, Vannais DB, Kronenberg A, Ueno A, Waldren CA: Gamma-ray mutagenesis studies in a new human-hamster hybrid, A(L)CD59(+/-), which has two human chromosomes 11 but is hemizygous for the CD59 gene. Radiat Res 156:10-19, 2001.

14. Kraemer SM, Waldren CA: Chromosomal mutations and chromosome loss measured in a new human-hamster hybrid cell line, ALC: studies with colcemid, ultraviolet irradiation, and 137Cs gamma-rays. Mutat Res 379:151-166, 1997.

15. McGregor DB, Brown AG, Howgate S, McBride D, Riach C, Caspary WJ: Responses of the L5178Y mouse Lymphoma cell forward mutation assay. V: 27 coded chemicals. Environ Mol Mutagen 17:196-219, 1991.

16. McGregor DB, Martin R, Cattanach P, Edwards I, McBride D, Caspary WJ: Responses of the L5178Y tk+/tk- mouse lymphoma cell forward mutation assay to coded chemicals. I: Results for nine compounds. Environ Mutagen 9:143-160, 1987.

17. McGuinness SM, Shibuya ML, Ueno AM, Vannais DB, Waldren CA: Mutant quantity and quality in mammalian cells (AL) exposed to cesium-137 gamma radiation: effect of caffeine. Radiat Res 142:247-255, 1995.

18. Moore MM, Clive D, Howard BE, Batson AG, Turner NT: In situ analysis of trifluorothymidine-resistant (TFTr) mutants of L5178Y/TK+/- mouse lymphoma cells. Mutat Res 151:147-159, 1985.

19. Moore MM, Harrington-Brock K, Doerr CL: Relative genotoxic potency of arsenic and its methylated metabolites. Mutat Res 386:279-290, 1997.

20. Oberly TJ, Michaelis KC, Rexroat MA, Bewsey BJ, Garriott ML: A comparison of the CHO/HGPRT+ and the L5178Y/TK+/- mutation assays using suspension treatment and soft agar cloning: results for 10 chemicals. Cell Biol Toxicol 9:243-257, 1993.

21. Ross CD, Lim CU, Fox MH: Assay to measure CD59 mutations in CHO A(L) cells using flow cytometry. Cytometry A 66:85-90, 2005.

22. Thacker J, Stretch A, Stephens MA: Th induction of thioguanine-resistant mutants of Chinese hamster cells by gamma-rays. Mutat Res 42:313-326, 1977.

23. Ueno A, Vannais D, Lenarczyk M, Waldren CA: Ascorbate, added after irradiation, reduces the mutant yield and alters the spectrum of. J Radiat Res (Tokyo) 43 Suppl:S245-S2492002.

24. Waldren C, Correll L, Sognier MA, Puck TT: Measurement of low levels of x-ray mutagenesis in relation to human disease. Proc Natl Acad Sci U S A 83:4839-4843, 1986.

25. Waldren C, Jones C, Puck TT: Measurement of mutagenesis in mammalian cells. Proc Natl Acad Sci U S A 76:1358-1362, 1979.

26. Waldren C, Vannais D, Drabek R, Gustafson D, Kraemer S, Lenarczyk M, Kronenberg A, Hei T, Ueno A: Analysis of mutant quantity and quality in human-hamster hybrid AL and AL-179 cells exposed to 137Cs-gamma or HZE-Fe ions. Adv Space Res 22:579-585, 1998.

27. Waldren CA, Ueno AM, Schaeffer BK, Wood SG, Sinclair PR, Doolittle DJ, Smith CJ, Harvey WF, Shibuya ML, Gustafson DL, Vannais DB, Puck TT, Sinclair JF: Mutant yields and mutational spectra of the heterocyclic amines MeIQ and PhIP at the S1 locus of human-hamster AL cells with activation by chick embryo liver (CELC) co-cultures. Mutat Res 425:29-46, 1999.

28. Waldren CA, Vannais DB, Ueno AM: A role for long-lived radicals (LLR) in radiation-induced mutation and persistent chromosomal instability: counteraction by ascorbate and RibCys but not DMSO. Mutat Res 551:255-265, 2004.

29. Wedemeyer N, Greve B, Uthe D, Potter T, Denklau D, Severin E, Hacker-Klom U, Kohnlein W, Gohde W: Frequency of CD59 mutations induced in human-hamster hybrid A(L) cells by low-dose X-irradiation. Mutat Res 473:73-84, 2001.

30. Zhou H, Xu A, Gillispie JA, Waldren CA, Hei TK: Quantification of. Mutat Res 594:113-119, 2006.